이학박사 학위논문

생분석을 위한
표면 기능화 연구:
바이러스가 고정된 금 마이크로
쉘과 변형된 시냅스 유도 단백질

Surface Functionalization for
Bioanalytical Applications:
Virus-decorated Gold Microshells and
Modified Synaptic Cell Adhesion Molecules

2016년 2월

서울대학교 대학원

화학부 분석화학 전공

전 창 수

생분석을 위한 표면 기능화 연구:
바이러스가 고정된 금 마이크로
쉘과 변형된 시냅스 유도 단백질

Surface Functionalization for Bioanalytical Applications:
Virus-decorated Gold Microshells and
Modified Synaptic Cell Adhesion Molecules

지도교수 정 택 동

이 논문을 이학박사 학위논문으로 제출함

2016 년 2 월

서울대학교 대학원

화학부 분석화학 전공

전 창 수

전창수의 박사학위논문을 인준함

2016 년 2 월

위 원 장 이 연 (인)

부 위 원 장 정 택 동 (인)

위 원 주 재 범 (인)

위 원 남 좌 민 (인)

위 원 김 석 희 (인)

A Ph. D. Dissertation

Surface Functionalization for Bioanalytical Applications:

Virus-decorated Gold Microshells and Modified Synaptic Cell Adhesion Molecules

By

Chang Su Jeon

Supervisor: Professor Taek Dong Chung

Major: Analytical Chemistry

Department of Chemistry

Graduate School of

Seoul National University

February 2016

Abstract

Surface Functionalization for Bioanalytical Applications:

Virus-decorated Gold Microshells and Modified Synaptic Cell Adhesion Molecules

Chang Su Jeon
Department of Chemistry, Analytical Chemistry
The Graduate School
Seoul National University

Solid-phase extraction (SPE) is a sample preparation method used as a means of separation, concentration, and purification for analysis of complex unknown samples in the analytical field. Recently, there have been efforts to increase binding affinity, sensitivity, and selectivity through biomimetic surface engineering. In the analysis of complex biological samples, like blood and cells, physical and chemical interactions between the solid-phase surface and target species are crucial. These interactions can be divided into those in which the target analyte directly interacts with the solid surface and those in which the secreted substance is observed upon the introduction of target analyte, including cells, to the surface. This dissertation

describes (i) bio-inspired surface modifications for enhanced analyte-solid surface interactions and (ii) the purification of synaptic cell adhesion proteins for induced artificial synapses and bioanalysis.

Part I. Analyte-solid surface interaction: virus-decorated magnetic gold microshells with biomimetic architectures for enhanced immunoassays

Filamentous phage virus has similar structural dimensions to many cellular threadlike structures that enhance the cellular functions. The aim of this study was to combine the virus and microshells to resemble biological systems, thereby harnessing the enhancement factors originating from the unique morphology. We implemented gold layer on a microshell to form a self-assembled monolayer that help with chemical modifications using streptavidin and protection from non-specific adsorptions. Phage virions that carry biotins within their tails were prepared for directional binding of the virions to streptavidin-modified gold microshells. We confirmed the augmented yield of antibody loading on virus-modified gold microshells because of the increased surface to volume ratio. Indeed, the sensitivity has increased up to nine-fold for the detection of cardiac marker proteins. This work demonstrates the feasibility of merging viruses with non-biological substrates to yield biomimetic tools for the enhanced analyte-decorated solid surface interactions.

Part II. Cell-solid surface interaction: purified synaptic cell adhesion molecules for induced artificial synapse

Conventional neural interfaces solely depend upon passive physical contact between nerve cells and their non-biological counterparts. Nerve cells in the brain, however, communicate via synapses of which spatiotemporal specificity is exquisitely regulated. Here, we report a newly engineered postsynaptic cell adhesion molecules (CAMs) that are fluorescent and biotinylated to facilitate its purification, quantification, tracking, and immobilization on inorganic substrates. The independence of synaptic CAMs on the lipid membranes, originating from the orientation-controlled immobilization, extends versatility of the protein to fit in artificial synapse formation between neurons and various types of inorganic solid substrates. Moreover, this method will be used as the basis for studying the interaction between the cell and solid surface.

Keywords: gold microshell, suspension array, non-specific binding, virus, artificial synapse, neuroligin, synaptic cell adhesion molecules

Student number: 2009-22920

Contents

List of Figures

magnet was placed beside the tube.

Figure 6. Verification of the stability of SAM-modified gold microshells. SAM-protected gold microshells were incubated in phosphate-buffered saline (PBS) buffer at (a) 4 ℃ or (b) 25 ℃ for 24 hours. Each of (a) and (b) samples was incubated at 4 ℃ , 25 ℃ , 40 ℃ for 24 hours and then treated with streptavidin and biocytin-alexa594 for 1 hour at 25 ℃ to observe fluorescence. Biocytin-Alexa Fluor 594 dye was used for the determination of mean fluorescence intensity (MFI).

Figure 7. (a) Schematic representation of antibody immobilization on carboxyl-terminated gold microshells. After the primary antibody was attached to the surface of the gold microshells using EDC/NHS, the reaction was observed via fluorescence with an alexa488 conjugated secondary antibody. (b) DIC image. (c) Fluorescence image.

Figure 8. Optimization of antibody loading on gold microshells. (a) Schematic representation of antibody immobilization on thiol SAM-decorated gold microshells. (b) DIC and fluorescence images with different amounts of primary antibody, and a fixed amount of secondary antibody. (c) Fluorescence intensity according to the ratio of experimental to theoretical antibody.

Figure 9. Results of streptavidin immobilization on gold microshells. In (a) and (c), experiments using biocytin-Alexa 488 (upper panels) did not show fluorescence due to quenching whereas biocytin-Alexa 594 (lower panels) showed strong fluorescence. (b) and (d) indicate pretreatments with free biotin, and no fluorescence was observed.

Figure 10. Detection of cardiac troponin I in human serum.

Figure 11. (a) Phage vector map, fd-tet with SfiI and NotI cloning site in front of pIII. (b) Wild-type fd-tet and AP-representing fd-tet-APpIII virions (1013) were treated with BirA, followed by western blot visualized using streptavidin-HRP. (c) The two primer, SfiI-Avitag-NotI-F and SfiI-Avitag-NotI-R, were annealed and ligated with fd-tet phage vector (a) that had been digested with SfiI and NotI.

Figure 12. TEM image of PEG/NaCl-purified fd-tet-APpIII phage after 2% uranyl acetate staining. Scale bar = 200 nm.

Figure 13. BirA-treated fd-tet (upper panel) and fd-tet-APpIII (lower panel) phage virions (1.0×10^{10}) on streptavidin-SAM gold microspheres were detected using (a) Alexa Fluor® 610 Succinimidyl Esters, (b) rabbit anti-fd antibody and anti-rabbit Alexa Fluor® 610-R-PE antibody.

Figure 14. Optimization of surface modifications of Au microspheres with streptavidin and phage virions. Various amount of biotinylated phage virions were used for the titration of virus loading with the same reaction conditions as in Figure 15 (b).

Figure 15. (a) SEM image of bare magnetic gold microspheres (scale bar = 10 μm). (b) Magnified image of gold microspheres reveals the morphology of gold layer (scale bar = 2 μm). Pt-sputtered surface morphology of the beads that had been modified with carboxyl-terminated hexa(ethylene glycol) undecane thiol SAM (c), then conjugated with streptavidin (d), and finally with pIII-biotinylated fd-tet phage virions (e). Scale bars for c-e = 100 nm.

Figure 16. (a) SEM images of independent areas of streptavidin-modified gold microshells with Pt sputtering. (b) SEM images of independent areas of streptavidin-gold microshells treated with phage virions at various magnifications with Pt sputtering.

Figure 17. 3D N-SIM super resolution image from a100 nm Z-stack step size and 0.1 reconstruction factor. w/o phage (a) and w/ phage (b) (scale bar = 1 μm) at 1 μm streptavidin-coated microsphere.

Figure 18. Optimization of Staudinger ligation using mouse antibody. (a) Gold microspheres, covered with streptavidin or phage virions, were treated with four different concentrations of Sulfo-NHS-Phosphine, while mouse antibody were incubated with 0.1 mM and 1.0 mM NHS-PEG_{12}-Azide. (b) streptavidin or phage-covered gold microspheres were incubated with fixed concentration of phosphine (0.5 mM), while the concentration of azide varied. Anti-mouse Alexa Fluor 594 antibody was used for the determination of mean fluorescence intensity (MFI).

Figure 19. Sandwich immunoassay profiles (top) and representative fluorescence images of each functionalized microspheres corresponding to the w/o initial and final concentrations (bottom) tested for cardiac marker proteins. A range of cTnI in PBS (a), myoglobin in PBS (b), and cTnI in serum (c) were detected using virus- and streptavidin-gold microspheres (a and b), as well as polymer microspheres (c).

Figure 20. Immunoassay of cTnI in PBS buffer (10 ng/mL) using 10 μm diameter polystyrene beads whose surfaces were modified with an anti-cTnI

antibody using EDC/NHS chemistry. (a) DIC image. (b) Fluorescence image.

Figure 21. Genetic engineering of postsynaptic CAMs for facile mass production with in vivo biotinylation. SS, signal sequence; HA, hemagglutinin affinity tag; H6, hexa-His tag; GS, Gly-Ser rich linker; H8, octa-His tag; AP, biotin acceptor peptide; IRES, internal ribosome entry site. The SS, HA and H6 vary depending upon the type of the postsynaptic CAMs

Figure 22. HEK-293H cell viability assay in 800 μg/ml G418 for (a) 0, (b), 1, (c) 2, (d) 3, (e) 5, (f) 7 days.

Figure 23. Optimization of transfection methods for a HEK-293H cell line. Fluorescent images of GFP-transfected HEK-293H cells in three independent transfection experiments. (a) Calcium phosphate, (b) Lipofectamine 2000, (c) Polyethyleneimine.

Figure 24. (a) 4, (b) 9 and (c) 12 days after transfection. (d) DIC image of a single colony in which G418 selected NL1-R was expressed two weeks after transfection.

Figure 25. Merged fluorescence and DIC images of stable cell lines in which synaptic CAMs of (a) Y-NL1-G, (b) Y-NL1, (c) R-NL1, (d) NL1-R, (e) NL2-R, and (f) SL3-R were expressed.

Figure 26. Western blot profiles for the partially purified and labeled NL1s. The YFP-tagged NL1-GPI (Y-NL1-G) rarely appeared in the elution fraction despite its presence in the total cell lysate. When the GPI motif was replaced with AP, the YFP-NL1-AP (Y-NL1) was secreted into the culture medium, and was retained in a Ni-NTA resin. Both in vitro and in vivo biotinylation revealed biotinylated NL1

regardless of the position of the fluorescence protein. Y-NL1-G was probed by anti-NL1 antibody while the AP-tagged NL1s were detected using streptavidin-HRP.

Figure 27. Partially purified NL1-R was quantified using BSA standards. The biotinylated band was verified using western blot (right panel). The relationship between fluorescence intensity and concentration of NL1-R was determined to be 19,000 MFI/μg NL1-R when measured using a microplate reader.

Figure 28. Purified biotin tagged NL1-R was immobilized on streptavidin contained 2.8 μm Dynabeads. (a) DIC image, (b) Fluorescence image. Since RFP is included, as shown in (b), red fluorescence was observed in addition to the shape of the bead.

Figure 29. NL1-R induces artificial synapse independently of SLB membrane. NL1-R has the strongest synaptogenic activity streptavidin coated Dynabeads when incubated with DIV14 hippocampal neuron culture for 2 days. Synapsin I (Syn I) aggregation were induced by NL1-R on streptavidin coated Dynabeads. Scale bars = 10 μm.

List of Schemes and Tables

surface modifications by thiol SAM followed by chemical conjugation of streptavdin. The resulting streptavidin-modified microspheres are decorated with pIII-biotinylated phage virions that have filamentous structure, resembling the surface morphology of specific types of cells. The surface-exposed anime groups of N-termini of the viral major coat proteins are conjugated with phosphine and mixed with azide-modified primary antibodies to yield microspheres covered with high-density antibodies via bioorthogonal Staudinger ligation (figures shown cross-sectional area of virions layer and not drawn to scale).

Scheme 5. (a) Schematic representation of artificially induced neuronal cell-solid surface interfaces.

Scheme 6. (a) Schematic structure of artificial synapse displaying postsynaptic NL1 homodimer (NL1-R), NL2 homodimer (NL2-R), and Slitrk3 (SL3-R). The structures were modeled after NL1 (PDB ID, 3BIX) and NL2 (PDB ID, 3BL8), while the structure of Slitrk3 (27-627 residues) was predicted using Slitrk1 (PDB ID, 4RCW)[16] as a template by the RaptorX server, showing two LRR1 and LRR2 domains. (b) Schematic structures of engineered synaptic CAMs used in this study in comparison to wild type NL1 (WT). (c) Predicted structure of NL1-R-Nrx1β complex. The C-terminal tagging module for ectodomain of postsynaptic CAMs minimizes steric hindrance in pre- and postsynaptic CMAs interaction.

Table 1. Sorted by category of blood analysis.

Table 2. List of commercialized beads builders.

Table 3. List of commercialized beads products and services.

Part 1

Analyte-solid surface interaction:

Virus-decorated magnetic gold microshells with biomimetic architectures for enhanced immunoassay

1. Background and Overview

1.1. Immunoassay

The first immunoassay was developed by Landsteiner in 1954, who detected small molecules called "haptens" using antibodies [1]. In 1971, E. Engvall and P. Perlmann introduced enzyme-linked immunoassay [2], which is now known as the representative enzyme-linked immune-sorbent assay (ELISA); it is used to observe color changes using antibodies. Such immunoassays are widely used as quantitative methods for detecting supramolecules (e.g., cells, proteins, and polypeptides) and small molecules (lipids, hormones, chemicals, etc.) in various fields of molecular biology and environmental science. Color changes of substrates such as tetramethylbenzidine (TMB) and p-nitrophenyl phosphate (p-NPP) following reaction with antibodies were observed in traditional ELISA, but recently, ELISA-like technologies that do not use enzymes, but use a new reporter that generates various signals, have been widely adopted [3-10].

Immunoassays are categorized into optical and non-optical methods (electrochemical, mass sensitive, calorimetric) depending on the transducing mechanism. Optical immunoassay can be classified into the following 6 types: 1. UV/VIS spectroscopy, which measures the optical or electronic properties of a material, such as absorption, transmission, and reflectivity; 2. fluorescence, which measures the shift in the wavelength of the fluorophore, time dependence of

fluorescence emission, and energy transfer phenomena; 3. surface plasmon resonance, which measures the changes in wavelength, intensity, and the phase or angle of incidence; 4. chemiluminescence, which measures characteristic light from a reaction product prepared by oxidation of a luminol reactant; 5. Raman spectroscopy, which measures vibrational energy states; and 6. Interferometry, which measure the changes in the evanescent field. The optical immunoassay has the advantages of high sensitivity and high speed and benefit from developing infrastructure. Especially, as the fluorescence immunoassay method does not require additional substrate (TMB, p-NPP, luminol) is being widely used. The fluorescence immunoassay can be carried out by one of two methods: by conjugating the fluorophore or the quantum dot to the antibody. Of these two, the fluorophore-based method is widely used.

The representative advantage of immunoassay over other binding assays is its low detection limit and high analyte selectivity. On the other hand, its representative disadvantages are that it is greatly influenced by antibody activity and its cross reactivity with the structural analogs of the target analyte [11]. As indicated by Prof. B. M. Spiegelman [12] and Prof. A. J. Wagers [13], immunoassays using antibodies have become controversial, so much so that an article named 'Blame it on the antibodies' was published in Nature 2015. Although errors due to incorrect molecular recognition may arise with use of antibodies in immunoassays, no other substitute binding has been developed, and the immunoassay remains one of the preferred methods for biological sample analysis [14].

1.2. Planar array and suspension array

The quality and average expectancy of human life have increased with rapid advancements of modern science. In terms of disease diagnosis, specific test items have also increased with the advancement of science and technology. For example, there are over 200 test items (Table 1), including chemicals, DNA, lipid protein, and cells in a blood test [15], and early diagnosis is critical for disease prevention/treatment [16, 17].

Table 1. Sorted by category of blood analysis

	category	# of test
1	Ions and trace metals	17
2	Acid-base and blood gases	9
3	Liver function	9
4	Cardiac marker	9
5	Lipids	6
6	Tumour markers	9
7	Endocrinology	29
8	Vitamins	8
9	Toxins	2
10	Hematology	31
11	Immunology	25
12	Other enzymes and proteins	7
13	Other electrolytes and metabolites	12

Rapid, accurate, low-cost, and efficient detection and quantification of various disease markers from a limited amount of samples is the hot topic of interest in

analytical chemistry. The conventional immunoassay format of ELISA requires about 500 ng of capture antibody and 50~100 μL of a sample to analyze one specimen. As a result, an array type binding assay technology has been developed as a miniaturized, parallel binding assay for multiplexed detection [18]. The first multiplexed immunoassay was developed by L. G. Feinberg in 1961 for microspot test of antibody-antigen reaction in the thin agar films on the cover glass [19]. Since then, various attempts have been made, but the main approach can be divided into 2 general methods: the use of 2D planar micro arrays or 3D suspension array.

A 2D planar array is an assay that captures molecules immobilized in microspots (diameter < 250 μm), with several thousand spots exist per square centimeter [20]. The individual microspots are located hundreds of micrometers apart to prevent mutual contamination, and may immobilize different capture molecules. DNA chip and Protein chip are examples of 2D planar arrays, often referred to as a planar array or a microarray [21]. The protocol of a 2D planar array is similar to that of conventional ELISA, and generally scans fluorescence or chemiluminescent signals. For multiplexed detection, the different capture molecules must be located at nearby spots and the array needs to remember the immobilized capture molecule at each spot. When the X and Y locations are memorized in a 2D planar array for multiplexed detection, it is easier to remember the locations of the capture molecules, which is a comparatively easier barcoding method than 3D suspension array.

A 3D suspension array is an analytic system that suspends a few micrometer-

sized microspheres (particles or beads) of the immobilized capture molecules in a solution, and reacts them with an unknown sample to detect the signals from these particles. The suspension array has the following advantages over planar array. First, the total assay time (TAT) is shorter and a smaller sample volume is required. As the Micrometer sized particles have fast diffusion and smaller steric hindrance with their high surface to volume ratio, compulsory-mixed by external force is possible. Furthermore, a planar array must set adjacent spots apart by a fixed distance to prevent their cross contamination, creating a dead surface that consequently increases the area contacted by the sample solution. Therefore, the suspension array requires shorter total analysis time compared to the planar array, with a smaller sample volume. Second, it has greater sensing flexibility with the different capture molecules that can be mix-and-matched at different combinational at will. Third, the suspension array can replicate each target molecule from hundreds to thousands in the single experiment, offering greater reproducibility and high precision measurements. Fourth, it is cost-effective because of the reduced TAT and improved reproducibility and precision by performing only one experiment [20]. Unlike a 2D planar array, a 3D suspension array has suspended micrometer-sized particles that move while in solution, requiring barcoding for individual particles. The most widely used barcoding method is the optical one, which uses an organic dye [22], quantum dots [23], IR [24], or a Raman probe [25]. Chemical [26], graphical [27], electronic [28], and physical methods [29] are also used.

A planar array obtains signals by scanning, but a suspension array obtains

information using flow cytometry. Flow cytometry hydrodynamically focuses the suspended particles in a solution and passes a beam of light (usually laser light) of single wavelength through the suspension for the analysis. Coulter counter and fluorescence-activated cell sorter (FACS) are representative analytical methods of flow cytometry. Since the first report of flow cytometry in the 1960s, it has been used in a variety of areas, and has become an essential technique in the diagnosis of health disorders [30]. A conventional Coulter counter or FACS has the disadvantages of being expensive and very large. To compensate for these disadvantages, microfluidic chip based flow cytometry has been introduced. J. M. Ramsey distinguished 1- and 2 μm particles through electrokinetic focusing in a microchip and reported a throughput of 34 particles [31]. T. D. Chung *et al.* distinguished white blood cells and red blood cells using a microfluidic chip and direct current (DC) impedance [32], and in 2010, developed a microflow-cytometry system that could simultaneously detect particle size by DC impedance and fluorescence by laser [33]. Recently, a mixed planar array system has been reported, which can lithographically build a wall to immobilize the particles while scanning to detect signals [34].

1.3. Microspheres

Polymer particles, such as poly(methyl methacrylate) (PMMA), polystyrene (PS), or silica particles of 1~100 μm (mostly 2~15 μm) are generally used in 3D suspension array systems. Polymer or silica particles are separated by centrifugation, but magnetic particles, which encapsulate magnetic pigments such as iron oxide and

nickel particles or whose surfaces have been introduced with a magnetic pigment, are widely used. Presently, microspheres are moving beyond the academic field (Figure 1) of experimentation and are being widely used commercially. These types of microspheres are being widely used in clinical diagnostics, molecular assays/cellular assays (drug targeting, cell isolation and purification, nucleic acid or protein purification and detection) [35].

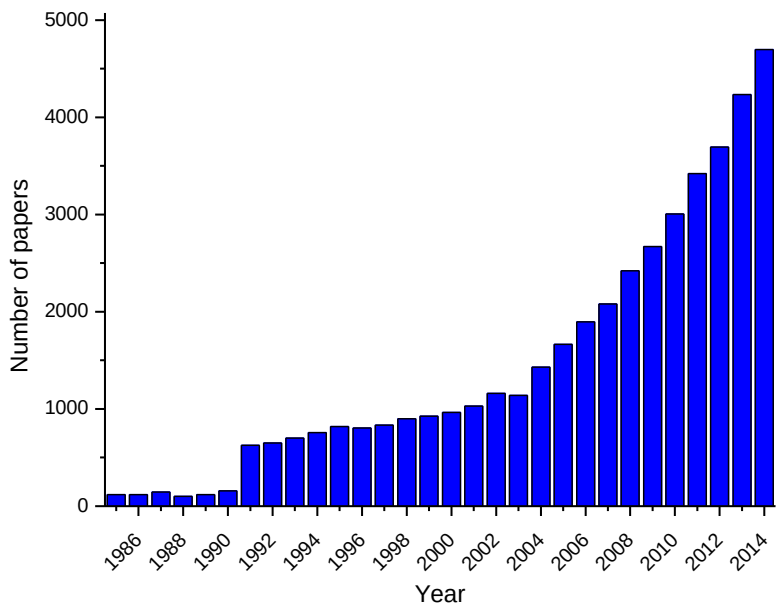

Figure 1. Number of papers published in each year between 1985 and 2014 in which terms microsphere and/or microspheres were used, according to the ISI Web of Knowledge scientific base search.

Many companies sell microspheres or microsphere-related products. For commercially available microspheres, certain beads builders sell naked beads (Table 2); however, most of the time, they sell surface-functionalized or modified beads, while also providing experimentation services (Table 3) [36].

Table 2. List of commercialized beads builders.

Company	Products	Location
Dynal Biotech Inc. → Thermo	Polymer	Norway
Merck Estabor → Millipore	Polymer/Silica	France
Seradyn Inc. →Thermo	Polymer	USA
Bnag's Lab.	Polymer/Silica	USA
Luminex Corp.	Polymer	USA
Immunico Corp. → Johnson&Johnson/Veridex	Polymer/Silica	USA
Spherotech Inc.	Polymer/Silica	USA
Advanced Magnetics Inc.	Polymer	U.K.
CPG Inc. → Millipore	Polymer	USA
Promega	Polymer	USA
Ferrofluidics Corp.	Polymer	USA
FeRx Inc.	Polymer	USA
Miltenyi Biotec	Polymer	Germany
PolyMicrospheres Inc.	Polymer	USA
Chemicell	Polymer/Silica	Germany

Bangs laboratories, Inc., established in 1988, provides 1–25 μm PS, PMMA, or SiO_2 particles whose surface have been aminated or caboxylated, or decorated with a certain antibody or protein [37]. Dynabeads, widely known as Thermo Fisher

Scientific Company, sells various products such as iron oxide type magnetism introduced 1, 2.8, 4.5 μm sized PS particles conjugated with glycidyl ether and having proteins on their surfaces [38]. The US microspheres-Nanospheres Company sells sub-micrometer sized particles of gold, silver, aluminum oxide, titanium oxide, silicon oxide and 1–100 μm particles of PS, PMMA, and SiO_2, as well as surface-functionalized products [39].

Table 3. List of commercialized beads products and services.

Company	**Products & Services**	**Location**
Marligen Biosciences	Transcription Factors	Maryland, USA
Panomics	mRNA, RNAi, Immunoassays	California, USA
Radix BioSolutions Ltd.	DNA Hybridization, Immunoassays	Texas, USA
Applied Cytometry Systems	Software & Assay Development	California, USA
Bio-Rad Life Science	Bio-Plex: Instruments, Cytokines, Isotyping, etc.	California, USA
Cayman Chemical Company	Cancer, Nitric Oxide, Apoptosis, etc.	Michigan, USA
Cogenics	Genotyping	North Carolina, USA
Eva Technologies Corp.	Autoimmunity, Cancer, etc.	Alberta, Canada
Exiqen	Gene Expression	Denmark
Expression Analysis	RNA Profiling & Genotyping	North Carolina, USA
INDOOR Biotechnologies, Inc.	Allergy	Virginia, USA
Invitrogen	Cytokines, Signal Transduction, Neuroscience, etc.	California, USA
Marligen Biosciences, Inc.	Genotyping & mRNA	Maryland, USA
Millipore Corp.	Cytokines, Apoptosis, Cardiac, Endocrine, etc.	Missouri, USA
MiraiBio	Equipment, Software & Materials	California, USA
Novagen	Cellular Signaling & Cancer	Wisconsin, USA
Panomics	Cellular Signaling, Cytokines, etc.	California, USA
PerkinElmer	Drug Discovery	Massachusetts, USA
QIAGEN	Instruments, Reagents & Cell Signaling	California, USA

R&D Systems, Inc.	Cytokines, MMP's, etc.	Minnesota, USA
Rules Based Medicine	Assay Services	Texas, USA
Wageningen University and Research Center	Plant pathogenic virus	The Netherlands
Abbott Molecular Inc.	FISH	Illinois, USA
Asuragen	Signature, Genetic Testing, Oncology	Texas, USA
BMD	Autoimmune & Infectious Disease	France
Bio-Rad Diagnostics	Autoimmune, etc.	California, USA
Celera Diagnostics	Infectious Disease &Cystic Fibrosis	California, USA
MiraiBio	Equipment, Software & Materials	California, USA
EraGen Biosciences	Genetic Analysis	Wisconsin, USA
Fisher Healthcare	Prima	Texas, USA
Focus Diagnostics	Assay Services	California, USA
INOVA Diagnostics, Inc.	Autoimmune Disease	California, USA
ImmuneTech	Allergy	California, USA
InnoGenetics NV	Neurodegeneration	Belgium
Inverness Medical Professional Diagnostics	Autoimmune Disease	New Jersey, USA
MICROBIONIX GmbH	Assay Services & Assay Development	Germany
Multimetrix GmbH	Infectious disease, Inflammation, Coagulation, etc.	Germany
One Lambda, Inc.	HTA Testing	California, USA
Tepnel Lifecodes	HLA Testing	Connecticut, USA
Zeus Scientific, Inc.	Autoimmune Disease	New Jersey, USA

The representative company that offers suspension arrays is Luminex Corp., established in 1996. They offer not only microspheres but also provide integrated support from signal readout devices to experimental services. Various chemical functional groups and oligomer or protein can be conjugated to a 5.6 μm size polystyrene particle, and 6.5 μm PS particles are used as magnetic microspheres [40]. Currently, 500-plex analysis is possible by swelling the polymer microspheres in an organic solvent and allowing two organic dyes of different proportions to enter the

microspheres, followed by shrinking them in an aqueous solution. Data can be acquired by flow cytometry, using the non-overlapping fluorophore wave as the target signal, and by barcoding and passing the microspheres through a fixed laser pathway. Like Luminex, Affymetrix also offers services related to microspheres that allow 100-plexed detection with an internal dye and 4–5 μm sized PS particles as the microspheres [41]. Miltenyi Biotec company offers 2, 3 μm microspheres, reagents; equipment; and total analysis service for flow cytometry and cell stimulation as a Magnetic Activated Cell Sorting (MACS) technology [42]. The Korean company Bioneer sells 1–5 μm SiO_2-based magnetic microspheres with various surface modifications [43].

In 2007, T. Nagaoka *et al.* made gold-coated microspheres on polystyrene and reported their applications. They attached gold nanoparticles to 6 μm polystyrene particles and plated them by electroless plating to form a gold layer, introducing various metal layers, such as nickel, silver and copper, on the polymers for application in electronic devices [44]. Furthermore, in 2009, they introduced a gold layer on plastic particles using a binder, describing its potential use as an anisotropic conductive film (ACF) [45]. M. E. Meyerhoff *et al.* reported the first instance of using magnetic gold microspheres for immunoassay in 2006. They introduced gold to 4.5 μm magnetic polystyrene microspheres through electroless plating, and covalently attached antibody fragments to a tosyl-activated surface; the absorbance signal was detected using alkaline phosphatase and p-NPP [46]. At the same time, M. Liu *et al.* proposed a fluorescence signal analysis system by attaching antibodies

after forming a gold layer on 100 μm PS particles [47]. In 2011, an immune-device system integrating gold microspheres with immobilized protein using self-assembled monolayers, microfluidic chip, and dielectrophoresis was reported [48]. Commercial gold microspheres can be purchased from the SEKISUI chemical corp. and the Nomadien corp. SEKISUI gold microspheres were developed for electric contact, and contain nickel inside with the surface gold layer [49]. Nomadien corp. introduced magnetism and a layer of gold on 2–15 μm polymer microspheres, and showed their potential use in detecting various biological molecules [50-54].

1.4 Viruses

Virus, a contagious particle of size less than a few hundred micrometers, replicates only inside the living cells of other organisms, and can be categorized into bacteriophages (shortened to phages), plant viruses, and animal viruses depending on the host. Early virus-related research was conducted in the fields of molecular and cell biology in the broad areas of life sciences and medicine. Recently, viruses have been used as chemical and biological sensors in material science and nanotechnology. Phages, which are used widely in sensing applications, have the following advantages. First is the well-established phage display technology. Phage display is a technique that selects the high-binding-affinity sequence by amplifying only the target-specific phage from a randomly sequenced phage library [55]. Second, they show high sensitivity and selectivity through target-specific recognition, an inherent virus function. Third, they exhibit multivalent interactions. A virus is composed of

several domain proteins, each domain having about 3000 copies. Therefore, a strong multivalence can be obtained if a target domain is given functionality [56, 57]. Fourth, they can be mass-produced in a cost-efficient manner in the host bacterial cell. Fifth, they have good chemical and thermal stability, allowing them to survive in acidic, basic, or non-aqueous media, and at temperatures up to 180 ℃. Sixth, they can be used as a template for self-assembly of uniform size and shape with a nucleation site [58].

Phages can be categorized into lytic phages, such as T4 and MS2 phages, which replicate in a bacterial cell and leave the host cell after killing it, and non-lytic phages, such as M13 and fd phages, which leave the host cell without killing it. The T4 bacteriophage, which is frequently shown in literature as having a spaceship-shaped icosahedral head and tail, has an inner diameter of 55 nm, tail length of 28.5 nm, and diameter of 19 nm. The MS2 phage, which looks like a nanosphere, has a diameter of 23–27 nm. Fd and M13 phages are nanofiber-shaped with a ~6 nm diameter and ~1 μm length. Filamentous M13 and fd phages have been the most-preferred genetically modified phages since G. P. Smith first introduced the phage display technology in 1985 [59].

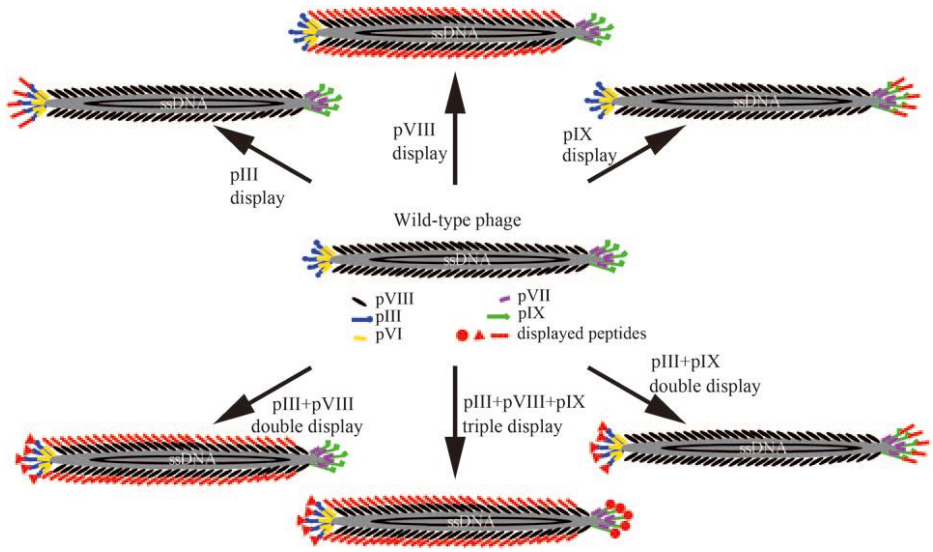

Figure 2. Structure of filamentous phage (M13 or fd) and the genetically engineered version. The phage DNA is encased in a capside made of four minor coat proteins (pIII, pIX, pVI, and pVII) located at one of the two distal ends of the phage and one major coat protein (pVIII), several thousand copies of which constitute the side wall of the phage. The landscape phaeg library was pioneered by V. A. Petrenko and G. P. Smith (adapted from reference [66]).

Of the 5 types of structural proteins that surround the internal single-strand DNA of the phages, genetic engineering techniques for the pIII and pVIII proteins have been reported most frequently, and two or more proteins can be genetically engineered simultaneously (Figure 2). For example, foreign peptides or proteins can be expressed in a certain structural protein by inserting the desired DNA sequence

in the gene of a phage vector. The yield of the structural protein with multiple copies is determined by the size and folding level of the expressed peptide; in general, a small peptide gives better expression than a large peptide.

As the filamentous phages are themselves nanoparticles, much attention has been paid not only for their sensing applications in terms of function and shape, but also as templates for nanostructure synthesis. They have been used as chemical and biological sensors [61] in a form that integrates the inherent target-recognition function of phages with the conventional methods of quartz crystal microbalance [62-64], ELISA [65-67], and optical [68, 69] and electrochemical methods [70, 71]. To use phages as a template to introduce metals or metal oxides, a nucleation site or affinity is needed; different combinations have been reported using phage display (PD) and cell-surface display (CSD) [72]. A. M. Belcher *et al.* at Massachusetts Institute of Technology conduct active research on the application of phages as a template. They reported the potential use of phage-templated nanowires as electrodes for lithium-ion batteries in their representative study published in Science in 2006 [73], with the nanowires made by expressing cobalt- and gold-nucleating motifs on phage body. J. N. Cha *et al.* detected surface-enhanced Raman spectroscopy signals after binding DNA-Raman-active nanoparticles to phages and loading the phages on silica microbeads [74]. K. T. Nam *et al.* successfully detected prostate-specific antigens using virus-probes, which were made by expressing the gold-binding peptide sequence on the phage body, integrating gold nanocubes, and immobilizing them on magnetic microbeads [75].

1.5 Purpose of this work

The major purpose of the current research was to develop a biocompatible and bio-inspired biosensor with high potential to be used for the improved analyte-solid surface interactions. In this work, we will focus on demonstrating the feasibility of our phage-decorated three-dimensional suspension array system using cardiac marker proteins, cardiac troponin I (cTnI) and myoglobin. While many assay systems based on microbeads lack quantitative mode of action, our virus-gold microshells clearly show the capability of quantitative assay.

2. Introduction

Recent outbreak of virus-based hybrid materials has enabled realization of highly selective and sensitive biosensors [58]. The benefits of the merger between virions and biosensing materials intuitively originate from the virion's capability of molecular recognition [76-80] and innate physical properties that stem from the phenotypic morphologies [81-88]. However, despite the functional advances in biosensors using virus hybrids, the detection systems largely remain in two-dimensional planar platforms, requiring relatively large sample volumes and greater time for analysis [58].

In this work, we demonstrate enhanced detection of protein biomarkers using gold-layered magnetic microspheres on which viral filaments are tethered in orientation-controlled manner. The magnetic gold microspheres, like many other typical microspheres, are compatible with flow cytometers, fluorescence activated cell sorting (FACS) systems, and conventional fluorescence microscopes, requiring minute sample volumes, and allowing statistical analysis that raises credibility [89]. Importantly, in contrast to nanoparticles, the gold microspheres are eligible for the detection of small molecule biomarkers in serum.

In biosensor development for immunoassays, preventing non-specific adsorption while providing high antibody loading is of primary importance. Since we had been experiencing a heavy non-specific binding to typical polymer beads

when using blood or serum samples, we envisioned that covering the porous and sticky surfaces of the polymer beads with gold and thiol self-assembled monolayers (SAMs) should resolve the adsorption problem. The SAM molecules, if properly chosen, are able to prevent non-specific interactions between gold surface and analytes as well as to provide functional groups for protein conjugation [90-92].

Filamentous bacteriophages, such as fd and M13, have nanostructured morphologies with contour length of ~ 1 μm and diameter of ~ 7 nm [93].

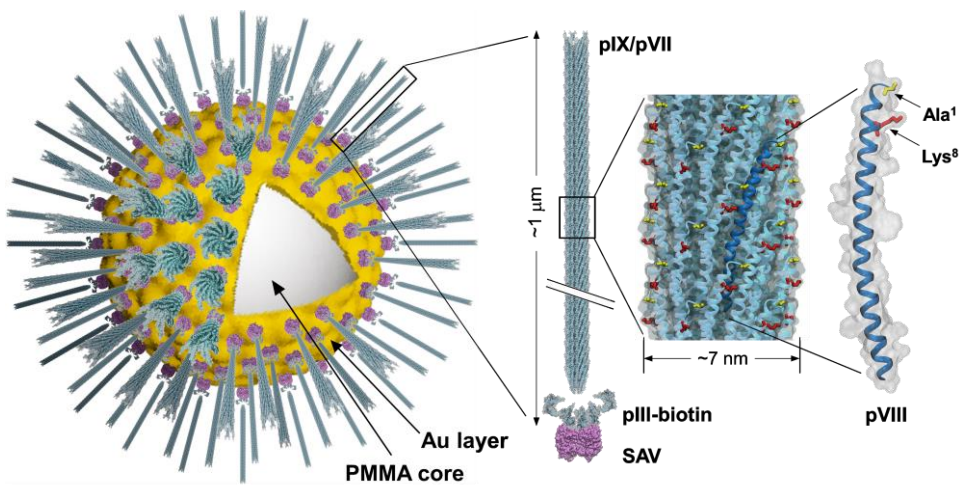

Scheme 1[i]. Schematic representation of the bioinspired virus-gold microsphere. A thin gold layer allows facile surface modifications by thiol SAMs followed by chemical conjugation of functional proteins, such as streptavidin (streptavidin,

[i] Dr. Inseong Hwang contributed to this scheme.

purple). The streptavidin-modified microspheres are decorated with pIII-biotinylated phage virions (pale blue) that have filamentous structure, resembling the surface morphology of some cells. The surface-exposed amine groups of N-terminal Ala-1 (yellow stick) and Lys-8 (red stick) of the viral major coat proteins (blue for a single pVIII unit) are used for the Staudinger ligation with primary antibodies to yield microspheres covered with high-density antibodies. Protein figures were generated using VMD [94] based on PDB code 1IFJ.

The viruses are comprised of five different kinds of structural proteins (pIII, pVI, pVII, pVIII, and pIX) that encase a single-stranded viral DNA. Among them, more than 2700 copies of the major coat protein pVIII serve for the assembly of filamentous structure with their ε-amino groups of Lys-8 and α-amino groups of N-termini being exposed, each of which have been successfully modified with macromolecules using chemical conjugation [80, 95-97]. A minor coat protein pIII, three to five copies per virion, has been dominantly used for the display of peptides and proteins (Scheme 1) [55].

The filamentous morphology of the filamentous (fd) virus provides unique opportunity to construct bioinspired architectures because the virus has similar structural dimensions to many cellular threadlike structures that leverage various cellular functions. Furthermore, in biorecognition processes, such as ligand-receptor interactions, longer and flexible tethers and polyvalency have proved to be beneficial

[98-101]. Indeed, in biological systems, neuronal cells are rich in neurites and filopodia that maximize the cellular interactions by forming synapses [102]. Leukocytes, macrophages, and some epithelial cells are covered with microvilli that facilitate cellular movement, adhesion, endocytosis, and exocytosis [103]. Similarly, some bacterial cells represent pili that help cell–cell interactions essential for mating; others have fimbriae that aid adhesion [104, 105]. Based on these observations, we reasoned that the surface of gold microspheres, once modified with nanostructured filamentous virions, would have greater surface to volume ratio, mimicking biological architectures and thus allowing high degree of conjugation with functional molecules, such as antibodies. Such an increased ratio of antibody to biomarkers, together with three-dimensional gold-SAM protected surface of microspheres and microvilli-like long virus tethers, would provide improved performance compared to conventional 2D or 3D detection systems.

3. Experimental methods

3.1. Reagents

Sulfo-N-hydroxysulfosuccinimide (Sulfo-NHS), sulfo-NHS-phosphine, NHS-PEG_{12}-azide, Streptavidin-coupled Dynabeads Myone T1 and 1-ethyl-3-[3-dimethylaminopropyl] carbodiimide hydrochloride (EDC) were purchased from Thermo Scientific (Rockford, IL). Carboxyl-terminated hexa(ethylene glycol) undecane thiol (CMT002) was obtained from Nanoscience Instruments (Phoenix, AZ). Biotin-terminated daca(ethylene glycon) ethane thiol (41156-1095) was purchased from Polypure (Oslo, Norway). Carbenicillin (Carb) and isopropyl β -D-1-thiogalactopyranoside (IPTG) were from Gold Biotechnology (St. Louis, MO). Streptavidin (SAV), bovine serum albumin (BSA), tetracycline (Tet), Tween-20, adenosine 5′-triphosphate (ATP), and cardiac troponin I (cTnI) were purchased from Sigma-Aldrich (St. Louis, MO). Plasmid pET21a-BirA was obtained from Addgene (Cambridge, MA). Magnetic gold microspheres (M-NG0501, Nomadien.com) were generated using proprietary methods including electroless plating of auric acids on proprietary magnetic poly(methyl methacrylate) (PMMA) beads (Nomadien.com) that were 15 μm in diameter. Nominal 10 μm diameter carboxylated polystyrene (PS) beads were from Polysciences (Warrington, PA). Phage vector, fd-tet with Sfi I and Not I cloning site in front of pIII, was kindly provided by Drs. Philipp Holliger and Chang-Hoon Nam. Rabbit polyclonal anti-fd (ab6188) and anti-cTnI (ab47003)

antibodies were purchased from Abcam (Cambridge, MA). Mouse monoclonal anti-cTnI antibody [19C7] was from GeneTex (Irvine, CA). Chicken Alexa Fluor 594 anti-mouse antibody (A21201), goat Alexa Fluor 610-R-Phycoerythrin (PE) anti-rabbit antibody, Alexa Fluor 594 biocytin, streptavidin conjugated with horseradish peroxidase (streptavidin-HRP), biotin, and bacterial cell lines for protein expression and phage amplification were obtained from Invitrogen (Carlsbad, CA). Myoglobin, rabbit polyclonal anti-myoglobin antibody (70-MR13), and mouse monoclonal anti-myoglobin antibody (10-M50A) were from Fitzgerald (North Acton, MA).

3.2. Fluorescence microscopy

Gold microspheres (~ 500) in phosphate buffered saline (PBS, 5 μL) were spotted on a glass slide. The fluorescence was monitored using Nikon Ti-E (Nikon, Japan) equipped with zyla sCMOS camera (Andor, Northern Ireland). At least thirty microspheres were chosen for the determination of mean fluorescence intensity (MFI) using NIS-Elements software version 4.2 (Nikon, Japan).

3.3. Field-Emission Scanning Electron Microscopy (FE-SEM)

The surface morphology of gold microspheres on a carbon tape was monitored using JSM 5410LV (JEOL, Japan) with 2 kV of acceleration voltage at the National Instrumentation Center for Environmental Management (NICEM), Seoul National University. To monitor the surface morphology of gold microspheres modified with

thiol SAM, streptavidin, and phage virions, Pt was sputtered using BAL-TEC SCD 005 sputter coater at 15 mA for 100 s.

3.4. N-SIM super resolution microscopy

Fd-tet-APpIII phage virions on streptavidin coated microspheres were detected using rabbio anti-fd antibody and anti-rabbit alexa Fluor 488 antibody. Phage decorated microspheres in PBS (5 μm) were spotted on a glass slide. The fluorescence was monitored using N-SIM super resolution microscope (Nikon, Japan) at the Boimedical Imaging Center (BIM) of Seoul National University.

3.5. Production of BirA

His-tagged BirA was prepared according to the provider's protocol with conditional modifications. Briefly, the pET21a- BirA plasmid was transformed into E. coli BL21(DE3)pLysS, plated on lysogeny broth (LB)-agar with Carb (100 μg/mL). A single colony was inoculated into LB-Carb media and was grown until the cell density reached mid-log phase when IPTG (1.0 mM) was added for induction. After overnight incubation at 37 ℃, the cells were harvested, broken by sonication, and centrifuged. The supernatant was loaded onto Co-NTA column to purify His-tagged BirA. Typically, a small-scale pilot test was performed using seven individual colonies when the best-expressing colony was used for the large-scale enzyme preparation.

3.6. Production of phages carrying biotinylation motif

The two primers, AP-F (5′-CGG CCA TGG CAG GTC TGA ACG ACA TCT TCG AGG CTC AGA AAA TCG AAT GGC ACG AAG GCT CCG GTG C-3′) and AP-R (5′- GGC CGC ACC GGA GCC TTC GTG CCA TTC GAT TTT CTG AGC CTC GAA GAT GTC GTT CAG ACC TGC CAT GGC CGG CT-3′), were annealed and ligated with fd-tet phage vector that had been digested with Sfi I and Not I. After the verification of the ligation by DNA sequencing, the phage vector was transformed into *E. coli* TG1 and grown in LB agar plate containing Tet (40 μg/mL) for 16 h at 37 ℃, the Next morning, a single colony was picked and inoculated into 3 mL of NZY liquid media with Tet (20 μg/mL) as a starter culture. For large-scale phage preparation, the starter culture was inoculated into NZY-Tet media (400 mL) and grown for 16 h at 37 ℃ with vigorous shaking. Phages were then purified by polyethylene glycol (PEG)/NaCl precipitation according to the standard protocols.

3.7. Biotinylation of phages

The purified phage virions (10^{13}) were incubated with BirA (30 nM), biotin (100 μM), and ATP (1 mM) in PBS-Mg (0.5 mL, pH 7.4 with 5 mM $MgCl_2$) for 2 h at 37 ℃. The phages were then precipitated by PEG/NaCl two times and the residual PEG/NaCl molecules were removed by buffer exchange using Centricon (MWCO = 100 kDa). The level of biotinylation was evaluated by western blot using streptavidin-HRP.

3.8. Surface modifications of gold microspheres

Gold microspheres (1 mg) was rotary incubated with thiol SAM molecules (1 mM) in 0.5 mL of ethanol for 16 h at 25℃. To the SAM-modified gold microspheres (5 μg) was added EDC (2 mM) and NHS (5 mM) in 0.5 mL of MES buffer, pH 5.0 for 30 min at 25 ℃. The beads were then washed with PBS (1 mL, pH 7.4) three times, followed by the addition of streptavidin (0.5 mg) in PBS (50 μL). The streptavidin-modified microspheres were treated with PBS-BT (PBS with 1% BSA, 0.1% Tween-20, pH 7.4) for 30 min and the streptavidin loading was verified using biocytin-Alexa Fluor 594.

3.9. Optimization of phage loading onto gold microspheres

A range of biotinylated phage virions were rotary incubated with streptavidin-modified gold microspheres (5 μg) in PBS-BT (50 μL) for 16 h at 25 ℃. As a negative control, wild-type fd-tet virions were used. After washing three times with PBS, the beads were treated with anti-fd rabbit IgG (37 ng) in PBS (50 μL) for 1 h at 25 ℃. After washing, the loading of phage virions were visualized by incubating with anti-rabbit Alexa Fluor 610-R-PE antibody (100 ng) in PBS (50 μL) for 1 h at 25 ℃, followed by the monitoring with a fluorescence microscope.

3.10. Optimization of staudinger ligation

Streptavidin-modified beads (5 μg) were incubated with varying amount of sulfo-

NHS-phosphine in PBS (0.5 mL) for 1 h at 25 ℃, which were used as a positive control. To build virus-immobilized beads, the streptavidin-modified beads were further incubated with 1.0×10^{10} of biotinylated phages in PBS-BT (50 μL) for 16 h at 25 ℃, washed three times with PBS-BT and three times with PBS, followed by an incubation with a range of Sulfo-NHS-Phosphine in PBS (0.5 mL) for 1 h at 25 ℃. For the Staudinger ligation, primary antibody from mouse (100 μg) was incubated with NHS-PEG_{12}-azide (0.1 and 1.0 mM) in of PBS (0.1 mL) for 1 h at 25 ℃, followed by overnight dialysis against PBS. The phosphine-treated streptavidin- and virus-gold microspheres (5 μg) were ligated with the azide-modified mouse antibody (0.5 μg) in PBS for 4 h at 37 ℃. The resulting beads were then washed three times with PBS-BT, followed by the incubation with anti-mouse Alexa Fluor 594 antibody for the fluorescence microscopic analysis. As a negative control, anti-mouse Alexa Fluor 594 antibody was directly treated with streptavidin- and virus-beads without azide-modified antibody and the background signals, if any, were subtracted.

3.11. Cardiac marker assays

Initially, the streptavidin- and virus-gold microspheres (5 μg) were treated with sulfo-NHS-phosphine (0.5 mM) in PBS (0.5 mL) for 1 h at 25 ℃, followed by the ligation with rabbit polyclonal anti-cTnI capture antibodies (0.5 μg) that had been incubated with NHS-PEG_{12}-azide (100 μM) in PBS (50 μL) for 4 h at 37 ℃. The resulting beads were then washed three times with PBS-BT and were mixed with cTnI (0.02, 0.2, 2, and 10 ng/mL) or myoglobin (0.02, 0.2, 2, 10, 40, and 100 ng/mL)

in PBS (0.5 mL) for 1 h at 25 ℃. For the detection of cTnI in human serum, PBS was replaced with cTnI-spiked human serum (0.02, 0.2, 2, and 10 ng/mL in 0.5 mL). The beads were then washed, incubated with mouse monoclonal anti-cTnI detection antibody [19C7] in PBS (500 ng, 50 μL) for 1 hr at 25 ℃, and visualized with anti-mouse Alexa Fluor 594 antibody (500 ng). For the determination of background signals, the assay was performed using the same conditions without marker proteins.

4. Results and Discussion

4.1. Characterization of magnetic gold microshells

Beads that are used in suspension arrays for bio-analysis are of low density and most of them use polymer microspheres, which are amenable to surface modification. However, these beads are not free from non-specific adsorption, which is a problem not only because it leads to adsorption of non-specific species into the microsphere surface, but also because of the introduction of these species into the polymer microsphere core. Therefore, in this study, we used gold microshells from Nomadien Corp. (www.nomadien.com), which consist of a thin gold layer that forms a metal barrier that blocks contact between the polymer core and external solution fundamentally while easily facilitating surface modification. Iron oxide was introduced into the poly(methyl methacrylate) (PMMA) surface to make the beads magnetic, and finally a gold layer was added using electroless plating (Figure 3a). The gold layer was approximately 200 nm thick, as verified by TEM (Figure. 3c), and its density was 2.64 g/mL.

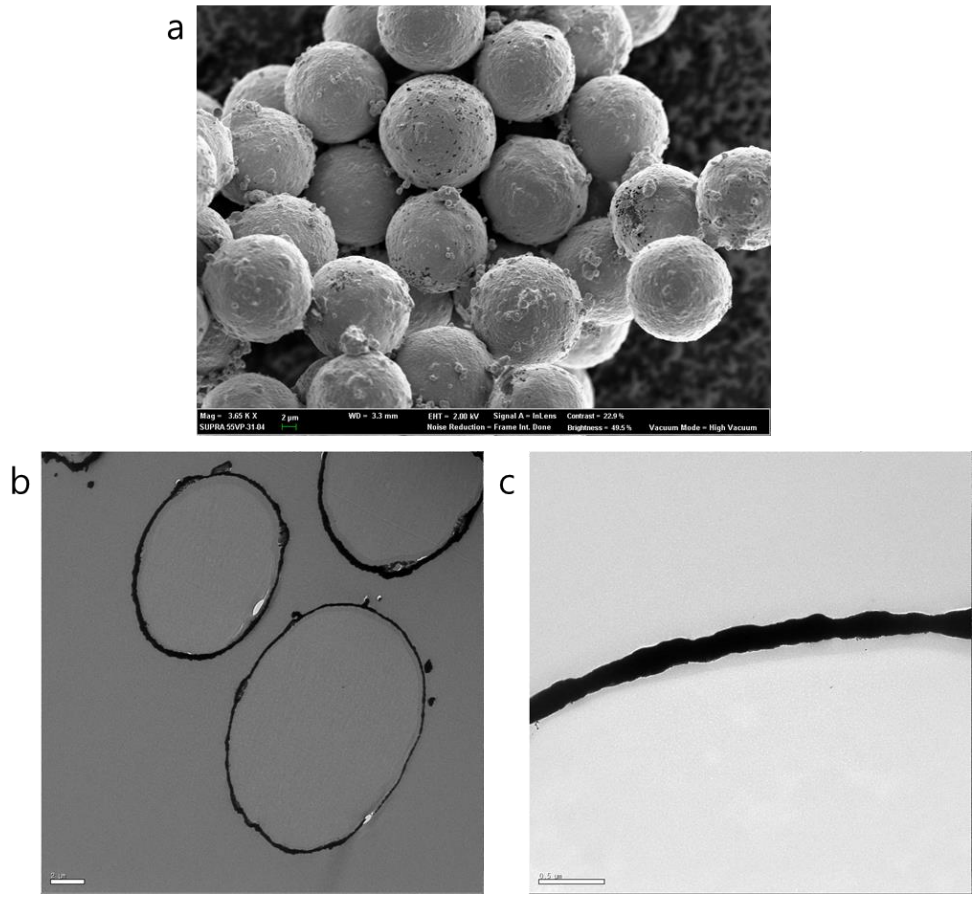

Figure 3. (a) SEM image of iron oxide embedded 15 μm magnetic gold microshells. TEM images of magnetic gold microshells (b) and (c). As shown in (c), the thin gold layer was less than 200 nm thick.

4.1.1. Testing the physical and chemical stability of gold microshells

To measure the physical and chemical stability of the gold microshells, a 5 μg gold microshell was added to ethanol, dimethyl sulfoxide, N,N-dimethylformamide or 1,4-dioxane solution. This was followed by sonication for 30 minutes and incubation for a further 15 hours.

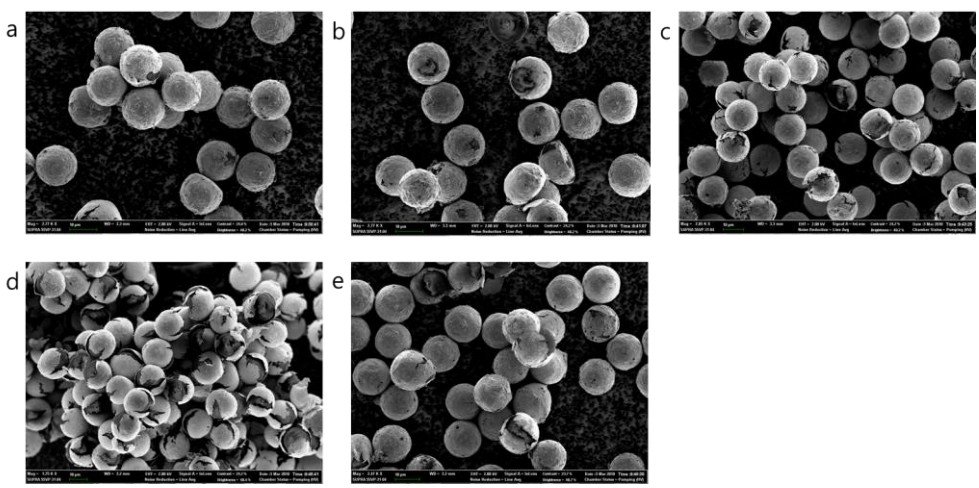

Figure 4. Solvent test of gold microspheres. SEM images of gold microshells that were put into (a) PBS buffer, (b) ethanol, (c) dimethyl sulfoxide, (d) N,N-dimethylformamide, or (e) 1,4-dioxane, followed by 30 minutes of sonication and a 16 h incubation at 25 ℃.

As shown in Figure 4, separation of the gold layer was observed as a swelling of the polymer microsphere in the organic solution. Separation of the gold layer was also observed when sonication was performed for more than 30 min. We did not observe cracking of the gold layer in the water and ethanol solution (Figure 4a-b). Thus, we confirmed that the gold layer is stable in an ethanol solution and remain stables even after up to three minutes of sonication.

Next, we prepared SAM-protected gold microspheres using carboxyl-terminated hexa(ethylene glycol) undecane thiol, followed by protein conjugation using 1-ethyl-3-(3-dimethylaminopropyl)-1-carbodiimide hydrochloride (EDC) and N-hydroxysuccinimide (NHS). The gold-layered microspheres were stable in ethanol for 16 h, enough time for SAM formation. The bead system facilitated chemical conjugation of protein on the SAM-modified gold microspheres using EDC-NHS in that the unreacted excessive EDC and NHS could be easily washed out. When gold microshell powder was added to the solution, the gold-gold affinity increased, resulting in aggregation (Figure 5a). However, because the SAM-protected gold microshells have a high affinity for gold-thiol, they formed single beads (Figure 5b). The SAM-protected gold microshells were well dispersed in the solution (Figure 5c) and could be collected using a magnet after 30 seconds (Figure 6d).

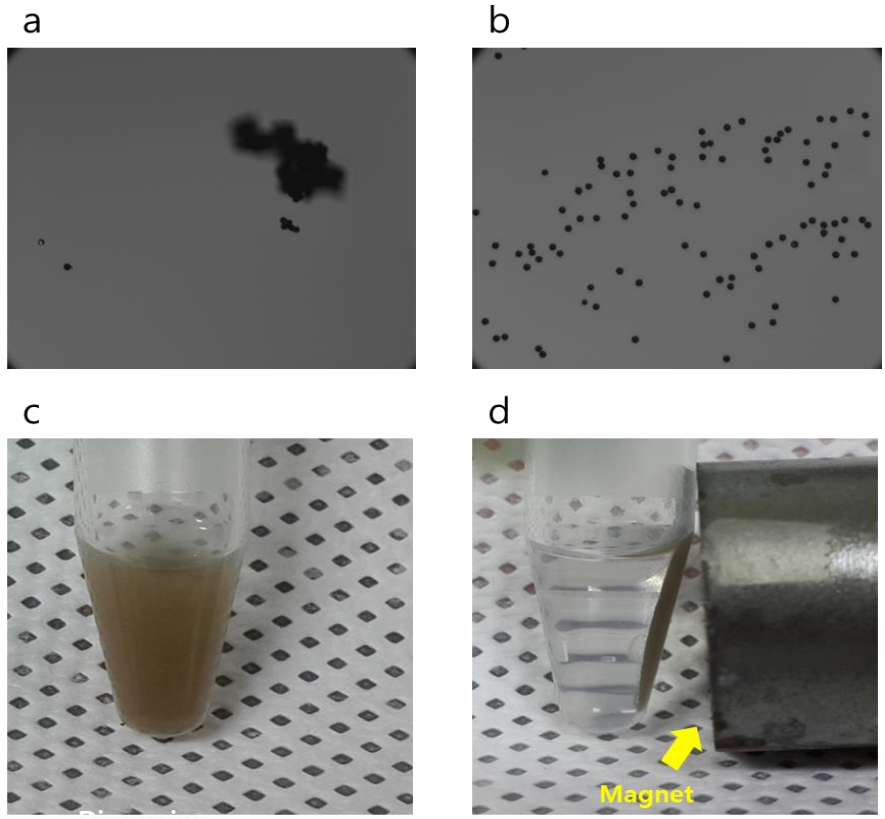

Figure 5. (a) Optical image of the gold microshell before the SAMs were formed (b) Optical image of the gold microshell after the SAMs were formed (c) Dispersion state in the solution after the SAMs were formed (d) Image at 30 seconds after a magnet was placed beside the tube.

To investigate the effect of temperature on SAM formation, SAM-modified gold microshells were incubated for 24 hours at either 4 ℃ or 25 ℃ and then

incubated with Alexa 594 conjugated biocytin at 4 ℃, 25 ℃ or 40 ℃. As shown in Figure 6, the fluorescence values for all samples were not significantly different within the error range. This result indicates that there was no desorption of SAM molecules at either 4 ℃ or 25 ℃ and there was no effect of temperature on streptavidin and biocytin-Alexa 594.

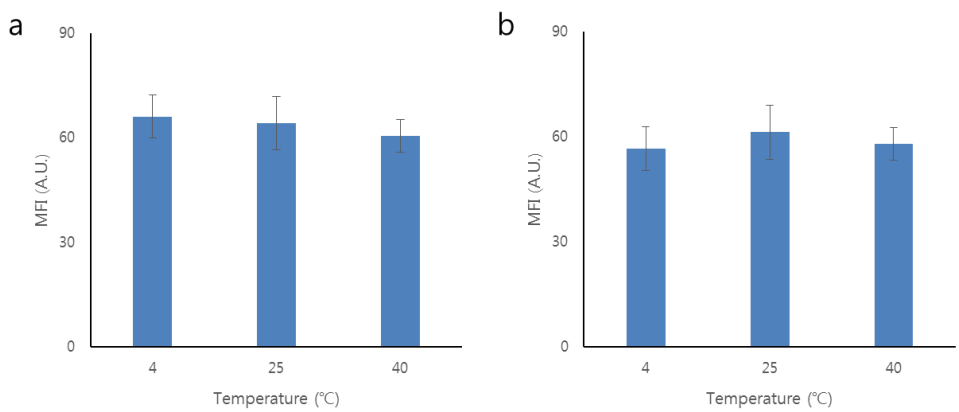

Figure 6. Verification of the stability of SAM-modified gold microshells. SAM-protected gold microshells were incubated in phosphate-buffered saline (PBS) buffer at (a) 4 ℃ or (b) 25 ℃ for 24 hours. Each of (a) and (b) samples was incubated at 4 ℃ , 25 ℃ , 40 ℃ for 24 hours and then treated with streptavidin and biocytin-alexa594 for 1 hour at 25 ℃ to observe fluorescence. Biocytin-Alexa Fluor 594 dye was used for the determination of mean fluorescence intensity (MFI).

4.1.2. Protein immobilization of gold microshells

Having verified the stability of the thiol SAMs-treated gold microshells, we wanted to determine whether the protein could be incorporated into them. After activating the carboxyl-terminated gold microshells using EDC/NHS, the primary antibody was covalently attached and fluorescence was observed using an alexa488 conjugated secondary antibody (Figure 8a). As shown in Figure 7c, green fluorescence was observed on the gold microshells, indicating that the protein had successfully attached.

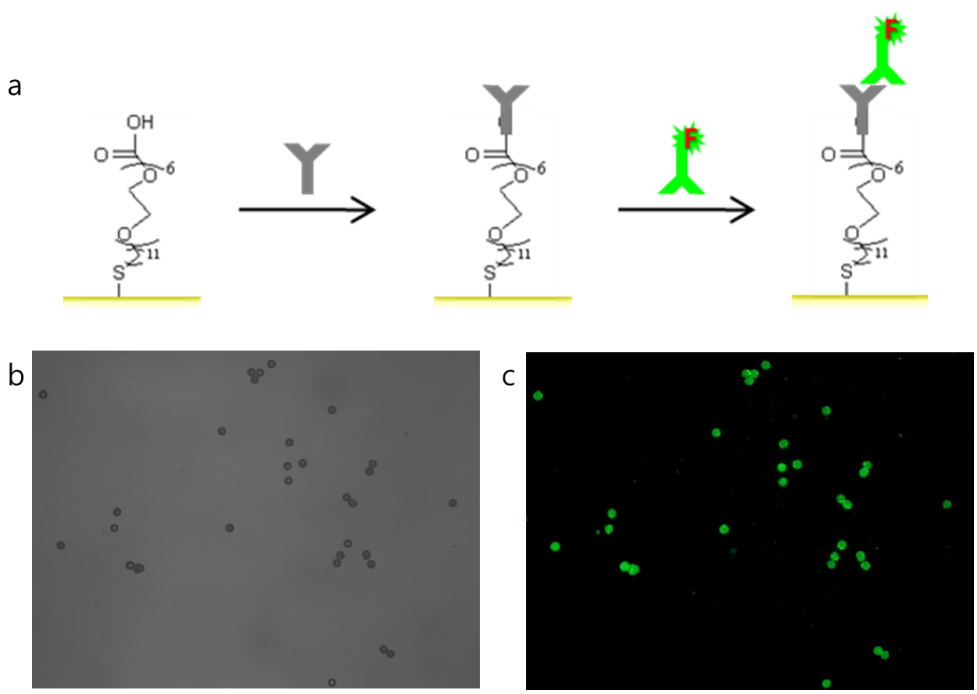

Figure 7. (a) Schematic representation of antibody immobilization on carboxyl-

terminated gold microshells. After the primary antibody was attached to the surface of the gold microshells using EDC/NHS, the reaction was observed via fluorescence with an alexa488 conjugated secondary antibody. (b) DIC image. (c) Fluorescence image.

To optimize protein immobilization on the gold microshells, we tested different numbers of gold microshells, antibody concentrations, working volumes, and reaction times. Full-length IgG antibodies have a molecular weight of 150 kDa and a size of 3 nm × 15 nm × 15 nm, and we assumed their area as 2 nm × 4 nm. Given the three-dimensional curvature of the microspheres, the degree of freedom of polyethylene glycol and the size of a single chain fixed at the surface, we estimated that 5 μg of 15 μm sized gold microshells would require 24 ng of antibody. The following conditions were fixed: 5 μg gold microshells, 500 μL working volume, 1 h reaction time, and 2 μg secondary antibody. Only the amount of primary antibody was changed, and the degree of protein attachment was determined by the level of fluorescence (Figure 8a). A fluorescence value for the ratio of experimental value to theoretical value of the antibody was determined (Figure 8c), and with the use of approximately more than 20 times the amount of antibody, saturated fluorescence was found such that 500 ng used with 5 μg of gold microshells was sufficient. Thus, results from this experiment indicate that when proteins were fixed and secondary antibody was used, 0.5 μg of protein was used in 5 μg gold microshells.

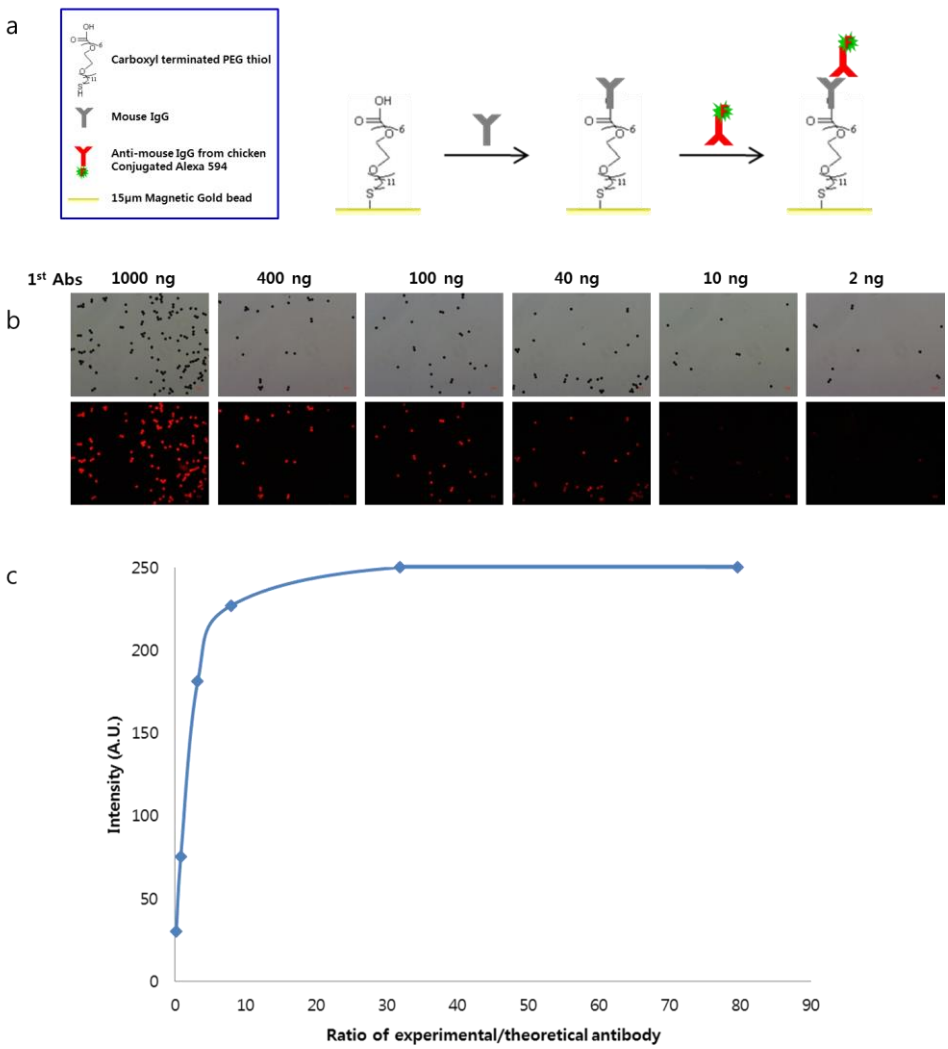

Figure 8. Optimization of antibody loading on gold microshells. (a) Schematic representation of antibody immobilization on thiol SAM-decorated gold microshells. (b) DIC and fluorescence images with different amounts of primary antibody, and a fixed amount of secondary antibody. (c) Fluorescence intensity according to the ratio of experimental to theoretical antibody.

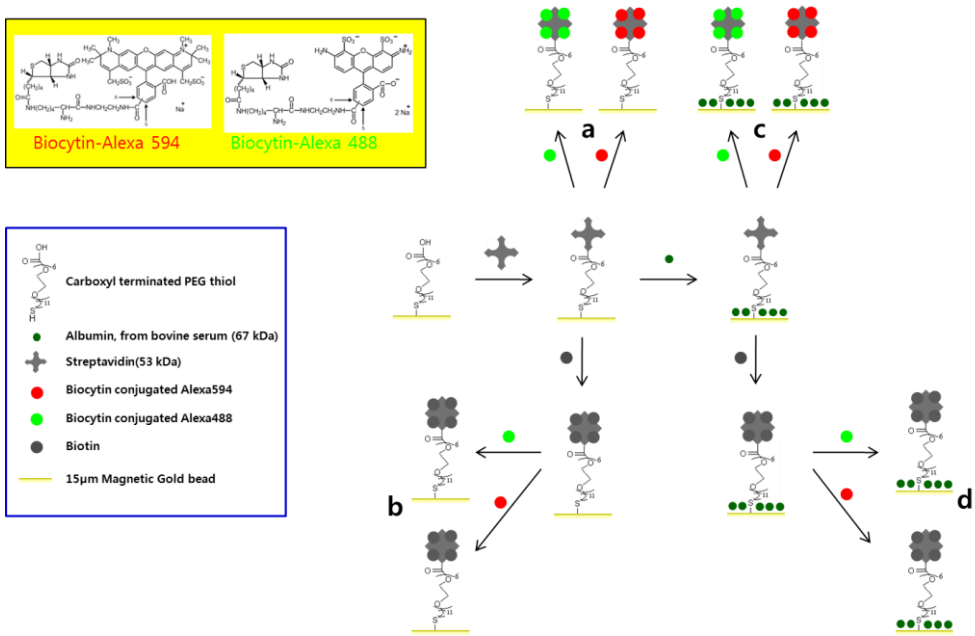

Scheme 2. Schematic representation of streptavidin immobilization on gold microshells to determine the quenching effect. (b) and (d) are a control experiment after pretreatment with free biotin. (a) and (b) are pretreatments without albumin.

Next, we evaluated streptavidin conjugation using biocytin-Alexa Fluor 594 and biocytin-Alexa Fluor 488 (Scheme 2). When the beads were pre-treated with free biotin, no fluorescence was observed after incubation with fluorescent biocytin (Figure 9b and d). In contrast, we observed strong fluorescence signals when the beads were directly incubated with the fluorescent biocytin (Figure 9 Lower panel a, c). Unexpectedly, no green fluorescence was observed following incubation with

biocytin-Alexa Fluor488 (Figure 9 Upper panels a, c). This could be because the green fluorescence was quenched by the gold because there is some overlap between the maximum absorption wavelength of the absorption spectrum in the gold visible light region and the green region. Thus, we repeated the experiments only using red based fluorescence (biocytin-Alexa 594) and were able to observe fluorescence on the beads (Figure 9). In addition, in bio-analysis experiments, and in particular those involving blood, it is possible that proteins in the serum, such as albumin, could be a problem when using the polymer microspheres. However, we showed that there was no significant difference in fluorescence values following pretreatment with albumin (Figure 9a and c, lower panel).

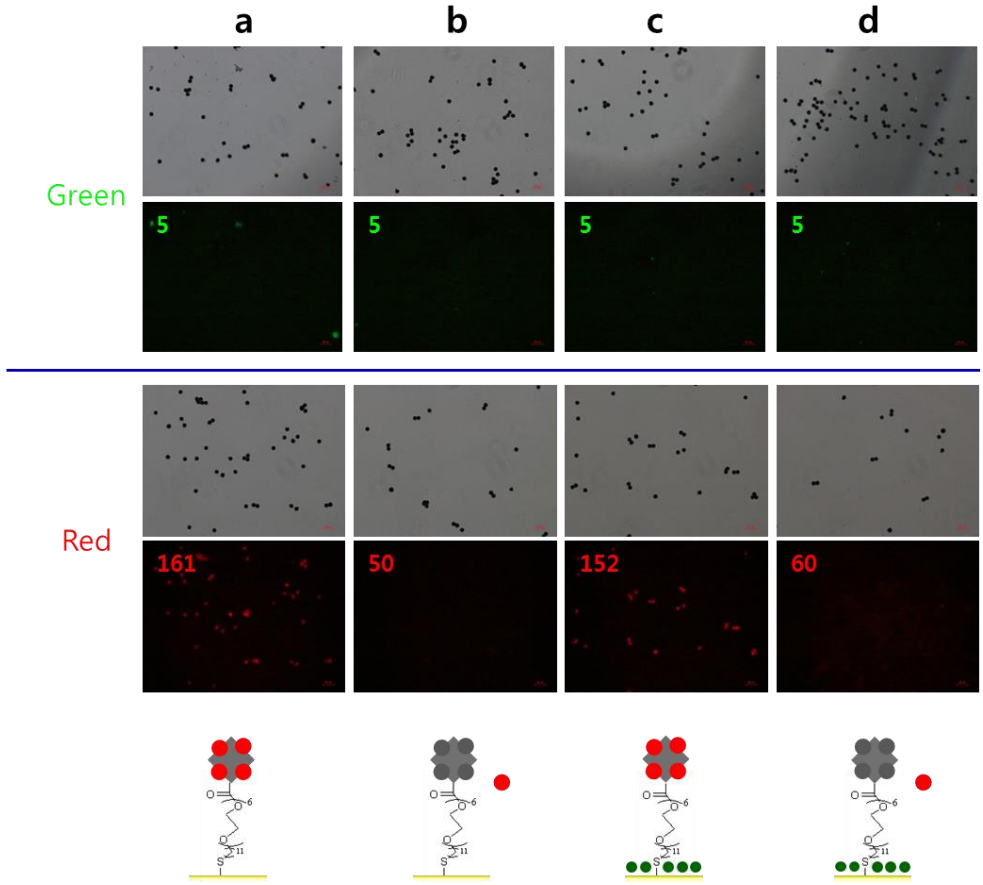

Figure 9. Results of streptavidin immobilization on gold microshells. In (a) and (c), experiments using biocytin-Alexa 488 (upper panels) did not show fluorescence due to quenching whereas biocytin-Alexa 594 (lower panels) showed strong fluorescence. (b) and (d) indicate pretreatments with free biotin, and no fluorescence was observed.

4.1.3. Sandwich immunoassay of antibody-decorated gold microshells

Using antibody-decorated gold microshells fixed directly with SAM molecules, a spike test of cardiac troponin I was conducted in human serum. A polyclonal antibody was covalently attached to the gold microshell using EDC/NHS and a sandwich-type immunoassay was performed after detecting a biomarker from the human serum (Scheme 3). For the control experiments, a carboxyl-terminated polymer microsphere was used and conditions without a biomarker or without a monoclonal antibody were compared to determine the level of fluorescence caused by non-specific binding.

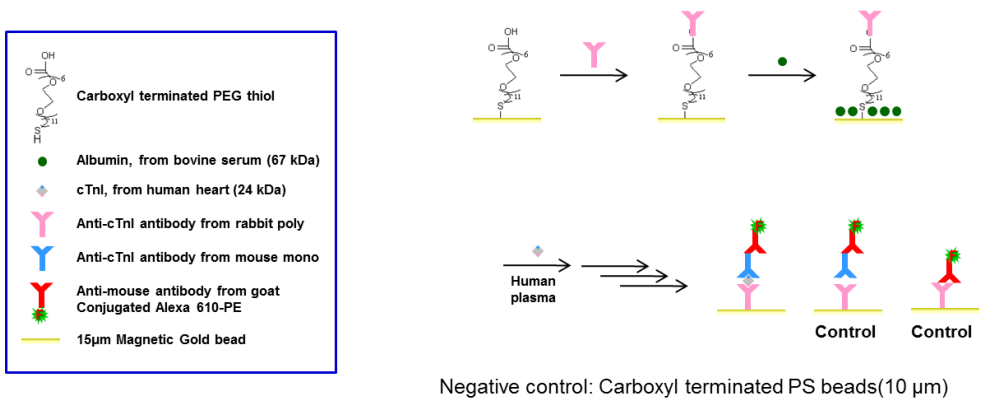

Scheme 3. Schematic representation of the 100 ng/mL cardiac troponin I assay in human serum.

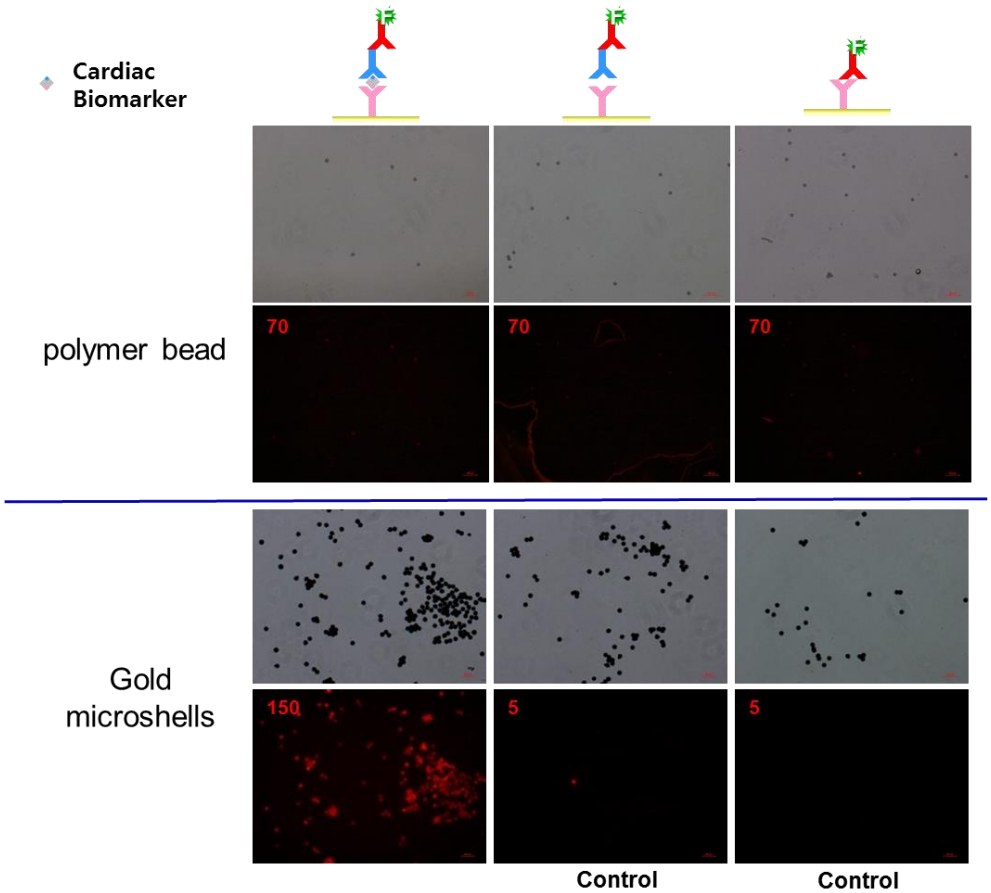

Figure 10. Detection of cardiac troponin I in human serum.

We verified that the mean fluorescence intensity (MFI) was approximately 150 for the gold microshells when 100 nm/mL cardiac troponin I was spiked in human serum. For polymer microspheres, high background fluorescence of 70 MFI was measured. This value was similar to that of a control sample in the absence of cardiac troponin I due to non-specific adsorption of secondary antibody. Gold microshells

in the absence of cardiac troponin I had a MFI value of approximately 5, which indicated significantly low non-specific adsorption. We inferred that this was due to the effect of the polyethylene glycol in the thiol SAM molecule and a thin gold layer that forms a metal barrier and blocks contact with the polymer core. Our colleague, S. R. Kwon, discovered how to prevent non-specific adsorption effectively using the same magnetic gold microshell and PEG-thiol SAM molecules that we used through MALDI analysis [106]. S. R. Kwon *et al*. shows the MALDI-TOF mass spectra for commercial polymer microspheres and for the magnetic gold microshells used in our experiments. A human serum albumin peak of non-specific adsorption was detected at 33 and 66 kDa , but was not detected with magnetic gold microshells. The detection ability of Myoglobin, which is a target biomarker, showed that the magnetic gold microshells had the best result. Based on the above results, polyethylene glycol and the metal barrier are both effective at suppressing non-specific adsorption.

4.2. Preparation and characterization of engineered phage virions

To prepare microshells covered with threadlike nanostructured surface, we employed fd-tet phage virus that has intriguing morphology similar to cellular microvilli-like edifice. A 14-mer bacterial biotin acceptor peptide (AP), GLNDIFEAQKIEWHE [107], was introduced using SfiI and NotI cloning sites in front of pIII of fd-tet (Figure 11) [108].

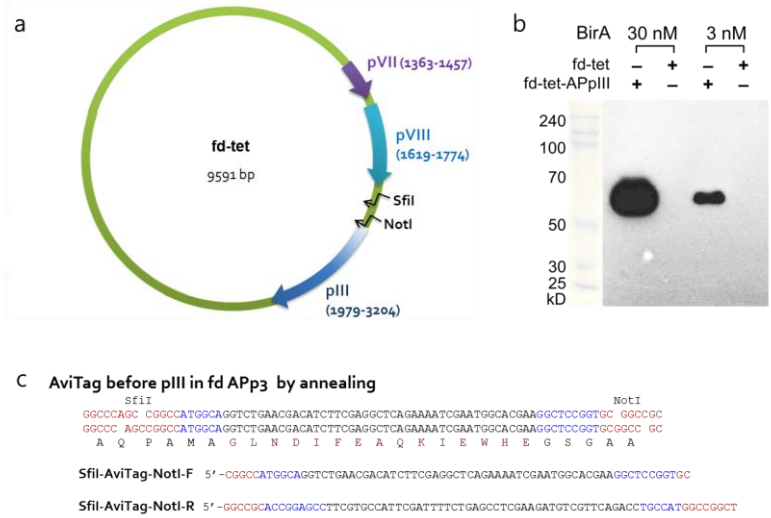

Figure 11. (a) Phage vector map, fd-tet with SfiI and NotI cloning site in front of pIII. (b) Wild-type fd-tet and AP-representing fd-tet-APpIII virions (10^{13}) were treated with BirA, followed by western blot visualized using streptavidin-HRP. (c) The two primer, SfiI-Avitag-NotI-F and SfiI-Avitag-NotI-R, were annealed and ligated with fd-tet phage vector (a) that had been digested with SfiI and NotI.

Since the ε-amino group of Lys, a specific biotinylation site within the AP tag, is vulnerable to chemical modification by NHS for the subsequent Staudinger ligation, we tried in vivo biotinylation of phages by endogenous biotin ligase BirA that recognize AP in bacterial cells [107]. The degree of in vivo biotinylation, however, was minute, making us to purify BirA and biotinylate the virions in vitro

[109]. When we incubated AP-containing phage (fd-tet-APpIII) with BirA, distinct bands (~60 kDa) appeared in a western blot using streptavidin-HRP (Figure 11b) and we were able to successfully visualize negatively stained virions using uranyl acetate (Figure 12).

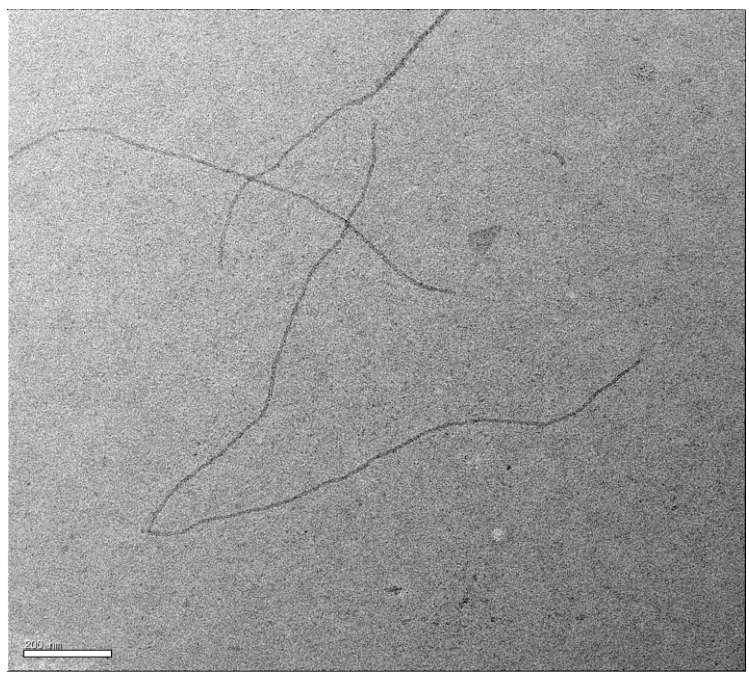

Figure 12. TEM image of PEG/NaCl-purified fd-tet-APpIII phage after 2% uranyl acetate staining. Scale bar = 200 nm.

4.3 Evaluation and optimization of virus-decorated gold microshells

We then briefly evaluated the loading of virions on streptavidin-gold microspheres and found saturated fluorescence signals using 1.0×10^{10} virions and 5 μg of streptavidin-gold microspheres (Figure 13). Given that the apparent diameter of terminal N1-N2 domain of pIII is ~6 nm and the tail part of the fd virus is composed of three to five copies of pIII [110], one virion may be ensconced in an area of ~8.5×10^{-17} - 1.4×10^{-16} m^2. Since 5 μg of gold microspheres corresponds to ~1,000 beads, the total surface area of the beads is ~7×10^{-7} m^2 on which ~$5\text{-}8 \times 10^9$ of virions can be accommodated without gaps in theory.

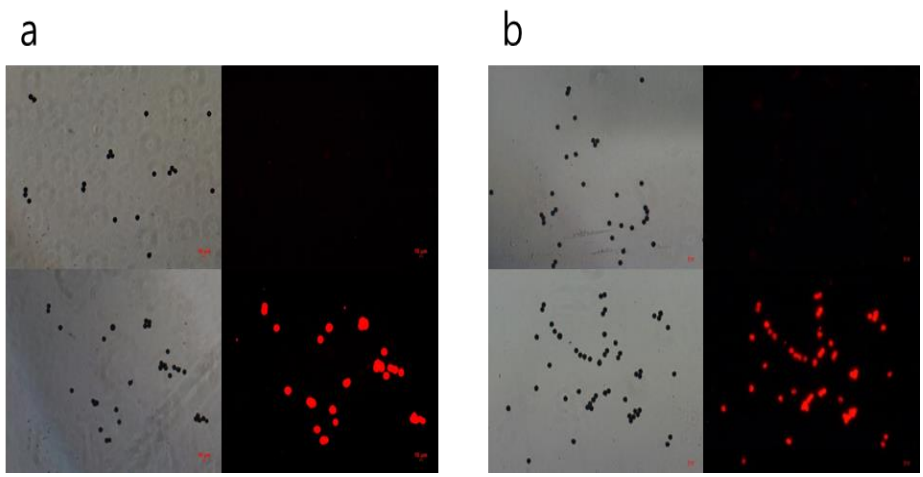

Figure 13. BirA-treated fd-tet (upper panel) and fd-tet-APpIII (lower panel) phage virions (1.0×10^{10}) on streptavidin-SAM gold microspheres were detected using (a) Alexa Fluor® 610 Succinimidyl Esters, (b) rabbit anti-fd antibody and anti-rabbit Alexa Fluor® 610-R-PE antibody.

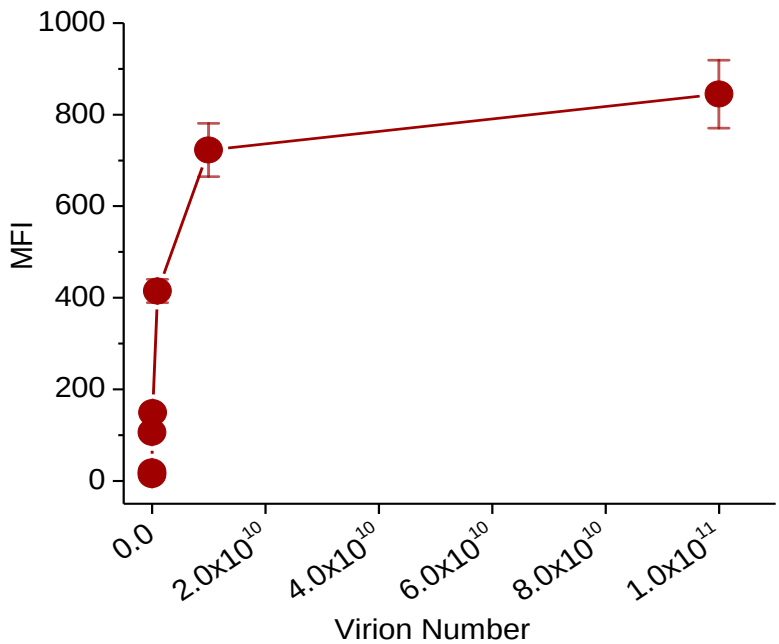

Figure 14. Optimization of surface modifications of gold microspheres with streptavidin and phage virions. Various amount of biotinylated phage virions were used for the titration of virus loading with the same reaction conditions as in Figure 13 (b).

Indeed, when we titrated the loading of virions on the microspheres, the fluorescence intensity began to plateau from 1.0×10^{10} virions near the theoretical value (Figure 14). Thus, we used 1.0×10^{10} virions to maximize antibody loading for subsequent immunoassays, while keeping the efficiency in phage preparation.

4.4 Visualization of virus-decorated gold microshells

We next compared the surfaces of gold microspheres before and after the phage immobilization. Figure 15a and b are the FE-SEM images of bare gold microspheres that reveal gold granules layered on the surface of microspheres. After thiol SAM formation, gold surface maintained the overall roughness similar to the bare gold surface (Figure 15c). By contrast, streptavidin-modified surface exhibited tiny pimples, believed to be Pt-coated streptavidin, added on the gold granular blocks (Figure 15d and Figure 16a). Furthermore, in the case of virus-modified surface, we could clearly identify the virion fibers on the streptavidin layer with the increased thicknesses of 10~15 nm due to the sputtered Pt (Figure 15e and Figure 16b). The virion strands appeared to lie down because of the dry conditions and Pt sputtering required for the FE-SEM operation.

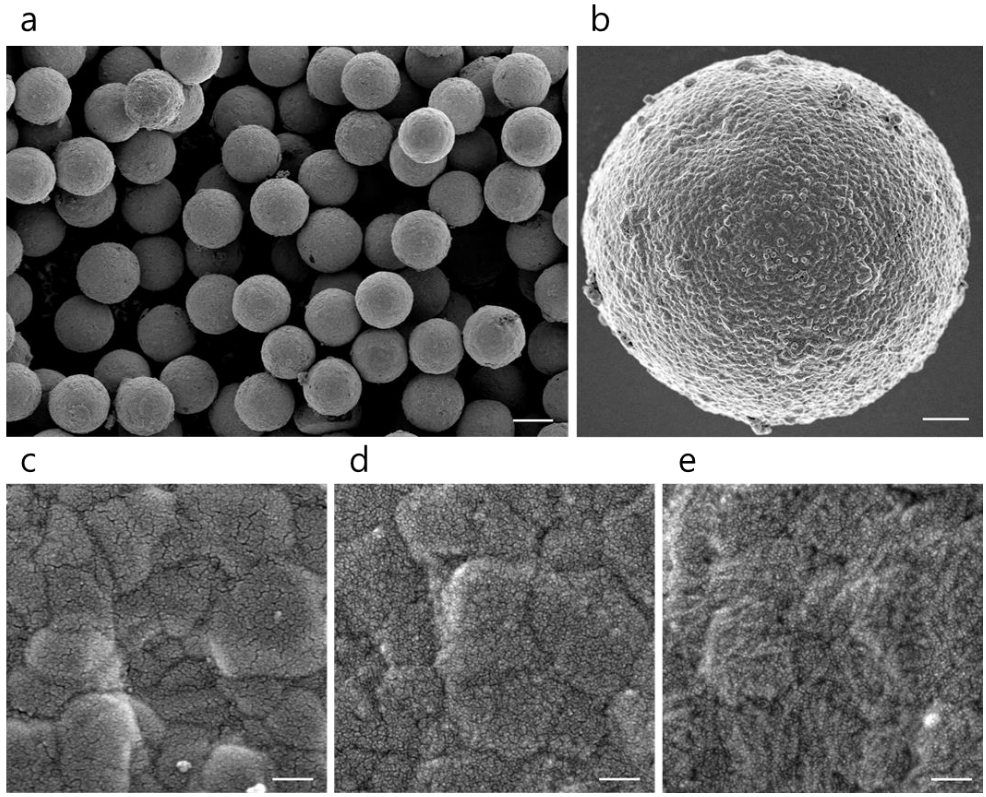

Figure 15. (a) SEM image of bare magnetic gold microspheres (scale bar = 10 μm). (b) Magnified image of gold microspheres reveals the morphology of gold layer (scale bar = 2 μm). Pt-sputtered surface morphology of the beads that had been modified with carboxyl-terminated hexa(ethylene glycol) undecane thiol SAM (c), then conjugated with streptavidin (d), and finally with pIII-biotinylated fd-tet phage virions (e). Scale bars for (c)-(e) = 100 nm.

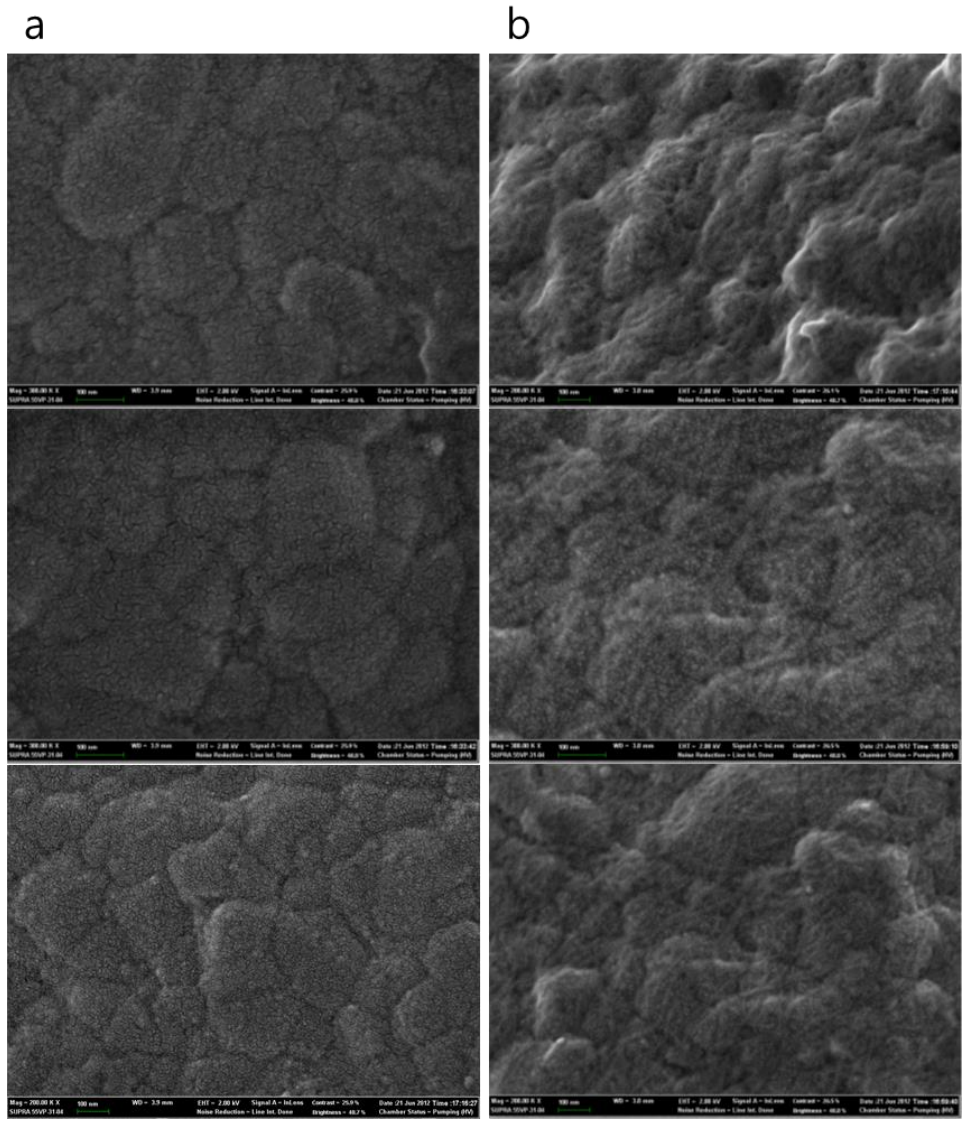

Figure 16. (a) SEM images of independent areas of streptavidin-modified gold microshells with Pt sputtering. (b) SEM images of independent areas of streptavidin-gold-microshells treated with phage virions at various magnifications with Pt sputtering.

The presence of virus on the streptavidin-decorated gold microshells was verified via FE-SEM imaging, however the actual location of the virus in the solution was not known. To determine this, we used Alexa Fluor® 488 Succinimidyl ester, which is an amine-reactive dye and introduced fluorescence to the primary amine of the protein fixed at the bead in order to visualize the location of the virus in the solution. In contrast to streptavidin-coated beads in the absence of virus, the virus-decorated beads were well established within the three-dimensional space (Figure 17). As such, fixation using a virus rather than fixing an antibody directly onto the bead will increase the availability of the antibody and ultimately increase the frequency of ligand-receptor interactions.

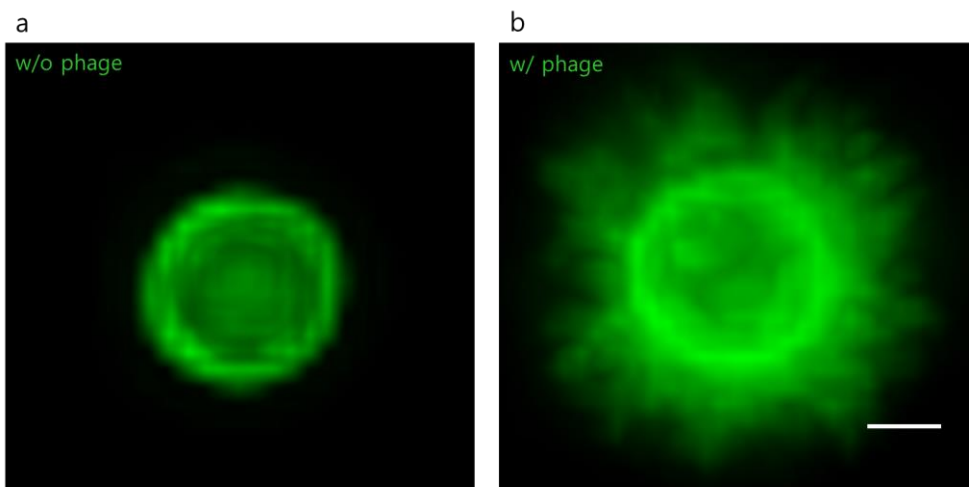

Figure 17. 3D N-SIM super resolution image from a 100 nm Z-stack step size and 0.1 reconstruction factor. w/o phage (a) and w/ phage (b) (scale bar = 1 μm) at 1 μm streptavidin-coated microsphere.

4.5 Optimization of the Staudinger ligation

Staudinger ligation, an extended version of classical Staudinger reaction, has been rediscovered by Saxon and Bertozzi [111]. Among several bioconjugation techniques, the Staudinger ligation has garnered much interest in that it has highly chemoselective and bio-orthogonal conjugation mechanism (Scheme 4). Consequently, the Staudinger ligation has been deployed not only to label glycans, lipids, nucleic acids, proteins, and cell surface, but also to manufacture glycopeptides, microarrays, and biopolymers. To keep the intact filamentous structure of the virions on microspheres, conjugation reactions should be devoid of intra- and inter-molecular crosslinking of the virions, while not interfering with a directional binding of virion tips to microspheres. To that end, we selectively biotinylated pIII parts for the orientation-controlled immobilization of fd virions and thereby used the Staudinger ligation, a bioorthogonal and chemoselective crosslinking between azide and phosphine, for the ligation of phage virions and antibodies (Scheme 4).

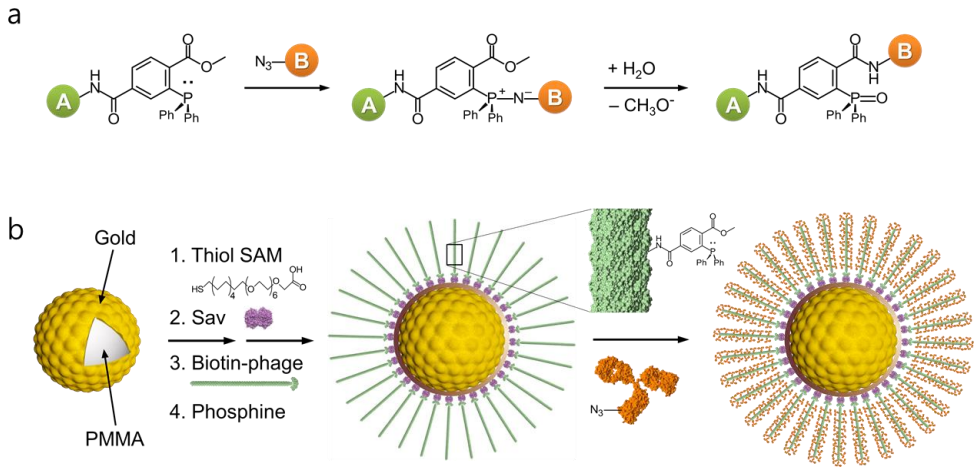

Scheme 4[ii]. Schematic representation of the fabrication of bio-inspired virus-gold microsphere. (a) The Staudinger ligation (azide-phosphine conjugation) between phosphine-activated A and azide-labeled B. An aza-ylide intermediate (middle) converts to a stable covalent amide bond (right). (b) A thin layer of gold allow facile surface modifications by thiol SAM followed by chemical conjugation of streptavidin. The resulting streptavidin-modified microspheres are decorated with pIII-biotinylated phage virions that have filamentous structure, resembling the surface morphology of specific types of cells. The surface-exposed anime groups of N-termini of the viral major coat proteins are conjugated with phosphine and mixed with azide-modified primary antibodies to yield microspheres covered with high-density antibodies via bioorthogonal Staudinger ligation (figures shown cross-sectional area of virions layer and not drawn to scale).

[ii] Dr. Inseong Hwang contributed to this scheme.

We then optimized antibody labeling with either amine-reactive NHS-PEG_{12}-Azide or Sulfo-NHS-Phosphine. In our experimental conditions, antibody precipitated after incubation with Sulfo-NHS-Phosphine probably because of the increased hydrophobicity stems from the phenyl groups of phosphine. On the contrary, no antibody precipitate was found with NHS-PEG_{12}-Azide, and no visible changes of streptavidin- and virus-beads were observed after labeling with Sulfo-NHS-Phosphine; streptavidin is already fixed on the beads, allowing no further aggregation, and phages are rich in surface charges that negate the effect of increased hydrophobicity. After ligation of the azide-modified primary antibody and the phosphine-modified beads, we stained the beads with fluorochrome-labeled secondary antibody and measured the fluorescence intensity of the beads.

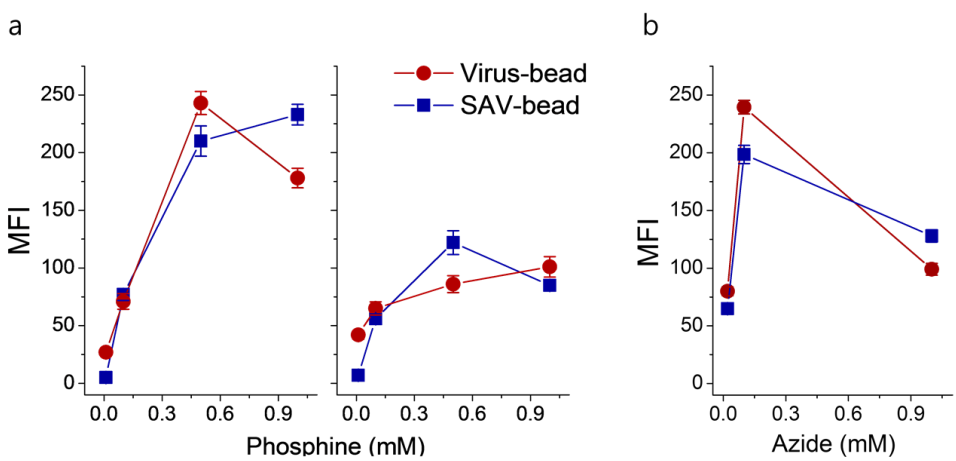

Figure 18. Optimization of Staudinger ligation using mouse antibody. (a) Gold microspheres, covered with streptavidin or phage virions, were treated with four

different concentrations of Sulfo-NHS-Phosphine, while mouse antibody were incubated with 0.1 mM and 1.0 mM NHS-PEG_{12}-Azide. (b) streptavidin or phage-covered gold microspheres were incubated with fixed concentration of phosphine (0.5 mM), while the concentration of azide varied. Anti-mouse Alexa Fluor 594 antibody was used for the determination of mean fluorescence intensity (MFI).

We found that the optimum concentration of phosphine was around 0.5 mM with 100 μM azide where, among others, the virus-tethered beads exhibited the highest fluorescence intensity (Figure 18a). The efficiency of antibody loading decreased at higher concentration of azide (1.0 mM) probably because of the limited access of secondary antibody to buried epitopes of the primary antibody. Lower amount of azide (20 μM) did not seem to push efficacious Staudinger ligation (Figure 18b). However, we cannot rule out the possibility that the lower the level of azide modification, the better the antibody activity.

4.6 Sandwich immunoassay of cardiac biomarkers

To demonstrate the effect of long virus threads, after antibody loading we compared the biomimetic virus-beads with streptavidin-coated beads in terms of antibody activity against cardiac marker proteins, cardiac troponin I (cTnI) and myoglobin.

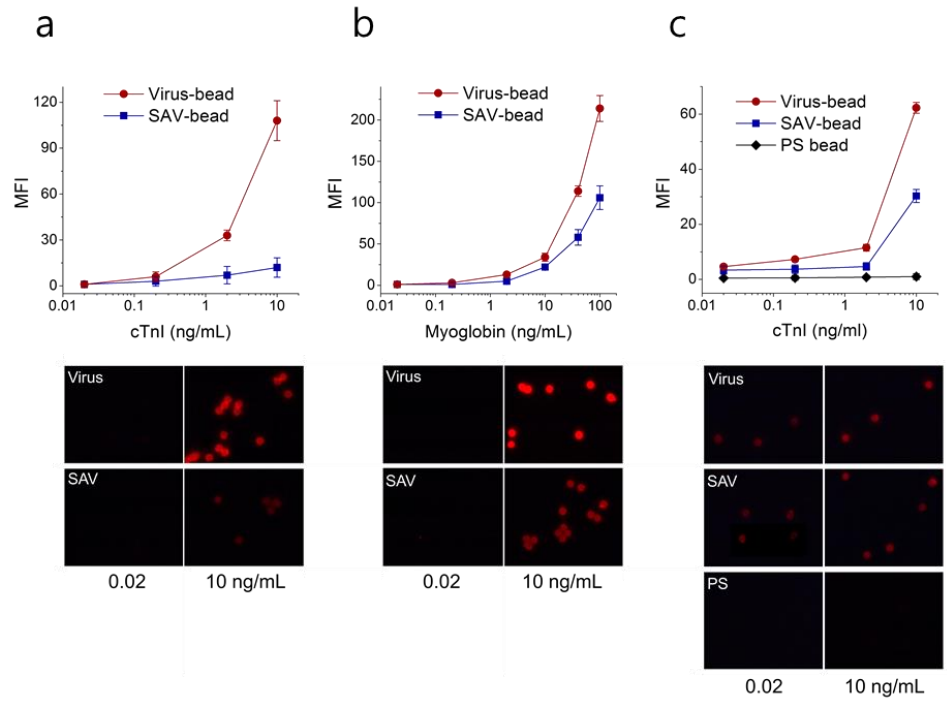

Figure 19. Sandwich immunoassay profiles (top) and representative fluorescence images of each functionalized microspheres corresponding to the w/o initial and final concentrations (bottom) tested for cardiac marker proteins. A range of cTnI in PBS (a), myoglobin in PBS (b), and cTnI in serum (c) were detected using virus- and streptavidin-gold microspheres (a and b), as well as polymer microspheres (c).

We focused on the low range of cTnI and relatively higher range of myoglobin concentrations on the basis of clinical applications [112]. In immunoassays using cTnI- and myoglobin-spiked PBS, virus-decorated gold microspheres showed markedly enhanced signals compared to streptavidin-modified gold microspheres (Figure 19a and b). We could detect as low as 0.2 ng/mL of cTnI and myoglobin using virus-beads. The signals from streptavidin-beads lingered with the background until the concentration reached 2.0 ng/mL of cTnI and myoglobin. The effect of virions was more dramatic in the higher range of cTnI concentration with up to 9-fold increase in fluorescence signal at 10 ng/mL, while the effect of virions on myoglobin showed 2-fold increase within the concentration range tested. The difference in fold increase may originate from the intrinsic variances of antigens, such as size, structure, and binding constant to primary antibodies. Note that the difference in assay performance is greater than the one in the antibody loading between the streptavidin- and virus-beads (see Figure 19). Furthermore, the effect of viral fibers stands out when the amount of captured antigens, and thus the detection antibodies in sandwich assay, is limiting. Therefore, the enhanced sensitivity of the virus-beads may be ascribed to the greater amount of antibody and the long and flexible virus filaments that increase receptor-ligand interactions.

The preventive role of SAM-gold layer for nonspecific adsorption was marked in immunoassays using serum samples that were spiked with cTnI. Interestingly, both the virus- and streptavidin-beads detected as low as 20 pg/mL of cTnI (Figure 19c), while the streptavidin-beads exhibited partial improvement at higher

concentration of cTnI (10 ng/mL) with two fold lower sensitivity than the virus-beads. Importantly, we observed concentration-dependent increase of fluorescence signals at lower range of cTnI only in the case of virus-beads. By contrast, typical carboxylated polystyrene (PS) beads, on which antibodies were conjugated with EDC-NHS chemistry, failed to produce any signals throughout the range tested in serum, although the beads were able to detect cTnI in PBS (Figure 20).

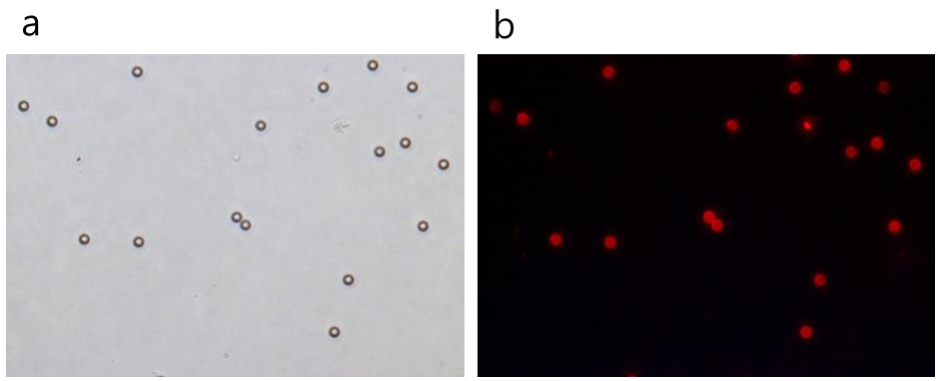

Figure 20. Immunoassay of cTnI in PBS buffer (10 ng/mL) using 10 μm-diameter polystyrene beads whose surfaces were modified with an anti-cTnI antibody using EDC/NHS chemistry. (a) DIC image. (b) Fluorescence image.

The reason why the sensitivity for cTnI in serum should increase remains obscure, although the results suggest that the dense antibodies on phage tentacles and the SAM-gold protection layer synergistically enhance the sensitivity for the lower range of marker proteins.

5. Conclusion and Perspective

In cellular systems, threadlike protruding structures have been evolved to sustain efficacious cellular functions, such as cellular uptake of small- and large molecules, cellular adhesions to biological and non-biological matrices, cell-cell interactions, and ligand-receptor interactions. Inspired by the cellular morphology and by the additive effect of long tethers on receptor-ligand interactions, we decorated SAM-protected gold microspheres with filamentous virions that mimic microvilli-like biological architectures. The SAM-protected virus-gold microspheres showed extremely low non-specific bindings, enhanced capacity of antibody loading, and superior performance in analyte-solid surface interactions when compared with bare polymer beads and non-viral streptavidin-gold beads. The gold-protected and virus-tethered microbeads that resemble biological architectures will open up new possibilities for developing biocompatible and bio-inspired solid surfaces for the improved analyte-solid surface interactions. The microsphere, which is the key to the multiplex suspension array, can be replaced with the virus-decorated gold microshells we developed. This is applicable to the entire field of in-vitro diagnoses and feasible for point-of-care testing (POCT) in combination with microfluidics. Also, since gold microshells with a thin gold layer themselves conduct electricity, they could be used in electrical connections in printed circuit boards or connections among semiconductor elements.

Part 2

Cell-solid surface interaction:

Purified synaptic cell adhesion molecules for induced artificial synapse and bioanalysis

1. Introduction

A neuron is the main cell constituting the nervous system. Unlike other cells, it can transfer electrical signals, and can be classified into various types according to location and function. A typical neuron is composed of the cell body, called a soma, the signal receptors, called dendrites, and the main channel of signal transmission, called an axon. In the nervous system, neuron-to-neuron communication occurs by electrical or chemical signals passing through the neuron junctions (synapses). A typical synapse consists of a connection between the axon of one neuron and a dendrite or soma of another. The electrical signals are transmitted by the presynaptic axons and are transformed into chemical signals (neurotransmitters) in synapses where the probability of the transmission of the electrical signals to postsynaptic dendrites is determined by the types of the neurotransmitters. Excitatory synapses allow postsynaptic transmission of electrical signals, inhibitory synapses block postsynaptic transmission of the signals.

In-depth analysis of the signal transmissions between the axon and synapse reveals that they are ultimately a local movement of chemical species, and such changes in their electrochemical potential allow external stimulation or measurements of signals within the cell. Currently, in most studies, excluding the patch clamp method, neuronal cells are simply developed on or near a solid electrode surface to receive cellular signals.

E.G. Gray elucidated the structure of a synapse using an electron microscope in

1959 [113]. Synapses are ~1 μm in diameter with an intercellular space called synaptic cleft, which is ~20 nm wide, and their formation requires mutual pairing between cell adhesion molecules (CAMs). Synaptic CAMs are proteins localized on the cell surface that adhere to the pre- and post- synaptic terminals and increase the mechanical stabilization of the synapse, while modulating its structure and function. Generally, synaptic CAMs consist of 3 domains: the intracellular domain that interacts with intracellular scaffold proteins, the transmembrane domain, and an extracellular domain that interacts with other Synaptic CAMs. Several families of Synaptic CAMs have been discovered [114], including neuroligins (NLs), neurexins (Nrxs), Slit and Trk-like family (Slitrks), netrin-G ligand proteins (NGLs), leucine-rich repeat transmembrane neuronal proteins (LRRTMs), neural cell adhesion molecules (NCAM), L1-cell adhesion molecules (L1-CAMs), synaptic adhesion-like molecules (SALMs), etc (Table 4).

Most attempts in the formation of artificial synapses started from the year 2000 when seminal experiments were reported on stable synaptic junctions between non-neuronal cells expressing synaptic CAMs and cultured neuronal cells [115, 116, 121]. Recently, the purified synaptic CAMs were immobilized on a solid surface to induce artificial synapses [117, 118].

Table 4. Locations and functions of selected cell adhesion molecules [114].

Molecules	Synaptic location	Pairing	Function
NLs	post	Nrxs, PSD-95	Excitatory synapse formation (NL1)
Slitrks	post	PTPδ	Inhibitory synapse formation (Slitrk3)
NGLs	post	PTPσ, etc	Maintain excitatory synaptic current (NGL3)
LRRTMs	post	Nrxs	Excitatory synapse formation
Nrxs	pre	NLs, LRRTMs	Induce post-synaptic differentiation (β-Nrx)
L1-CAMs	pre	-	Decrease of inhibitory synaptic response (L1)
SALMs	both	NMDAR, etc	Control of excitatory synapse maturation (SALM2)

pre, pre-synaptic; post, post-synaptic; both, pre- and post-synaptic; PSD-95, post-synaptic density-95; PTPδ, protein tyrosine phosphatase δ; NMDAR, N-Methyl-D-aspartate receptor.

Among other synaptic CAMs, NLs and Nrxs are the most studied proteins; rats and mice have three genes encoding NLs, whereas humans have five. Previously in 1995, Südhof *et al*. first purified NL1 using affinity chromatography with immobilized Nrx-1β [119], and the complete paired structure of NL1 and Nrx-1β was revealed in 2007 [120]. Scheiffele *et al* expressed NLs in HEK-293 cells, co-cultured them with neuronal cells [121], and discovered that NL1 triggers pre-synaptic development. Similarly, Südhof *et al*. transfected NL1 derivatives into COS

cells and showed that this induced the formation of an artificial synapse [122]. Furthermore, Groves and coworkers immobilized a glycosylphosphatidylinositol (GPI)-linked NL1 ectodomain on silica microbeads covered with supported lipid bilayer (SLB) membrane, and confirmed the synaptogenic activity of the GPI-anchored NL1 ectodomain [118]. On the other hand, Colman group used poly-D-lysine (PDK)–coated polymer beads to induce the formation of artificial synapses without using synaptic CAMs [123]. Recently, research is being actively conducted on various synaptic CAMs and induced artificial synapses, but the function and mechanisms of these are yet to be completely revealed.

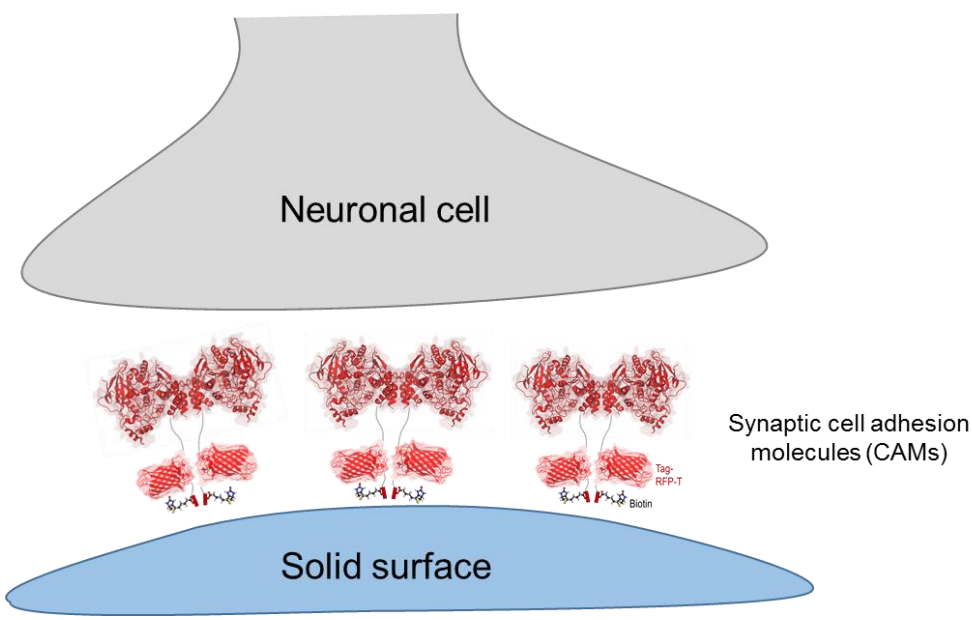

Scheme 5. Schematic representation of artificially induced neuronal cell-solid surface interfaces.

Unlike the detection of delocalized analytes in solutions, the detection of extremely local neuronal signals (e.g., electrical signal or neurotransmitter) needs sophisticated regulation of distances between an electrode surface and cells. Studies have so far only stochastically localized the cells on a solid surface, which causes a loss in sensitivity, selectivity, and reproducibility. If we allow the cells to meet electrodes through the synaptic connections, we not only ensure the reproducible physical geometry of the cell-electrode interfaces, but also have the possibility to measure neurotransmitters otherwise impossible (Scheme 5). Therefore, it is expected that the synaptic CAMs, which were developed to induce artificial synapses on a solid surface, will allow us to consistently position the neuronal cells evenly, thereby providing reproducible and selective signal exchanges. Furthermore, the induced artificial synapses using synaptic CAMs will ultimately provide the foundation for the systematic study of interactions between the solid surface and the cells, as well as the understanding of the information processes in neural networks.

To understand and mimic neuronal network behavior, the ability to monitor, and thus distinguish between, the excitatory and inhibitory signals is essential. In biological systems, excitatory and inhibitory synapses are determined by synaptic CAMs [124, 125]. Notably, chemical conjugation of NL1 on polystyrene beads, despite their capability of adhering to Nrx-expressing cells, failed to induce presynaptic differentiation, suggesting that NL1 requires fluidic lipid bilayer environment for its activity [117]. As a consequence, the use of synaptic CAMs such as NL1 to build artificial synapses has been blocked by the lipid membranes that

create a huge insulating barrier between neurons and the signal recording materials, e.g., electrodes. When it comes to direct recording of neuronal signals via artificial synapses induced by synaptic CAMs, an electrode is expected to act as a 'fake' postsynaptic bouton, and thus the requirement of lipid bilayer on the electrode is a significant challenge. NL isoforms (NL1, 3, and 4) are well-known to induce the formation of excitatory (glutamatergic) presynapses, while NL2 and recently found Slitrk3 inhibitory (GABAergic) presynpases [126-129]. As synaptic CAMs for inhibitory synapses are quite rare, unprecedented specificity to inhibitory synapses of Slitrk3 is of importance [130, 131].

Here, we demonstrate functional interactions of fluorescent and biotinylated synaptic CAMs with cultured hippocampal neurons, independent of SLB media. The fluorescence tag should aid in establishing stable cell lines, and thus mass production, quantification, and tracking of synaptic CAMs on a given artificial substrate.

2. Experimental Methods

2.1. Materials

Plasmids encoding cholinesterase-like domain (CLD) of neuroligin-1 (NL1) followed by GPI anchoring motif (pNICE-HA-H6-NL1-GPI) and full length NL1 and NL2 (pNICE-HA-H6-NL1 and pNICE-HA-NL2) were a generous gift from Peter Scheiffele. A plasmid carrying EYFP-tagged full length NL1 (pNICE-YFP-NL1) was a kind gift from Ann Marie Craig. A plasmid encoding full length Slitrk3, pGW1-Slitrk3, was a kind gift from Jaewon Ko. A plasmid expressing TagRFP-T (pcDNA3-TagRFP-T) was kindly provided by Roger Y. Tsien. BirA expressing plasmids pDisplay-BirA-ER (Addgene plasmid #20856) and pET21a-BirA (Addgene plasmid #20857) were provided by Alice Ting. pAd:CMV-rtTA-IRES-BirA was a gift from William Pu (Addgene plasmid #31375).

Carbenicillin (Carb) was from Gold Biotechnology (St. Louis, MO). Streptavidin, bovine serum albumin (BSA) (A3059), adenosine 5'-triphosphate (ATP), polyethyleneimine (Mw: 25,000), Kanamycin sulfate, and G418 (Geneticin) were from Sigma-Aldrich (St. Louis, MO). QIAprep Spin Miniprep, QIAGEN Plasmid Plus Midi, QIAquick Gel Extraction, Phusion DNA polymerase, and Ni–NTA resin were obtained from Qiagen (Seoul, Korea). Restriction enzymes and T4 ligase were obtained from New England Biolabs (Ipswich, MA). Alexa-labeled secondary antibodies, bacterial cell line DH10B, mammalian cell line HEK293-H,

HEK-293, streptavidin conjugated with horseradish peroxidase (streptavidin-HRP), Opti-MEM® I Reduced Serum Medium, Biocytin-Alexa 594, D-biotin, and Dynabeads® M-280 Streptavidin were obtained from Life Technologies (Invitrogen, Carlsbad, CA). Goat NL1 polyclonal antibody (sc-14084) was from Santa Cruz Biotechnology, Inc. (Santa Cruz, CA)

2.2. Molecular biology

2.2.1. Y-NL1-G

pNICE-YFP-NL1 was cut by KpnI and NotI to remove the predicted O-glycosylation motif (OG), transmembrane domain (TMD), and cytosolic domain of NL1 was replaced by GPI linker from pNICE-HA-H6-NL1-GPI by cutting with the same enzymes, yielding pNICE-YFP-NL1-GPI.

2.2.2. Y-NL1

The GPI portion of the pNICE-YFP-NL1-GPI was replaced with GS-linker (PHLHNLDI639 GGGSGGGSEGGGSGGGSGGGSEGGGSGG) fused with a 14-mer biotin acceptor peptide (AP or AviTag, GLNDIFEAQKIEWHE). First, pNICE-YFP-NL1-GPI and the staggered PCR product (primers N38, N39, N40 and N41) were digested with KpnI and NotI and ligated together. To aid purification, His×8 encoding primers, N43 and N44, were annealed and introduced in front of the YFP sequence using a single PvuI site, yielding pNICE-H8-YFP-NL1-AP (encoding Y-NL1).

2.2.3. R-NL1

TagRFP-T was PCR amplified from the pcDNA3-TagRFP-T plasmid using primers N48 and N49, cut by PvuI and SalI, and ligated with pNICE-H8-YFP-NL1-AP that had been digested with the same restriction enzymes, resulting in pNICE-H8-RFP-NL1-AP (encoding R-NL1).

2.2.4. NL1-R

First, we replaced the GPI tag of pNICE-HA-H6-NL1-GPI with a new GS linker containing additional cloning sites, PvuI and SalI, and AP tag (PHLHNLDI639GGGSGGGSEGGGSGGGSGGGSEG-RS(PvuI)GVD(SalI)-(AP)). The GS linker was synthesized using primers N38, N39, N50 and N41 by staggered PCR, cut by KpnI and NotI, and ligated with pNICE-HA-H6-NL1-GPI that had been cut by KpnI and NotI, yielding pNICE-HA-H6-NL1-GS-PS-AP. The TagRFP-T PCR product obtained from primers N48 and N49 and pNICE-HA-H6-NL1-GS-PS-AP were then digested with PvuI and SalI, followed by a ligation to give pNICE-HA-H6-NL1-H8-RFP-AP (encoding NL1-R).

2.2.5. NL2-R

NL2 was amplified from pNICE-HA-NL2 using primers N55 and N56. The GS linker was PCR amplified from pNICE-HA-H6-NL1-H8-RFP-AP using primers N103 and N104. The pNICE-HA-H6-NL1-H8-RFP-AP was but by BamH I and SalI and served as a vector for three-piece Gibson assembly.

2.2.6. SL3-R

Ectodomain of Slitrk3 was copied from pGW1-Slitrk3 using primers N83 and N74-2 and cut by HindIII and KpnI. The GS linker fused with H8-RFP, GT(KpnI)GSGGGSEGGGSGGGSGGGSEG-RS(PvuI)-(H8-RFP)-VD(SalI)-(AP), was PCR copied from pNICE-HA-H6-NL1-H8-RFP-AP using N38-2 and N41 and cut by KpnI and NotI. The pNICE-HA-H6-NL1-GS-AP was cut by HindIII and NotI and served as a vector for three-piece ligation, finally giving pNICE-SL3-H8-RFP-AP encoding SL3-R. To screen linker sequences, pNICE-SL3-H8-RFP-AP was cleaved by KpnI and PvuI where other linkers with various lengths were inserted. The active SL-R was obtained using annealed primers N106 and N107, yielding GT(KpnI)GSGGGSEGRS(PvuI)-(H8-RFP)-VD(SalI)-(AP).

Bicistronic synaptic encoding of postsynaptic CAMs and BirA: To make a bicistronic expression vector that allows a simultaneous expression of BirA-ER with the postsynaptic CAMs, the internal ribosome entry site (IRES) followed by BirA-ER gene was introduced (Figure 21). The pNICE-(HA-H6)-CAM-H8-RFP-AP (CAM = ectodomain of NL1, NL2, or Slitrk3) were cleaved by NotI to insert IRES-BirA that was amplified from pAd:CMV-rtTA-IRES-BirA using primers N86 and N87 and cut by NotI, generating pNICE-CAM-RAP-BirA after ligation.

Bacterial expression and purification of bacterial BirA biotin ligase was conducted using pET21a-BirA plasmid. The major primers used in this study are listed in Table 5.

Table 5. Primers used for the generation of protein NL1-R. Sequences underlined are crossover area for the staggered PCR.

Primer name	DNA oligomer sequence from 5' end (length)
N38_KpnI-AP-1F	ggcggt***GGTACC***TCATCTGCATAATCTCAATGACATTGG CGGCGGCAGCGGCGGAGGCAGCGAGGG (66)
N38-2_KpnI-GS-F	ggcggt ***GGTACC***GGCAGCGGCGGAGGCAGCGAGGG (35)
N39_AP-2R	GCCCTCGCTGCCGCCTCCGCTGCCGCCTCCGCTGCC TCCGCCCTCGCTGCCTCCGCCGCT (60)
N40_AP-3F	GCGGAGGCGGCAGCGAGGGCGGAGGCAGCGGCGG CGGCCTGAACGACATCTTCGAGGCCC (60)
N41_AP-NotI-4R	ggcagc***GCGGCCGC***TTACTCGTGCCACTCGATCTTCTG GGCCTCGAAGATGTCGTTC (57)
N50_AP-PvuI-SalI-3F	GCGGAGGCGGCAGCGAGGGC***CGATCG***GGT***GTCGA C***GGCCTGAACGACATCTTCGAGGCCC (60)
N43_H8-PvuI-F	***CG***CACCATCACCACCACCACCATCACCGAT (30)
N44_H8-PvuI-R	CGGTGATGGTGGTGGTGGTGATGGTG***CGAT*** (30)
N49_PvuI-H8-TagRFP-F	ggc***CGATCG***CACCATCACCACCACCACCATCACATGG TGTCTAAGGGCGAAGAG (54)
N48_EK-SalI-R	gccacc***GTCGAC***CTTGTCGTCGTCGTCCTTGTACAGCT CGTCCATGC (47)
N55_NL2-BamHI-F	GTGTGGTCCACAGG ***GGATCC*** (20)
N56_NL2-631-639-R	TCTGTGTGCAGGTTGTGCAGGTG (23)
N74-2_Slitrk3-Ecto-KpnI-R	accgcc***GGTACC***GCCCCCAGGAGGAGAAAACTC (33)
N83_pGW1-HindIII-F	CACCGTCCTTGACACG***AAGC*** (20)
N86_NotI-IRES-F	ct***GCGGCCGC***cgagcatagtcatctagcacaatTCCGCCCCTCTCC

	CTCCCCCCCCCCTAA (61)
N87_BirA-ER-NotI-R	ga***GCGGCCGC***TCACAGCTCGTCCTTTGAACCcccagatc cagatgtagacccTTTTTCTGCACTACGCAGGG (72)
N103_NL2-631-639-F	CTGCACAACCTGCACACAGAGGGCGGCGGCAGCG G (35)
N104_SalI-AP-R	CGAAGATGTCGTTCAGGCC***G*** (20)
N106_SL3-shortGS-F	***C***GGCAGCGGCGGAGGCAGCGAGGGC***CGAT*** (29)
N107_SL3-shortGS-R	***CG***GCCCTCGCTGCCTCCGCCGCTGCCG***GTAC*** (31)

2.3. Stable cell lines

For the initial screening of synaptogenic activity of NL1 ectodomains, 24 μg of each NL1-encoding plasmid DNA (pNICE-H8-YFP-NL1-AP, pNICE-H8-RFP-NL1-AP, and pNICE-HA-H6-NL1-H8-RFP-AP) was added to the 1.5 mL of Opti-MEM I Reduced Serum Media. Likewise, 60 μl of 1.0 mg/mL PEI solution was added to the 1.5 mL of Opti-MEM solution. After 5 min incubation at 25 ℃, the two solutions were mixed at room temperature for 30 min and added to HEK293 cells grown to ~20% confluence in a culture dish of 10 cm diameter at 37 ℃. The DMEM medium was replaced after 4 h incubation. After three days, the cells were treated with G418 with final concentration of 0.8 mg/mL. The G418 treatment was repeated with fresh medium after two days. After two weeks, single colonies with brightest fluorescence signals were picked and seeded on a 24-well plate. Among them, the best fluorescent

colonies were repeatedly selected until only one colony was left and seeded on a culture dish of 10 cm diameter for the subsequent passage. The established stable cell line was kept in DMEM medium containing 100 μg/mL G418.

2.4. Preparation of biotinylated synaptic CAMs

Plasmid pDisplay-BirA-ER (24 μg) in 1.5 mL of Opti-MEM solution was mixed with 1.5 mL of Opti-MEM solution containing 60 μg of PEI for 20 min at 25 ℃. The mixture was added to the established HEK293-H stable cell lines at ~20% confluence in a culture dish of 10 cm diameter. After 4 h incubation, the DMEM medium was replaced with a fresh one containing 100 μg/mL G418 and 10 μM biotin. The in vivo biotinylated synaptic CAM was allowed to secrete into culture medium for three days at 37 ℃. Then, 10 mL of the medium was saved and the whole cells were transferred to a culture dish of 15 cm diameter and filled with 30 mL of DMEM containing 100 μg/mL G418 and 10 μM biotin. After another three days, the culture media were combined and subjected to column purification using 2 mL of Ni-NTA resin according to the manufacturer's protocol. The three 1 mL elution fractions were subjected to fluorescence analysis using Synergy Mx fluorescence microplate reader (BioTek, Seoul, Korea).

For in vitro biotinylation, the stable cell line was grown without BirA transfection. To the 1 mL of column elution fraction showing the highest fluorescence signal was added 5 mM $MgCl_2$, 1 mM ATP, 0.1 mM biotin, and 30 nM BirA enzyme as final concentration and shake incubated for 2 h at 37 ℃. The level

of in vivo and in vitro biotinylation was analysed via western blot using streptavidin-HRP or using goat or mouse anti-NL1 antibody and HRP-conjugated secondary antibody. The purity of NL1 was analysed by SDS-PAGE with silver staining

2.5. Immunocytochemistry

Cells were fixed using formaldehyde (4%) for 25 min and rinsed three times with PBS (100 mM, pH 7.4). The cells were then incubated in blocking solution (PBS containing 4% BSA and 0.1% Triton X-100) for 30 min, followed by incubation in primary antibodies diluted in TBS (Tris-buffered saline, pH 7.4) containing BSA (0.5%) and Triton X-100 (0.1%) overnight at 4℃. The samples were then washed three times with TBS and the fluorescent secondary antibodies were applied for 1 h at room temperature in TBS containing BSA (0.5%). The samples were washed again three times with TBS and once with DDW, and stored in VECTASHIED Mounting Medium with DAPI at -80℃ until microscopic examination. Fluorescence images were taken with a Zeiss LSM710 confocal laser scanning microscope equipped with ZEN 2009 software at the National Center for Inter-university Research Facilities (NCIRF) at Seoul National University.

3. Results and Discussion

3.1. Construction of labelled NL1 ectodomains

To generate type-specific artificial dendrites, ectodomains of NL1 (48-639), NL2 (15-614), and Slitrk3 (28-649) were exerpted from their full sequences (Scheme 5). NL1 ectodomain was determined by the crystal structure of NL1/Nrx-1β complex that reveals Leu636 as the end of the α-helix required for NL1 dimerization [120, 132]. Indeed, NL1 (46-638) was the minimum domain functionally secreted to the culture medium, whereas NL1 (46-626) and NL1 (46-633) were not [133]. Intriguingly, the functional GPI-anchored NL1 contains Leu48-Pro631 [117, 125, 134], lacking several C-terminal amino acids required for the formation of α-helix bundle. Since the GPI motif linked to NL1 (48-631) begins with KLLSATA that has high α-helical propensity [135], the overall dimeric structure of GPI-anchored NL1 may have remained unaltered despite the absence of 631-638 helical residues. Ectodomain of NL2 (15-614) was determined by sequence homology with NL1. The border of Slitrk3 ectodomain was conservatively set further away from the C-terminal Leu-rich repeat domain (LRR-CT), seven residues before the transmembrane domain (TMD) (Scheme 6).

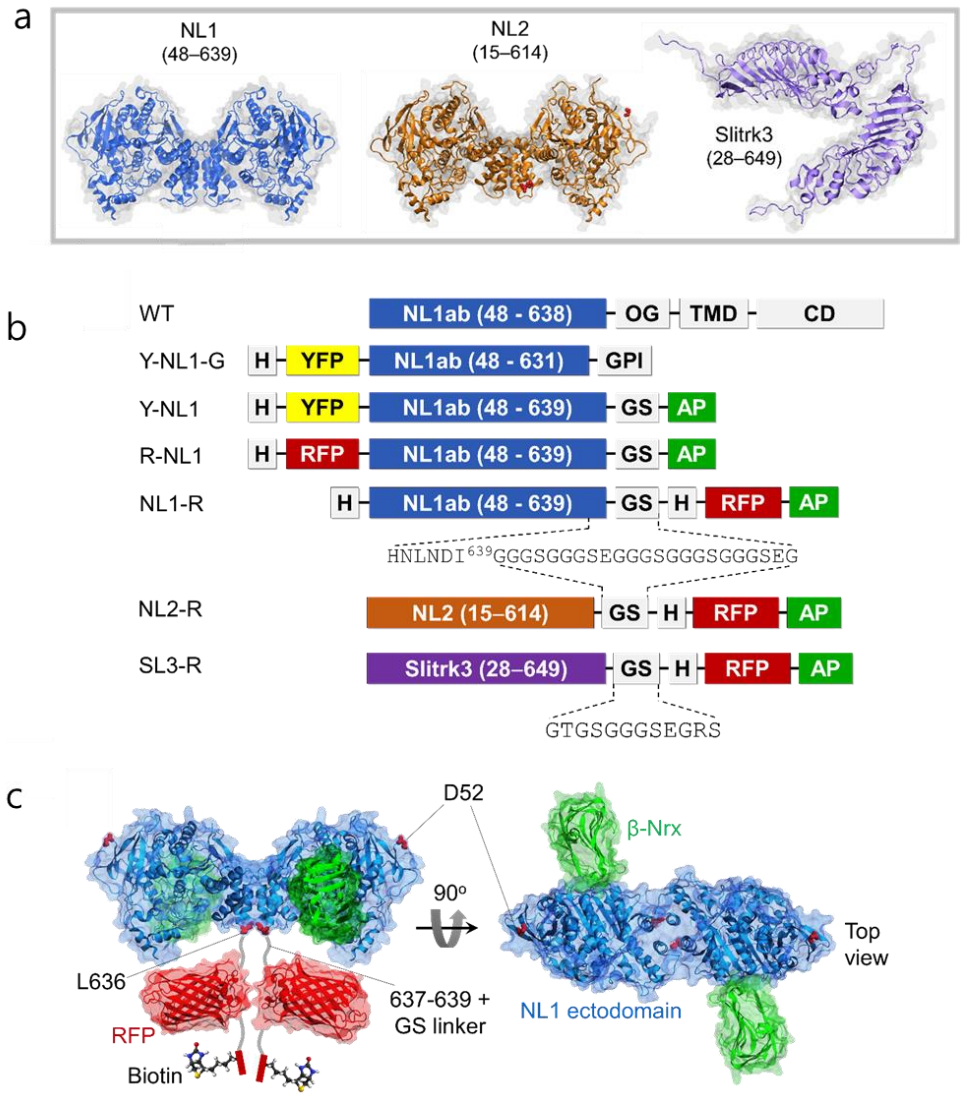

Scheme 6[iii]. (a) Schematic structure of artificial synapse displaying postsynaptic NL1 homodimer (NL1-R), NL2 homodimer (NL2-R), and Slitrk3 (SL3-R). The

[iii] Dr. Inseong Hwang contributed to this scheme.

structures were modeled after NL1 (PDB ID, 3BIX) [120] and NL2 (PDB ID, 3BL8) [136], while the structure of Slitrk3 (27-627 residues) was predicted using Slitrk1 (PDB ID, 4RCW)[137] as a template by the RaptorX server [138], showing two LRR1 and LRR2 domains. (b) Schematic structures of engineered synaptic CAMs used in this study in comparison to wild type NL1 (WT). (c) Predicted structure of NL1-R-Nrx1β complex. The C-terminal tagging module for ectodomain of postsynaptic CAMs minimizes steric hindrance in pre- and postsynaptic CMAs interaction.

To facilitate massive production, purification, quantification, and localization of the ectodomains as well as immobilization of the ectodomains on solid supports, we further engineered the NL1 ectodomain, seeking a general tagging module that can be applied to the other synaptic CAM molecules. On the basis of previous studies showing that both N-terminally YFP-tagged full-length NL1 [139] and glycosylphosphatidylinositol (GPI)-linked NL1 ectodomain [117, 125, 129] are able to instruct excitatory presynaptic differentiation, we first generated N-terminally YFP-tagged and C-terminally GPI-anchored NL1 (Y-NL1-GPI). Unfortunately, the purification yield of the Y-NL1-GPI was extremely low, making us replace the GPI-anchoring motif with AP, a biotin acceptor peptide [140], yielding C-terminally biotinylated Y-NL1. To prevent possible dimerization of YFP, we replaced YFP with TagRFP-T, a photostable monomeric red fluorescence protein (RFP) [141], to

generate R-NL1. We also moved the fluorescence tag from N-terminus to C-terminus of NL1 ectodomain, while keeping the AP-tag at the ultimate C-terminal end of the engineered protein, yielding NL1-R.

The in vivo biotinylation was further simplified by bicistronic expression of ER-specific bacterial biotin holoenzyme synthetase (BirA) (Figure 21).

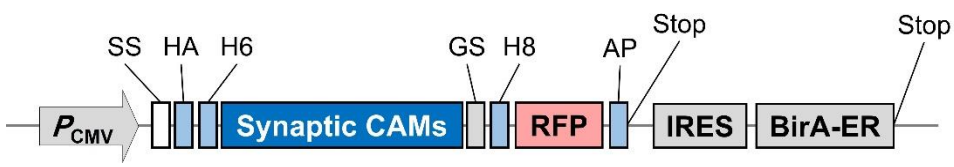

Figure 21[iv]. Genetic engineering of postsynaptic CAMs for facile mass production with in vivo biotinylation. SS, signal sequence; HA, hemagglutinin affinity tag; H6, hexa-His tag; GS, Gly-Ser rich linker; H8, octa-His tag; AP, biotin acceptor peptide; IRES, internal ribosome entry site. The SS, HA and H6 vary depending upon the type of the postsynaptic CAMs

3.2. Generation of stable cell lines

In order to make a stable cell line, the appropriate cell line and antibiotics must be selected. G418 is an antibiotic that is widely used to produce genetically engineered

[iv] Dr. Inseong Hwang contributed to this figure.

proteins in mammalian cells, and HEK-293T cells are resistant to G418. Thus, we selected HEK-293H cells to perform the viability assay using G418. Figure 25 shows a DIC image that demonstrates viability over time in an 800 μg/ml concentration of G418. HEK-293H cells, which are adherent cells, grew well at first, while they were attached to the dish (Figure 22a) but were all dead after one week, when they became detached.

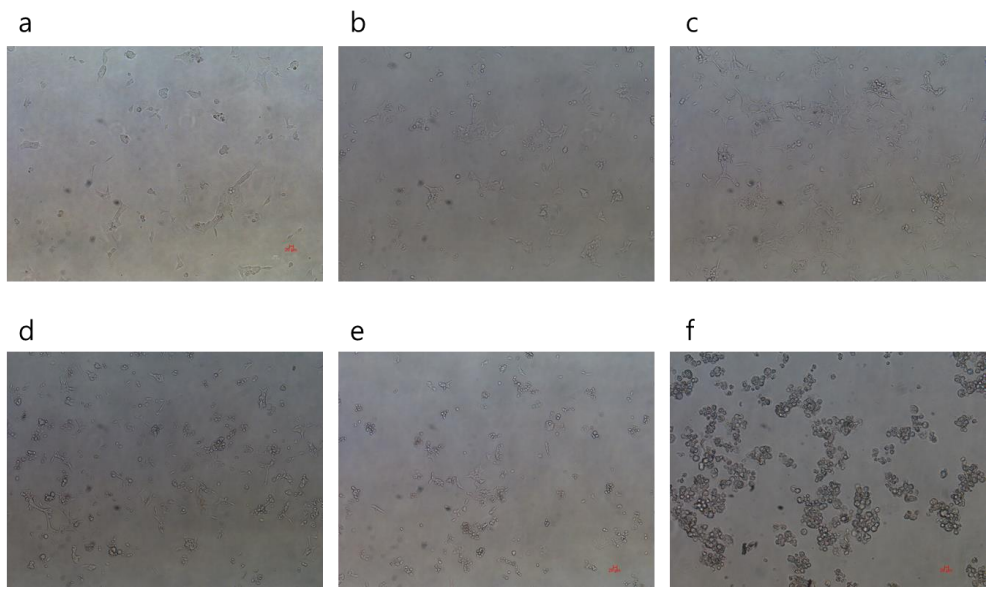

Figure 22. HEK-293H cell viability assay in 800 μg/ml G418 for (a) 0, (b), 1, (c) 2, (d) 3, (e) 5, (f) 7 days.

Next, we optimized the conditions for transient transfection. As shown in Figure 25, green fluorescent protein (GFP) was expressed in HEK-293H cells using either

calcium phosphate, lipofectamine 2000, or polyethyleneimine. The experimental results showed that the best transfection efficiency was obtained using polyethyleneimine (Figure 23c). The highest fluorescence levels were seen after 72 hours, and this became reduced at 100 hours after transfection, due to GFP gene deletion. Thus, we added G418 to the culture media on the third day after transfection to select for synaptic CAMs-expressing cells.

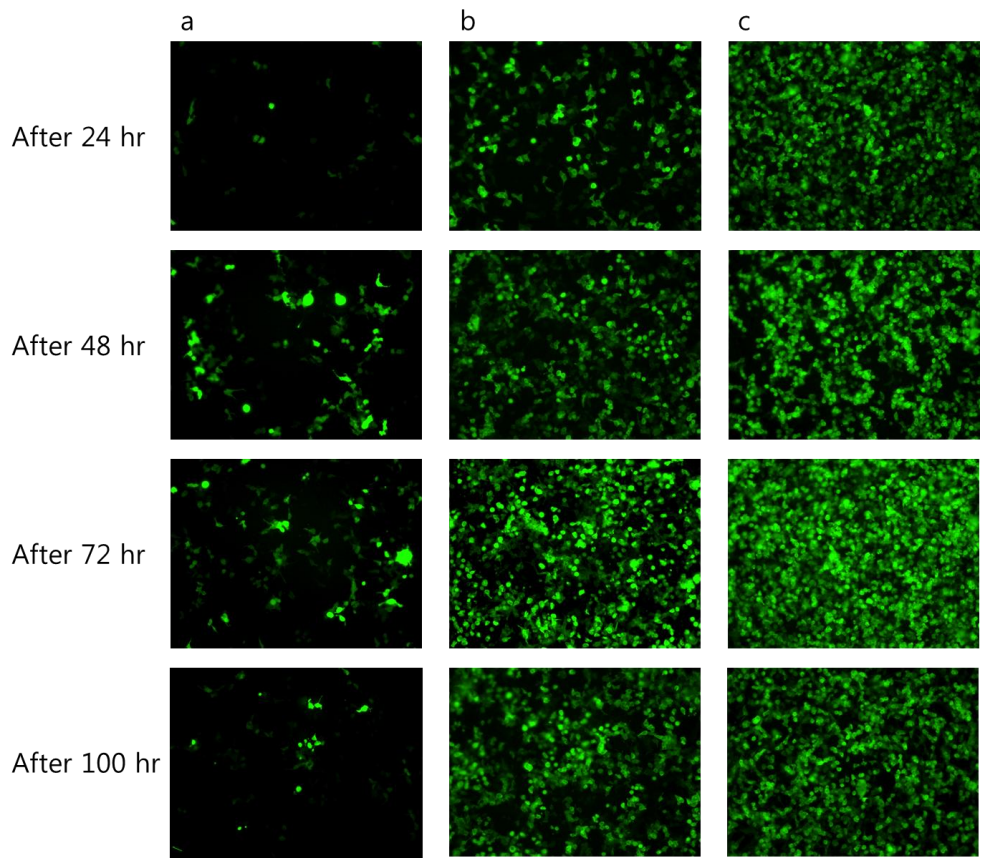

Figure 23. Optimization of transfection methods for a HEK-293H cell line.

Fluorescent images of GFP-transfected HEK-293H cells in three independent transfection experiments. (a) Calcium phosphate, (b) Lipofectamine 2000, (c) Polyethyleneimine.

Figure 24 shows the transfection and selection results using the aforementioned conditions. It also shows the results of selection over time via fluorescence (Figure 24a-c), and a single colony whose size was 0.5–1 mm (Figure 24d). We monitored expression, purification, and immobilization by tagging fluorescent proteins at the synaptic CAMs. It took at least 2 weeks to generate a stable cell line from G418-treated HEK-293H cells. Two to four weeks after transfection, a selected cell had formed into a single colony that could be picked.

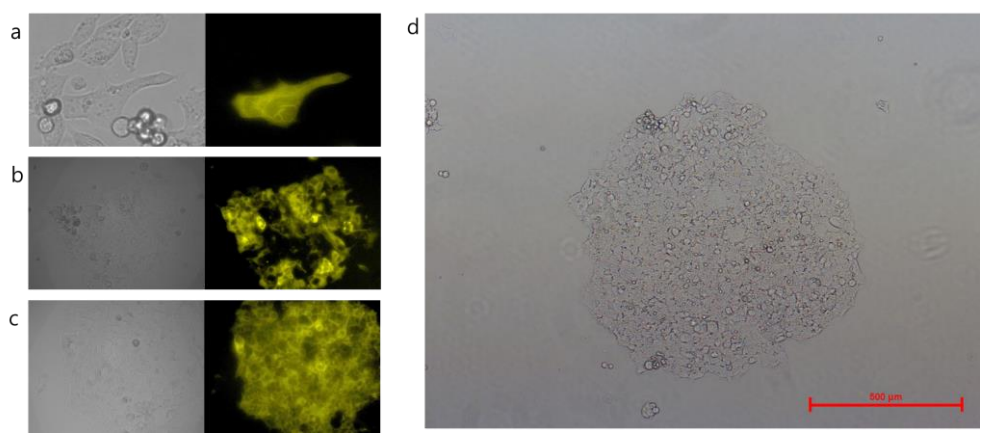

Figure 24. (a) 4, (b) 9 and (c) 12 days after transfection. (d) DIC image of a single colony in which G418 selected NL1-R was expressed two weeks after transfection.

After identifying a colony that was the appropriate size and that displayed bright fluorescence, it was picked using a micropipette on a fluorescence microscope and seeded into a 24-well plate. The established stable cell line was sub-cultured in the presence of 100 μg/mL G418 in a 10 cm-diameter culture dish (Figure 25). Each of the synaptic CAMs were well expressed, as verified by fluorescence. Synaptic CAMs in the cell media, which were secreted during sub-culture, were purified.

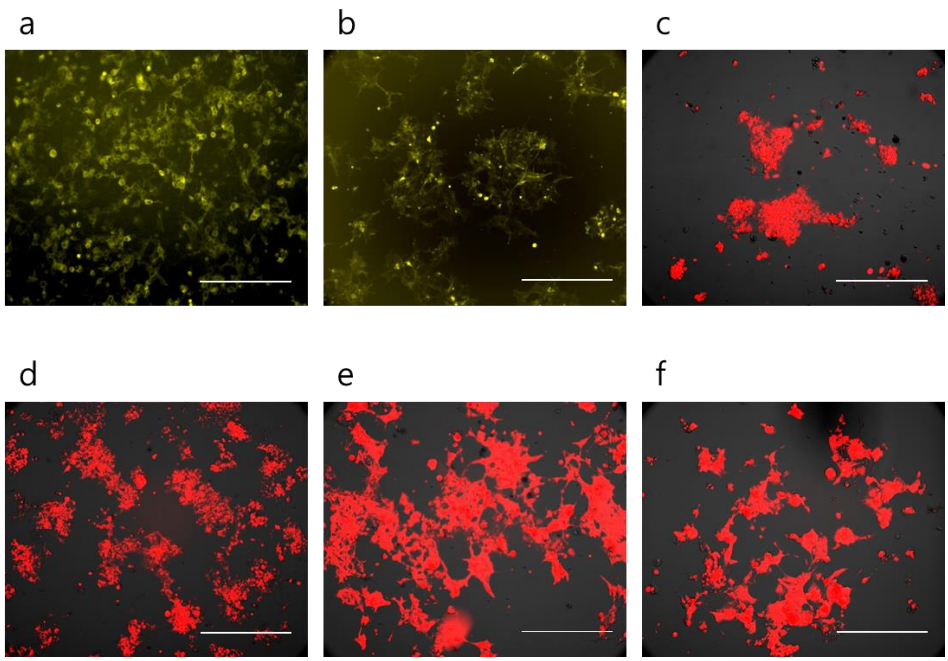

Figure 25. Merged fluorescence and DIC images of stable cell lines in which synaptic CAMs of (a) Y-NL1-G, (b) Y-NL1, (c) R-NL1, (d) NL1-R, (e) NL2-R, and (f) SL3-R were expressed.

3.3. Purification of synaptic CAMs

We employed biotin-streptavidin binding as a strategy to attach the synaptic CAMs to the solid surface. Two methods for binding biotin to synaptic CAMs are *in vivo* biotinylation, which expresses the BirA enzyme inside cells via transfection, and *in vitro* biotinylation, which uses the BirA enzyme in purified synaptic CAMs. The former purifies secreted biotin-conjugated synaptic CAMs by transfecting ER-specific BirA plasmid into the stable cell line, while the latter purifies secreted synaptic CAMs in the stable cell line to perform additional biotinylation. Culture media containing synaptic CAMs were subjected to column purification using 2 mL of Ni-NTA resin according to the manufacturer's protocol. Western blotting (Figure 26) verified that the NL1 derivatives band was successfully purified.

Quantification of the purified synaptic CAMs was verified by silver staining, western blot, and fluorescence intensity. A known amount of BSA was loaded and compared with a known volume of the synaptic CAMs elution fraction to yield the synaptic CAMs concentration (Figure 27). However, despite successful experimental results from *in vivo* and *in vitro* biotinylation of synaptic CAMs, those that were generated by *in vitro* biotinylation did not induce an artificial synapse. Thus, synaptic CAMs were attached to the streptavidin-coated dynabeads using the *in vivo* biotinylation method to induce an artificial synapse. Figure 30 shows the fluorescence image of NL1-R immobilized dynabeads. Since RFP is included, as shown in (Figure 30b), red fluorescence was observed in addition to the shape of the bead. However, RFP fluorescence was disappeared during the

immunocytochemistry (ICC) process for the synaptogenic activity test.

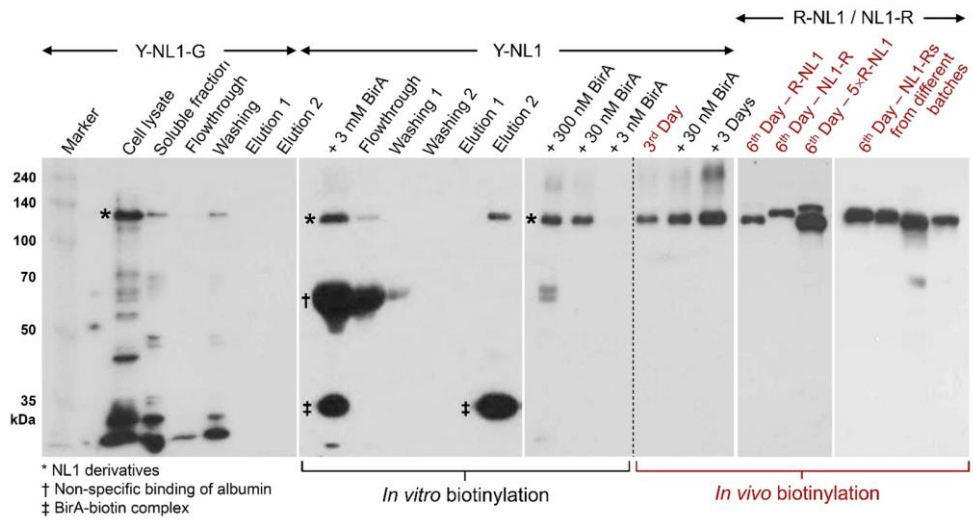

Figure 26. Western blot profiles for the partially purified and labeled NL1s. The YFP-tagged NL1-GPI (Y-NL1-G) rarely appeared in the elution fraction despite its presence in the total cell lysate. When the GPI motif was replaced with AP, the YFP-NL1-AP (Y-NL1) was secreted into the culture medium, and was retained in a Ni-NTA resin. Both *in vitro* and *in vivo* biotinylation revealed biotinylated NL1 regardless of the position of the fluorescence protein. Y-NL1-G was probed by anti-NL1 antibody while the AP-tagged NL1s were detected using streptavidin-HRP.

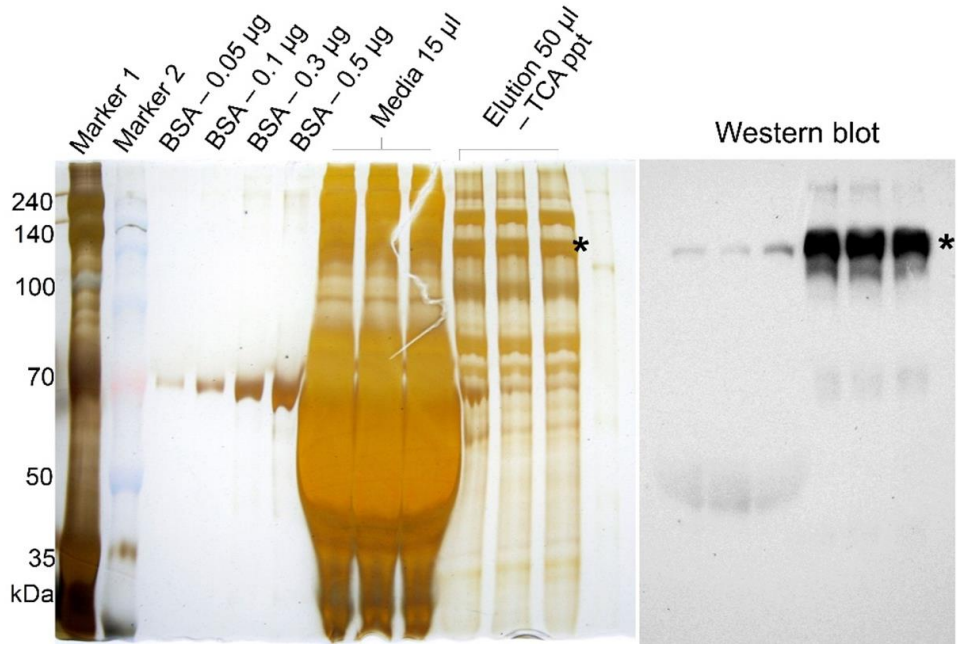

Figure 27. Partially purified NL1-R was quantified using BSA standards. The biotinylated band was verified using western blot (right panel). The relationship between fluorescence intensity and concentration of NL1-R was determined to be 19,000 MFI/µg NL1-R when measured using a microplate reader.

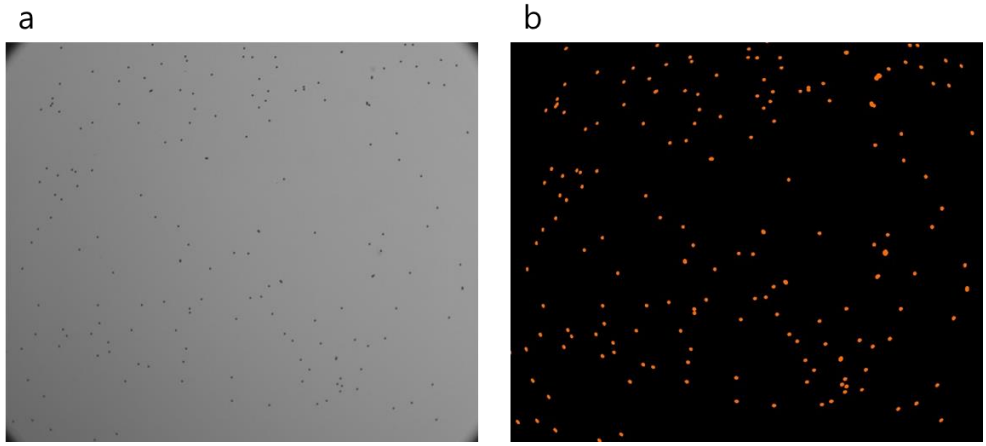

Figure 28. Purified biotin tagged NL1-R was immobilized on streptavidin contained 2.8 μm Dynabeads. (a) DIC image, (b) Fluorescence image. Since RFP is included, as shown in (b), red fluorescence was observed in addition to the shape of the bead.

3.4. Identification of induced artificial synapse

We then compared the synaptogenic activity of the engineered NL1 ectodomains by incubating them with DIV16 cultured neuronal cells for 24 h followed by immunocytochemistry (ICC) to identify immunopositive beads where synapsin I, a representative synaptic marker protein, was prominently clustered as a result of the formation of hemisynaptic boutons (figure 29).

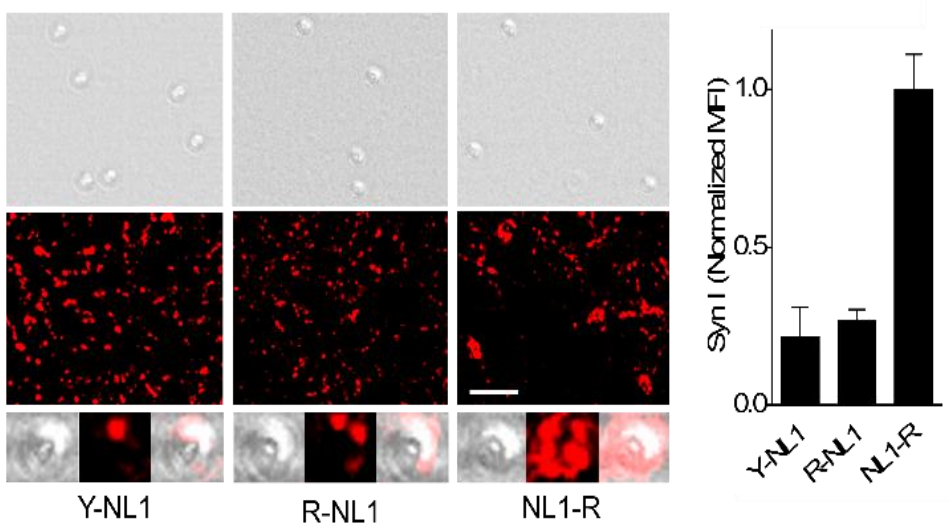

Figure 29[v]. NL1-R induces artificial synapse independently of SLB membrane. NL1-R has the strongest synaptogenic activity streptavidin coated Dynabeads when incubated with DIV14 hippocampal neuron culture for 2 days. Synapsin I (Syn I) aggregation were induced by NL1-R on streptavidin coated Dynabeads. Scale bars = 10 μm.

The dynabeads (Figure 29, left, upper images) to which each of the biotinylated NLs derivatives was fixed formed an artificial synapse by joining with randomly cultured hippocampal neurons. We found that although the N-terminally YFP-tagged NL1 was proven to have synaptogenic activity, biotin-tagged Y-NL1 was barely

[v] Eun Joong Kim contributed to this experiment.

functional compared to NL1-R when immobilized on the dynabeads. On the other hand, we observed that strong fluorescence was emitted by the C-terminally RFP-tagged NL1 on the microspheres and the most robust artificial synapse was induced. This indicated that the structural difference was important because synapses were induced through pairing with Nrxs even when the other components were the same. Furthermore, we separated and purified not only NL1 derivatives that induced an excitatory synapse but also NL2-R and SL3-R that induced an inhibitory synapse using the same experimental procedure, thereby verifying that an artificial synapse could be successfully induced.

4. Conclusion and Perspective

We have demonstrated the feasibility of engineered synaptic CAMs for the induction of artificial synapses. The synaptic CAMs can easily be biotinylated *in vivo*, purified, and quantified from their initial production to the final assay steps. The NL1 ectodomain allows C-terminal tagging for optical tracking and surface immobilization that dispenses with lipid bilayers for its synaptogenic activity. Removal of the lipid bilayer on inorganic substrates can greatly reduce the complexity and workload for establishing artificial synapses. This biased preference to a specific type of synapse induced by synaptic CAMs, if combined with other neuroengineering techniques such as micro- and nano-architectures for neural stimulation and recording, will provide unique possibilities for novel artificial neural interfaces. Moreover, this method will be used as the basis for studying the interaction between the cell and solid surface.

References

[1] K. Landsteiner, Harvard University Press, Cambridge, Massachusetts, 1945

[2] E. Engvall, P. Perlmann, *Immunochemistry* 1971, 8, 871-874

[3] N. Leffers, M. J. Gooden, R. A. Jong, B. N. Hoogeboom, K. A. Hoor, H. Hollema,H. M. Boezen,A. G. Zee, T. Daemen, H. W. Nijman, *Cancer Immunol. Immunother.* 2009, 58, 449-459

[4] S. Birtwell, H. Morgan, *Integr. Biol.* 2009, 1, 345-362

[5] M. Han, X. Gao, J. Z. Su, S. Nie, *Nat. Biotechnol.* 2001, 19, 631-635

[6] H. Fenniri, S. Chun, L. Ding, Y. Zyrianov, K. Hallenga, *J. Am. Chem. Soc.* 2003, 125, 10546-10560

[7] F. Cunin, T. A. Schmedake, J. R. Link, Y. Y. Li, J. Koh, S. N. Bhatia, M. J. Sailor, *Nat. Mater.* 2002, 1, 39-41

[8] Z. L. Zhi, Y. Morita, Q. Hasan, E. Tamiya, *Anal. Chem.* 2003, 75, 4125-4131

[9] D. C. Pregibon, M. Toner, P. S. Doyle, *Science* 2007, 315, 1393-1396

[10] E. J. Moran, S. Sarshar, J. F. Cargill, M. M. Shahbaz, A. Lio, A. M. Mjalli, R. W Armstrong, *J. Am. Chem. Soc.* 1995, 117, 10787-10788

[11] G. Shan, C. Lipton, S. J. Gee, B. D. Hammock, Handbook of Residue Analytical Methods for Agrochemicals, 2003

[12] P. Bostrom, J. Wu, M. P. Jedrychowski, A. Korde, L. Ye, J. C. Lo, K. A. Rasbach, E. A. Bostrom, J. H. Choi, J. Z. Long, S. Kajimura, M. C. Zingaretti, B. F. Vind, H. Tu, S. Cinti, K. Hohlund. S. P. Gygi, B. M. Spiegelman, *Nature.*

2012, 481, 463-469

[13] M. Sinha, Y. C. Jang, J. Oh, D. Khong, E. Y. Wu, R. Manohar, C. Miller, S. G. Regalado, F. S. Loffredo, J. R. Pancoast, M. F. Hirshman, J. Lebowitz, J. L. Shadrach, M. Cerletti, M. Kim, R. Serwold, L. J. Goodyear. B. Rosner, R. T. Lee, A. J. Wagers, *Science* 2014, 344, 649-652

[14] J. K. Lee, K. C. Ahn, O. S. Park, S. Y. Kang, B. D. Hammock, *J. Agric. Food Chem.* 2001, 49, 2159-2165

[15] https://en.wikipedia.org/wiki/Reference_ranges_for_blood_tests

[16] P. Lode, *Clin. Biochem.* 2005, 38, 591-606

[17] G. Amodia, G. Antonelli, F. D. Serio, *Curr. Vasc. Pharmacol.* 2010, 8, 388-393

[18] B. B. Haab, *Curr. Opin. Biotechnol.* 2006, 17, 415-421

[19] L. G. Feinberg, *Nature* 1961, 192, 985-986

[20] W. Zheng, L. He, *Advances in Immunoassay Technology.* 2012, 143-164

[21] M. F. Templin, D. Stoll, M. Schrenk, P. C. Traub, C. F. Vohringer, T. O. Joos, Trends Biotechnol. 2002, 20, 160-166

[22] D. A. Vignali, *J. Immunol. Methods* 2000, 243, 243-255

[23] Y. Li, E. C. Y. Liu, N. Pickett, P. J. Skabara, S. S. Cummins, S. Ryley, A. J. Sutherland, P. OKBrien, *J. Mater. Chem.* 2005, 15, 1238-1243

[24] H. Fenniri, L. H. Ding, A. E. Ribbe, Y. Zyrianov, *J. Am. Chem. Soc.* 2001, 123, 8151-8152

[25] R. Jin, Y. C. Cao, C. S. Thaxton, C. A. Mirkin, *Small* 2006, 2, 375-380

[26] N. P. Gerry, N. E. Witowski, J. Day, R. P. Hammer, G. Barany, F. Barany, *J. Mol. Biol.* 1999, 292, 251-262

[27] M. J. Dejneka, A. Streltsov, S. Pal, A. G. Frutos, K. Yost, P. K. Yuen, U. Muller, J. Lahiri, Proc. *Natl. Acad. Sci. USA* 2003, 100, 389-393

[28] K. C. Nicolaou, X. Y. Xiao, Z. Parandoosh, A. Senyei, M. P. Nova, Angew. Chem. Int. Ed. 1995, 34, 2289-2291

[29] M. J. Benecky, D. R. Post, S. M. Schmitt, M. S. Kochar, *Clin. Chem.* 1997, 43, 1764-1770

[30] F. E. Craig, K. A. Foon, *Blood* 2008, 111, 3941-3967

[31] D. P. Schrum, C. T. Culbertson, S. C. Jacobson, J. M. Ransey, *Anal. Chem.* 1999, 71, 4173-4177

[32] K. B. Kim, H. Chun, H. C. Kim, T. D. Chung, *Electrophoresis* 2009, 30, 1464-1469

[33] S. Joo, K. H.. Kim, H. C. Kim, T. D. Chung, *Biosens. Bioelectron.* 2010, 25, 1509-1515

[34] J. R. Askim, M. Mahmoudi, K. S. Suslick, *Chem. Soc. Rev.* 2013, 42, 8649-8682

[35] http://www.cardiogenics.com/market_advantages/CGNH_Magnetic_Beads_The_Needs.pdf

[36] M. J. Fritzler MJ, M. L. Fritzler, *Expert Opin. Med. Diagn.* 2009, 3, 81-89

[37] www.bangslabs.com

[38] www.thermofisher.com

[39] www.microspheres-nanospheres.com

[40] www.luminexcorp.com

[41] www.affymetrix.com

[42] www.miltenyibiotec.com

[43] www.bioneer.com

[44] Y. Yamamoto, S. Takeda, H. Shiigi, T. Nagaoka, *J. Electrochem. Soc*. 2007, 154, D462-D466

[45] S. Tokonami, Y. Yamamoto, Y. Mizutani, I. Ota, H. Shiigi, T. Nagaoka, *J. Electrochem. Soc.* 2009, 156, D558-D563

[46] H. Zhang, M. E. Meyerhoff, *Anal. Chem.* 2006, 78, 609-616

[47] Y. Cao, X. Hua, X. Zhu, Z. Wang, Z. Huang, Y. Zhao, H. gro, M. Lie, *J. Immunol. Methods* 2006, 317, 163-170

[48] R. Javier, Y. Tomoyuki, M. Fumio, *Biosens. Bioelectron.* 2011, 28, 443-449

[49] www.sekisuichemical.com

[50] J. R. Lee, J. Lee, S. K. Kim, K. P. Kim, H. S. Park, W. Yeo, *Angew. Chem. Int. Ed.* 2008, 47, 9518-9521

[51] J. Lee, J. Lee, T. D. Chung, W. Seo, *Anal. Chim. Acta* 2012, 736, 1-6

[52] J. Lee, J. Lee, H. Oh, H. Mok, W. Yeo, *Bull. Korean Chem. Soc.* 2012, 33, 3076-3078

[53] H. Seo, S. Kim, J. I. Kim, H. Kang, W. Jung, W. Yeo, *Anal. Biochem.* 2013, 434, 199-201

[54] S. Kwon, C. S. Jeon, N. Y. Hong, K. P. Kim, I. Hwang, T. D. Chung, *Chem.*

Commun. 2014, 50, 10066-10069

[55] G. P. Smith, V. A. Petrenko, *Chem. Rev.* 1997, 97, 391-410

[56] M. Mammen, S. Choi, G. Whitesides, *Angew. Chem. Int. Ed.* 1998, 37, 2754-2794

[57] C. Fasting, C. A. Schalley, M. Weber, O. Seitz, S. Hecht, B. Koksch, J. Dernedde, C. Graf, E. Knapp, R. Haag, *Angew. Chem. Int. Ed.* 2012, 51, 10472-10498

[58] C. B. Mao, A. Liu, B. Cao, *Angew. Chem. Int. Ed.* 2009, 48, 6790-6810

[59] G. P. Smith, *Science* 1985, 228, 1315-1317

[60] I. Hwang, *Sensors* 2014, 14, 13592-13612

[61] V. A. Petrenko, G. P Smith, X. Gong, T. Quinn, *Protein Eng*. 1996, 9, 797-801

[62] F. N. Dultsev, R. E. Speight, M. T. Fiorini, J. M. Blackburn, C. Abell, V. P. Ostanin, D. Klenerman, *Anal. Chem.* 2001, 73, 3935-3939

[63] E. Uttenthaler, M. Schraml, J. Mandel, S. Drost, *Biosens. Bioelectron.* 2001, 16, 735-743

[64] E. V. Olsen, I. B. Sorokulova, V. A. Petrenko, I.-H. Chen, J. M. Barbaree, V. J. Vodyanoy, *Biosens. Bioelectron.* 2006, 21, 1434-1442

[65] J. Brigati, D. D. Williams, I. B. Sorokulova, V. Nanduri, I.-H. Chen, C. L. Turnbough, Jr., V. A. Petrenko, *Clin. Chem.* 2004, 50, 1899-1906

[66] V. A. Petrenko, G. P. Smith, *Protein Eng.* 2000, 13, 589-592

[67] M. D. Sheets, P. Amersdorfer, R. Finnern, P. Sargent, E. Lindqvist, R. Schier, G. Hemingsen, C. Wong, J. C. Gerhart, J. D. Marks, *Proc. Natl. Acad. Sci.*

USA 1998, 95, 6157-6162

[68] T. Pulli, M. Hoyhtya, H. Soderlund, K. Takkinen, *Anal. Chem.* 2005, 77, 2637-2642

[69] M. Wikman, E. Rowcliffe, M. Friedman, P. Henning, L. Lindholm, S. Olofsson, S. Stahl, *Biotechnol. Appl. Biochem.* 2006, 45, 93-105

[70] S. Daly, P. Dillon, B. Manning, L. Dunne, A. Killard, R. OKennedy, *Food Agric. Immunol.* 2002, 14, 155-274

[71] Y. Jia, M. Qin, H. Zhang, W. Niu, X. Li, L.Wang, X. Li, Y. Bai, Y. Cao, X. Feng, *Biosens. Bioelectron.* 2007, 22, 3261-3266

[72] M. Sarikaya, C. Tamerler, A. Jen, K. Schulten, F. Baneyx, *Nat. Mater*. 2003, 2, 577-585

[73] K. T. Nam, D. Kim, P. J. Yoo, C. Chiang, N. Meethong, P. T. Hammond, Y. Chiang, A. M. Belcher, *Science* 2006, 312, 885-888

[74] J. H. Lee, P. F. Xu, D. W. Domaille, C. Choi, S. Jin, J. N. Cha, *Adv. Funct. Mater.* 2014, 24, 2079-2084

[75] H. Lee, H. K. Lee, H. Chang, H. Ahn, N. Erdene, H. Lee, Y. Lee, D. H. Jeong, J. Chung, K. T. Nam, *Small* 2014, 10, 3007-3011

[76] L. M. Chen, A. J. Zurita, P. U. Ardelt, R. J. Giordano, W. Arap, R. Pasqualini, *Chem. Biol.* 2004, 11, 1081-1091

[77] R. Edgar, M. McKinstry, J. Hwang, A. B. Oppenheim, R. A. Fekete, G. Giulian, C. Merril, K. Nagashima, S. Adhya, *Proc. Natl. Acad. Sci. U.S.A.* 2006, 103, 4841-4845

[78] K. Li, Y. Chen, S. Q. Li, G. N. Huong, Z. W. Niu, S. J. You, C. M. Mello, X. B. Lu, Q. A. Wang, *Bioconjugate Chem.* 2010, 21, 1369-1377

[79] S. Horikawa, D. Bedi, S. Q. Li, W. Shen, S. C. Huang, I. H. Chen, Y. T. Chai, M. L. Auad, M. J. Bozack, J. M. Barbaree, V. A. Petrenko, B. A. Chin, *Biosens. Bioelectron.* 2011, 26, 2361-2367

[80] J. A. Arter, J. E. Diaz, K. C. Donavan, T. Yuan, R. M. Penner, G. A. Weiss, *Anal. Chem.* 2012, 84, 2776-2783

[81] G. R. Souza, D. R. Christianson, F. I. Staquicini, M. G. Ozawa, E. Y. Snyder, R. L. Sidman, J. H. Miller, W. Arap, R. Pasqualini, *Proc. Natl. Acad. Sci. U.S.A.* 2006, 103, 1215-1220

[82] L. M. C. Yang, P. Y. Tam, B. J. Murray, T. M. McIntire, C. M. Overstreet, G. A. Weiss, R. M. Penner, *Anal. Chem*. 2006, 78, 3265-3270

[83] L. M. C. Yang, J. E. Diaz, T. M. McIntire, G. A. Weiss, R. M. Penner, *Anal. Chem*. 2008, 80, 933-943

[84] N. F. Steinmetz, E. Bock, R. P. Richter, J. P. Spatz, G. P. Lomonossoff, D. J. Evans, *Biomacromolecules* 2008, 9, 456-462

[85] J. S. Park, M. K. Cho, E. J. Lee, K. Y. Ahn, K. E. Lee, J. H. Jung, Y. J. Cho, S. S. Han, Y. K. Kim, J. Lee, *Nat. Nanotechnol*. 2009, 4, 259-264

[86] J. A. Arter, D. K. Taggart, T. M. McIntire, R. M. Penner, G. A. Weiss, Nano Lett. 2010, 10, 4858; g) J. H. Lee, J. N. Cha, *Anal. Chem*. 2011, 83, 3516-3519

[87] K. C. Donavan, J. A. Arter, R. Pilolli, N. Cioffi, G. A. Weiss, R. M. Penner, *Anal. Chem*. 2011, 83, 2420-2424

[88] J. H. Lee, D. W. Domaille, J. N. Cha, *ACS Nano* 2012, 6, 5621-5626

[89] R. Wilson, A. R. Cossins, D. G. Spiller, *Angew. Chem. Int. Ed*. 2006, 45, 6104-6117

[90] J. C. Love, L. A. Estroff, J. K. Kriebel, R. G. Nuzzo, G. M. Whitesides, *Chem. Rev*. 2005, 105, 1103-1169

[91] M. Schaeferling, S. Schiller, H. Paul, M. Kruschina, P. Pavlickova, M. Meerkamp, C. Giammasi, D. Kambhampati, *Electrophoresis* 2002, 23, 3097-3105

[92] C. J. Huang, Y. T. Li, S. Y. Jiang, *Anal. Chem*. 2012, 84, 3440-3445

[93] C. F. Barbas, Phage display : a laboratory manual Cold Spring Harbor Laboratory Press, Cold Spring Harbor, NY 2001

[94] W. Humphrey, A. Dalke, K. Schulten, *J. Mol. Graph. Model*. 1996, 14, 33-38

[95] Y. S. Nam, T. Shin, H. Park, A. P. Magyar, K. Choi, G. Fantner, K. A. Nelson, A. M. Belcher, *J. Am. Chem. Soc*. 2010, 132, 1462-1463

[96] J. R. Newton, Y. B. Miao, S. L. Deutscher, T. P. Quinn, *J. Nucl. Med*. 2007, 48, 429-436

[97] J. Muzard, M. Platt, G. U. Lee, *Small* 2012, 8, 2403-2411

[98] C. Jeppesen, J. Y. Wong, T. L. Kuhl, J. N. Israelachvili, N. Mullah, S. Zalipsky, C. M. Marques, *Science* 2001, 293, 465-468

[99] B. E. Collins, J. C. Paulson, *Curr. Opin. Chem. Biol*. 2004, 8, 617-625

[100] S. H. Wang, E. E. Dormidontova, *Soft Matter* 2011, 7, 4435

[101] D. Reeves, K. Cheveralls, J. Kondev, *Phys. Rev. E* 2011, 84, 021914

[102] M. F. Bear, B. W. Connors, M. A. Paradiso, Neuroscience : exploring the brain, Lippincott Williams & Wilkins, Philadelphia, PA 2007

[103] G. Greicius, L. Westerberg, E. J. Davey, E. Buentke, A. Scheynius, J. Thyberg, E. Severinson, *Int. Immunol*. 2004, 16, 353-364

[104] H. Connell, W. Agace, P. Klemm, M. Schembri, S. Marild, C. Svanborg, *Proc. Natl. Acad. Sci. U.S.A.* 1996, 93, 9827-9832

[105] J. Lederberg, E. L. Tatum, *Nature* 1946, 158, 558

[106] S. R. Kwon, C. S. Jeon, N. Y. Hong, K. P. Kim, I. Hwang, T. D. Chung, *Chem. Commun.* 2014, 50, 10066-10069

[107] M. Howarth, A. Y. Ting, *Nat. Protoc*. 2008, 3, 534-545

[108] A. N. Zacher, C. A. Stock, J. W. Golden, G. P. Smith, *Gene* 1980, 9, 127-140

[109] M. D. Scholle, U. Kriplani, A. Pabon, K. Sishtla, M. J. Glucksman, B. K. Kay, *Chembiochem* 2006, 7, 834-838

[110] P. Holliger, L. Riechmann, R. L. Williams, *J. Mol. Biol*. 1999, 288, 649-657

[111] E. Saxon, C. R. Bertozzi, *Science* 2000, 287, 2007-2010

[112] R. H. Christenson, H. M. E. Azzazy, *Clin. Biochem*. 2009, 42, 150-157

[113] E. G. Gray, *J. Anat*. 1959, 93, 420–433

[114] X. Yang, D. Hou, W. Jiang, C. Zhang, *Protein Cell* 2014, 5, 420–444

[115] E. R. Graf, X. Z. Zhang, S. X. Jin, M. W. Linhoff, A. M. Craig, *Cell* 2004, 119, 1013-1026

[116] C. Nam, L. Chen. *Proc Natl Acad Sci U S A*. 2005, 102, 6137-6142

[117] M. M. Baksh, C. Dean, S. Pautot, S. DeMaria, E. Isacoff, J. T. Groves,

Langmuir 2005, 21, 10693-10698

[118] K. Czöndör, M. Garcia, A. Argento, A. Constals, C. Breillat, B. Tessier, O. Thoumine. *Nat Commun.* 2013, 4, 2252

[119] K. Ichtchenko, Y. Hata, T. Nguyen, B. Ullrich, M. Missler, C. Moomaw, T. C. Sudhof, *Cell* 1995, 81, 435-443

[120] D. Arac, A. A. Boucard, E. Ozkan, P. Strop, E. Newell, T. C. Sudhof, A. T. Brunger, *Neuron* 2007, 56, 992-1003

[121] P. Scheiffele, J. H. Fan, J. Choih, R. Fetter, T. Serafini, *Cell* 2000, 101, 657-669

[122] Chubykin AA1, Liu X, Comoletti D, Tsigelny I, Taylor P, Südhof TC. J Biol Chem. 2005 Jun 10;280(23):22365-74

[123] A. Lucido, Suarez Sanchez F, Thostrup P, Kwiatkowski AV, Leal-Ortiz S, Gopalakrishnan G, Liazoghli D, Belkaid W, Lennox RB, Grutter P, Garner CC, Colman DR. J Neurosci. 2009 Oct 7;29(40):12449-66. doi: 10.1523/JNEUROSCI.1381-09.2009.

[124] M. B. Dalva, A. C. McClelland, M. S. Kayser, *Nat. Rev. Neurosci.* 2007, 8, 206-220

[125] C. Dean, F. G. Scholl, J. Choih, S. DeMaria, J. Berger, E. Isacoff, P. Scheiffele, *Nat. Neurosci*. 2003, 6, 708-716

[126] B. Chih, H. Engelman, P. Scheiffele, *Science* 2005, 307, 1324-1328

[127] B. Chih, L. Gollan, P. Scheiffele, *Neuron* 2006, 51, 171-178

[128] J. Y. Song, K. Ichtchenko, T. C. Sudhof, N. Brose, *Proc. Natl. Acad. Sci. U.S.A.*

1999, 96, 1100-1105

[129] G. Giannone, M. Mondin, D. Grillo-Bosch, B. Tessier, E. Saint-Michel, K. Czöndör, M. Sainlos, D. Choquet, O. Thoumine, *Cell Reports* 2013, 3, 1996-2007

[130] H. Takahashi, K. Katayama, K. Sohya, H. Miyamoto, T. Prasad, Y. Matsumoto, M. Ota, H. Yasuda, T. Tsumoto, J. Aruga, A. M. Craig, *Nat. Neurosci.* 2012, 15, 389-398

[131] Y. S. Yim, Y. Kwon, J. Nam, H. I. Yoon, K. Lee, D. G. Kim, E. Kim, C. H. Kim, J. Ko, *Proc. Natl. Acad. Sci. U.S.A.* 2013, 110, 4057-4062

[132] X. Chen, H. Liu, A. H. R. Shim, P. J. Focia, X. He, *Nat. Struct. Mol. Biol.* 2008, 15, 50-56

[133] D. Comoletti, R. Flynn, L. L. Jennings, A. Chubykin, T. Matsumura, H. Hasegawa, T. C. Sudhof, P. Taylor, *J. Biol. Chem.* 2003, 278, 50497-50505

[134] S. Pautot, H. Lee, E. Y. Isacoff, J. T. Groves, *Nat. Chem. Biol*. 2005, 1, 283-289

[135] K. T. Oneil, W. F. Degrado, *Science* 1990, 250, 646-651

[136] J. Koehnke, K. Jin, E. C. Budreck, S. Posy, P. Scheiffele, B. Honig, L. Shapiro, *P Natl Acad Sci USA* 2008, 105, 1873-1878

[137] J. W. Um, K. H. Kim, B. S. Park, Y. Choi, D. Kim, C. Y. Kim, S. J. Kim, M. Kim, J. S. Ko, S. G. Lee, G. Choii, J. Nam, W. D. Heo, E. Kim, J. O. Lee, J. Ko, H. M. Kim, *Nat Commun* 2014, 5, 5423

[138] M. Kallberg, H. P. Wang, S. Wang, J. Peng, Z. Y. Wang, H. Lu, J. B. Xu, *Nat.*

Protoc. 2012, 7, 1511-1522

[139] E. R. Graf, X. Z. Zhang, S. X. Jin, M. W. Linhoff, A. M. Craig, *Cell* 2004, 119, 1013-1026

[140] M. Howarth, A. Y. Ting, *Nat. Protoc*. 2008, 3, 534-545

[141] N. C. Shaner, M. Z. Lin, M. R. McKeown, P. A. Steinbach, K. L. Hazelwood, M. W. Davidson, R. Y. Tsien, *Nat. Methods* 2008, 5, 545-551

List of Publications

1. **Chang Su Jeon**, Inseong Hwang* and Taek Dong Chung*, "Virus-tethered Magnetic Gold Microshells with Biomimetic Architectures for Enhanced Immunoassay", *Adv. Fucnt. Mater*. 2013, 23, 1484-1489 (Cover paper)
2. Changrok Choi, Inseong Hwang, Young-Lai Cho, Sang Han, Donghyun Cho, Donggeun Jung, Dae Won Moon, Eun Joong Kim, **Chang Su Jeon**, Jeong Hun Kim*, Taek Dong Chung* and Tae Geol Lee*, "Fabrication and characterization of plasma-polymerized poly(ethylene glycol) film with superior biocompatibility", *ACS Appl. Mater. Interfaces* 2013, 5, 697-702
3. Hyoungseon Choi, Kwang Bok Kim, **Chang Su Jeon**, Inseong Hwang, Saram Lee, Hark Kyun Kim*, Hee Chan Kim* and Taek Dong Chung*, "Label-Free DC Impedance-based Microcytometer for Circulating Rare Cancer Cell Counting", *Lab Chip* 2013, 13, 970-977
4. Saram Lee, **Chang Su Jeon**, Inseong Hwang, Taek Dong Chung* and Hee Chan Kim*, "Simultaneous Detection of SERS and Fluorescence Signals Using a Single Excitation Laser Source for Microbead-Based Analysis", *J. Biomed. Nanotechnol.* 2013, 9, 1241-1244
5. Hyoungseon Choi, **Chang Su Jeon**, Inseong Hwang, Juhui Ko, Saram Lee, Jaebum Choo, Jin-Hyo Boo, Hee Chan Kim* and Taek Dong Chung*, "Flow Cytometry–based Submicron-Sized Bacterial Detection System using Movable Virtual Wall", *Lab Chip* 2014, 14, 2327-2333

6. Seung-Ryong Kwon, **Chang Su Jeon**, Nam Yong Hong, Kwang Pyo Kim*, Inseong Hwang* and Taek Dong Chung*, "Gold-plated magnetic polymers for highly specific enrichment and label-free detection of blood biomarkers under physiological conditions", *Chem. Commun.* 2014, 50, 10066-10069
7. Jangho Kim, Subeom Park, Yoen Ju Kim, **Chang Su Jeon**, Ki Teak Lim, Hoon Seonwoo, Sung-Pyo Cho, Taek Dong Chung, Yun-Hoon Choung*, Byung Hee Hong* and Jong Hoon Chung*, "Monolayer graphene-directed growth and neuronal differentiation of mesenchymal stem cells" J. Biomed. Nanotechnol. 11, 1-10 (2015), 2015
8. Eun Joong Kim‡, **Chang Su Jeon**‡, Soo Youn Lee, Inseong Hwang* and Taek Dong Chung*, "Fabrication of Robust Type-specific Hemisynapses Using Artificial Dendrites", *submitted*

요약 (국문초록)

고체상 추출은 시료를 전처리 하는 방법의 하나로 분석 분야에서는 복잡한 미지시료에서 관심 종을 분석하기 위한 분리, 농축 및 정제의 수단으로 사용되며, 최근에는 생체 모사 표면 공학을 통해 결합 친화성을 높이고 민감도와 선택성을 증가시키려는 노력들이 진행되고 있다. 혈액과 세포와 같은 복잡한 생체시료를 분석하기 위해서는 고체상 표면과 관심 종과의 물리/화학적 상호작용이 매우 중요하며, 관심 분석물질이 고체표면에 직접적으로 상호작용하는 유형과 세포와 같은 분석대상을 표면에 도입하여 분비되는 물질을 관찰하는 유형으로 구분할 수 있다. 본 학위 논문은 (i) 향상된 분석물질−고체표면 상호작용을 위한 생체 영감 표면 수식화 와 (ii) 인공시냅스 유도와 생분석을 위한 신경 세포 부착 단백질 정제의 응용사례를 보고했다.

파트1. 분석물질−고체 표면 상호작용: 향상된 면역분석법을 위한 생체 모사 건축물을 가진 바이러스로 꾸며진 자성 금 마이크로쉘

섬사상 파지 바이러스는 세포의 기능을 높이는 많은 가늘고 긴 구조와 유사한 구조적 차원들을 가지고 있다. 이 연구의 목적은 생물체의 시스템을 닮은 바이러스와 마이크로 입자의 결합이며, 그렇게 함으로써 독특한 형태에서 유래된 증가요소가 있다. 우리는 자기조립분자층을 형성하기 위해 마이크로 쉘 위에 금 층을 형성하고 이는 스트렙타아비딘을 사용한 화학조작과 비특이적 흡착을 방지하는데 도움이 된다. 파지 비리온들은 스트렙타아비딘으로 개질 된 금 마이크로쉘에 선택적으로 결합하기 위해 그들의 꼬리에 바이오틴이 결합되어 있다. 우리는 표면 대 부피 비

율 증가로 인해 바이러스 개질 된 금 마이크로쉘 위에 고정되는 항체의 양이 증가되는 것을 확인했다. 실제로 카디악 트로포닌I 와 마이오글로빈 각각이 검출되는 민감도가 증가했다. 이 연구는 바이러스와 비 생체 물질의 결합이 정량분석 가능한 향상된 면역분석을 위한 생체모방 수단이 될 가능성을 설명하고 있다.

파트2. 세포-고체 표면 상호작용: 인공 시냅스 유도를 위한 신경 세포 부착 물질 정제

전통적인 신경 인터페이스는 오로지 신경세포와 비 생물체의 수동적인 물리적 접촉에 의존한다. 하지만 뇌에서의 신경세포는 시·공간상의 특수함이 정교하게 조절된 시냅스를 통해 의사소통 한다. 이 시점에 우리는 새롭게 조작된 형광과 바이오틴이 붙어 정제, 정량, 추적, 무기 기질 위에 고정이 가능하게 하는 시냅스 후 세포 부착 물질을 보고한다. 방향성이 조절된 고정으로부터 유래된 지질 막 위의 시냅스 후 세포 부착 물질의 독립성은 신경세포와 다양한 무기 고체 기질간에 인공 시냅스 형성에 맞게 단백질의 기능성을 확장한다. 또한 세포와 고체 표면과의 상호작용을 연구하기 위한 기초로 활용될 것이다.

주요어: 골드 마이크로쉘, 서스펜션 어레이, 비특이적 흡착, 바이러스, 인공 시냅스, 뉴로라이긴, 신경세포 접착물질

학번: 2009-22920

이학박사 학위논문

생분석을 위한
표면 기능화 연구:
바이러스가 고정된 금 마이크로
쉘과 변형된 시냅스 유도 단백질

Surface Functionalization for
Bioanalytical Applications:
Virus-decorated Gold Microshells and
Modified Synaptic Cell Adhesion Molecules

2016년 2월

서울대학교 대학원

화학부 분석화학 전공

전 창 수

생분석을 위한 표면 기능화 연구:
바이러스가 고정된 금 마이크로
쉘과 변형된 시냅스 유도 단백질

Surface Functionalization for Bioanalytical Applications:
Virus-decorated Gold Microshells and
Modified Synaptic Cell Adhesion Molecules

지도교수 정 택 동

이 논문을 이학박사 학위논문으로 제출함

2016 년 2 월

서울대학교 대학원

화학부 분석화학 전공

전 창 수

전창수의 박사학위논문을 인준함

2016 년 2 월

위 원 장 이 연 (인)

부 위 원 장 정 택 동 (인)

위 원 주 재 범 (인)

위 원 남 좌 민 (인)

위 원 김 석 희 (인)

A Ph. D. Dissertation

Surface Functionalization for Bioanalytical Applications:

Virus-decorated Gold Microshells and Modified Synaptic Cell Adhesion Molecules

By

Chang Su Jeon

Supervisor: Professor Taek Dong Chung

Major: Analytical Chemistry

Department of Chemistry

Graduate School of

Seoul National University

February 2016

Abstract

Surface Functionalization for Bioanalytical Applications:

Virus-decorated Gold Microshells and Modified Synaptic Cell Adhesion Molecules

Chang Su Jeon
Department of Chemistry, Analytical Chemistry
The Graduate School
Seoul National University

Solid-phase extraction (SPE) is a sample preparation method used as a means of separation, concentration, and purification for analysis of complex unknown samples in the analytical field. Recently, there have been efforts to increase binding affinity, sensitivity, and selectivity through biomimetic surface engineering. In the analysis of complex biological samples, like blood and cells, physical and chemical interactions between the solid-phase surface and target species are crucial. These interactions can be divided into those in which the target analyte directly interacts with the solid surface and those in which the secreted substance is observed upon the introduction of target analyte, including cells, to the surface. This dissertation

describes (i) bio-inspired surface modifications for enhanced analyte-solid surface interactions and (ii) the purification of synaptic cell adhesion proteins for induced artificial synapses and bioanalysis.

Part I. Analyte-solid surface interaction: virus-decorated magnetic gold microshells with biomimetic architectures for enhanced immunoassays

Filamentous phage virus has similar structural dimensions to many cellular threadlike structures that enhance the cellular functions. The aim of this study was to combine the virus and microshells to resemble biological systems, thereby harnessing the enhancement factors originating from the unique morphology. We implemented gold layer on a microshell to form a self-assembled monolayer that help with chemical modifications using streptavidin and protection from non-specific adsorptions. Phage virions that carry biotins within their tails were prepared for directional binding of the virions to streptavidin-modified gold microshells. We confirmed the augmented yield of antibody loading on virus-modified gold microshells because of the increased surface to volume ratio. Indeed, the sensitivity has increased up to nine-fold for the detection of cardiac marker proteins. This work demonstrates the feasibility of merging viruses with non-biological substrates to yield biomimetic tools for the enhanced analyte-decorated solid surface interactions.

Part II. Cell-solid surface interaction: purified synaptic cell adhesion molecules for induced artificial synapse

Conventional neural interfaces solely depend upon passive physical contact between nerve cells and their non-biological counterparts. Nerve cells in the brain, however, communicate via synapses of which spatiotemporal specificity is exquisitely regulated. Here, we report a newly engineered postsynaptic cell adhesion molecules (CAMs) that are fluorescent and biotinylated to facilitate its purification, quantification, tracking, and immobilization on inorganic substrates. The independence of synaptic CAMs on the lipid membranes, originating from the orientation-controlled immobilization, extends versatility of the protein to fit in artificial synapse formation between neurons and various types of inorganic solid substrates. Moreover, this method will be used as the basis for studying the interaction between the cell and solid surface.

Keywords: gold microshell, suspension array, non-specific binding, virus, artificial synapse, neuroligin, synaptic cell adhesion molecules

Student number: 2009-22920

Contents

List of Figures

magnet was placed beside the tube.

Figure 6. Verification of the stability of SAM-modified gold microshells. SAM-protected gold microshells were incubated in phosphate-buffered saline (PBS) buffer at (a) 4 ℃ or (b) 25 ℃ for 24 hours. Each of (a) and (b) samples was incubated at 4 ℃ , 25 ℃ , 40 ℃ for 24 hours and then treated with streptavidin and biocytin-alexa594 for 1 hour at 25 ℃ to observe fluorescence. Biocytin-Alexa Fluor 594 dye was used for the determination of mean fluorescence intensity (MFI).

Figure 7. (a) Schematic representation of antibody immobilization on carboxyl-terminated gold microshells. After the primary antibody was attached to the surface of the gold microshells using EDC/NHS, the reaction was observed via fluorescence with an alexa488 conjugated secondary antibody. (b) DIC image. (c) Fluorescence image.

Figure 8. Optimization of antibody loading on gold microshells. (a) Schematic representation of antibody immobilization on thiol SAM-decorated gold microshells. (b) DIC and fluorescence images with different amounts of primary antibody, and a fixed amount of secondary antibody. (c) Fluorescence intensity according to the ratio of experimental to theoretical antibody.

Figure 9. Results of streptavidin immobilization on gold microshells. In (a) and (c), experiments using biocytin-Alexa 488 (upper panels) did not show fluorescence due to quenching whereas biocytin-Alexa 594 (lower panels) showed strong fluorescence. (b) and (d) indicate pretreatments with free biotin, and no fluorescence was observed.

Figure 10. Detection of cardiac troponin I in human serum.

Figure 11. (a) Phage vector map, fd-tet with SfiI and NotI cloning site in front of pIII. (b) Wild-type fd-tet and AP-representing fd-tet-APpIII virions (1013) were treated with BirA, followed by western blot visualized using streptavidin-HRP. (c) The two primer, SfiI-Avitag-NotI-F and SfiI-Avitag-NotI-R, were annealed and ligated with fd-tet phage vector (a) that had been digested with SfiI and NotI.

Figure 12. TEM image of PEG/NaCl-purified fd-tet-APpIII phage after 2% uranyl acetate staining. Scale bar = 200 nm.

Figure 13. BirA-treated fd-tet (upper panel) and fd-tet-APpIII (lower panel) phage virions (1.0×10^{10}) on streptavidin-SAM gold microspheres were detected using (a) Alexa Fluor® 610 Succinimidyl Esters, (b) rabbit anti-fd antibody and anti-rabbit Alexa Fluor® 610-R-PE antibody.

Figure 14. Optimization of surface modifications of Au microspheres with streptavidin and phage virions. Various amount of biotinylated phage virions were used for the titration of virus loading with the same reaction conditions as in Figure 15 (b).

Figure 15. (a) SEM image of bare magnetic gold microspheres (scale bar = 10 μm). (b) Magnified image of gold microspheres reveals the morphology of gold layer (scale bar = 2 μm). Pt-sputtered surface morphology of the beads that had been modified with carboxyl-terminated hexa(ethylene glycol) undecane thiol SAM (c), then conjugated with streptavidin (d), and finally with pIII-biotinylated fd-tet phage virions (e). Scale bars for c-e = 100 nm.

Figure 16. (a) SEM images of independent areas of streptavidin-modified gold microshells with Pt sputtering. (b) SEM images of independent areas of streptavidin-gold microshells treated with phage virions at various magnifications with Pt sputtering.

Figure 17. 3D N-SIM super resolution image from a100 nm Z-stack step size and 0.1 reconstruction factor. w/o phage (a) and w/ phage (b) (scale bar = 1 μm) at 1 μm streptavidin-coated microsphere.

Figure 18. Optimization of Staudinger ligation using mouse antibody. (a) Gold microspheres, covered with streptavidin or phage virions, were treated with four different concentrations of Sulfo-NHS-Phosphine, while mouse antibody were incubated with 0.1 mM and 1.0 mM NHS-PEG_{12}-Azide. (b) streptavidin or phage-covered gold microspheres were incubated with fixed concentration of phosphine (0.5 mM), while the concentration of azide varied. Anti-mouse Alexa Fluor 594 antibody was used for the determination of mean fluorescence intensity (MFI).

Figure 19. Sandwich immunoassay profiles (top) and representative fluorescence images of each functionalized microspheres corresponding to the w/o initial and final concentrations (bottom) tested for cardiac marker proteins. A range of cTnI in PBS (a), myoglobin in PBS (b), and cTnI in serum (c) were detected using virus- and streptavidin-gold microspheres (a and b), as well as polymer microspheres (c).

Figure 20. Immunoassay of cTnI in PBS buffer (10 ng/mL) using 10 μm diameter polystyrene beads whose surfaces were modified with an anti-cTnI

antibody using EDC/NHS chemistry. (a) DIC image. (b) Fluorescence image.

Figure 21. Genetic engineering of postsynaptic CAMs for facile mass production with in vivo biotinylation. SS, signal sequence; HA, hemagglutinin affinity tag; H6, hexa-His tag; GS, Gly-Ser rich linker; H8, octa-His tag; AP, biotin acceptor peptide; IRES, internal ribosome entry site. The SS, HA and H6 vary depending upon the type of the postsynaptic CAMs

Figure 22. HEK-293H cell viability assay in 800 μg/ml G418 for (a) 0, (b), 1, (c) 2, (d) 3, (e) 5, (f) 7 days.

Figure 23. Optimization of transfection methods for a HEK-293H cell line. Fluorescent images of GFP-transfected HEK-293H cells in three independent transfection experiments. (a) Calcium phosphate, (b) Lipofectamine 2000, (c) Polyethyleneimine.

Figure 24. (a) 4, (b) 9 and (c) 12 days after transfection. (d) DIC image of a single colony in which G418 selected NL1-R was expressed two weeks after transfection.

Figure 25. Merged fluorescence and DIC images of stable cell lines in which synaptic CAMs of (a) Y-NL1-G, (b) Y-NL1, (c) R-NL1, (d) NL1-R, (e) NL2-R, and (f) SL3-R were expressed.

Figure 26. Western blot profiles for the partially purified and labeled NL1s. The YFP-tagged NL1-GPI (Y-NL1-G) rarely appeared in the elution fraction despite its presence in the total cell lysate. When the GPI motif was replaced with AP, the YFP-NL1-AP (Y-NL1) was secreted into the culture medium, and was retained in a Ni-NTA resin. Both in vitro and in vivo biotinylation revealed biotinylated NL1

regardless of the position of the fluorescence protein. Y-NL1-G was probed by anti-NL1 antibody while the AP-tagged NL1s were detected using streptavidin-HRP.

Figure 27. Partially purified NL1-R was quantified using BSA standards. The biotinylated band was verified using western blot (right panel). The relationship between fluorescence intensity and concentration of NL1-R was determined to be 19,000 MFI/μg NL1-R when measured using a microplate reader.

Figure 28. Purified biotin tagged NL1-R was immobilized on streptavidin contained 2.8 μm Dynabeads. (a) DIC image, (b) Fluorescence image. Since RFP is included, as shown in (b), red fluorescence was observed in addition to the shape of the bead.

Figure 29. NL1-R induces artificial synapse independently of SLB membrane. NL1-R has the strongest synaptogenic activity streptavidin coated Dynabeads when incubated with DIV14 hippocampal neuron culture for 2 days. Synapsin I (Syn I) aggregation were induced by NL1-R on streptavidin coated Dynabeads. Scale bars = 10 μm.

List of Schemes and Tables

surface modifications by thiol SAM followed by chemical conjugation of streptavdin. The resulting streptavidin-modified microspheres are decorated with pIII-biotinylated phage virions that have filamentous structure, resembling the surface morphology of specific types of cells. The surface-exposed anime groups of N-termini of the viral major coat proteins are conjugated with phosphine and mixed with azide-modified primary antibodies to yield microspheres covered with high-density antibodies via bioorthogonal Staudinger ligation (figures shown cross-sectional area of virions layer and not drawn to scale).

Scheme 5. (a) Schematic representation of artificially induced neuronal cell-solid surface interfaces.

Scheme 6. (a) Schematic structure of artificial synapse displaying postsynaptic NL1 homodimer (NL1-R), NL2 homodimer (NL2-R), and Slitrk3 (SL3-R). The structures were modeled after NL1 (PDB ID, 3BIX) and NL2 (PDB ID, 3BL8), while the structure of Slitrk3 (27-627 residues) was predicted using Slitrk1 (PDB ID, 4RCW)[16] as a template by the RaptorX server, showing two LRR1 and LRR2 domains. (b) Schematic structures of engineered synaptic CAMs used in this study in comparison to wild type NL1 (WT). (c) Predicted structure of NL1-R-Nrx1β complex. The C-terminal tagging module for ectodomain of postsynaptic CAMs minimizes steric hindrance in pre- and postsynaptic CMAs interaction.

Table 1. Sorted by category of blood analysis.

Table 2. List of commercialized beads builders.

Table 3. List of commercialized beads products and services.

Part 1

Analyte-solid surface interaction:

Virus-decorated magnetic gold microshells with biomimetic architectures for enhanced immunoassay

1. Background and Overview

1.1. Immunoassay

The first immunoassay was developed by Landsteiner in 1954, who detected small molecules called "haptens" using antibodies [1]. In 1971, E. Engvall and P. Perlmann introduced enzyme-linked immunoassay [2], which is now known as the representative enzyme-linked immune-sorbent assay (ELISA); it is used to observe color changes using antibodies. Such immunoassays are widely used as quantitative methods for detecting supramolecules (e.g., cells, proteins, and polypeptides) and small molecules (lipids, hormones, chemicals, etc.) in various fields of molecular biology and environmental science. Color changes of substrates such as tetramethylbenzidine (TMB) and p-nitrophenyl phosphate (p-NPP) following reaction with antibodies were observed in traditional ELISA, but recently, ELISA-like technologies that do not use enzymes, but use a new reporter that generates various signals, have been widely adopted [3-10].

Immunoassays are categorized into optical and non-optical methods (electrochemical, mass sensitive, calorimetric) depending on the transducing mechanism. Optical immunoassay can be classified into the following 6 types: 1. UV/VIS spectroscopy, which measures the optical or electronic properties of a material, such as absorption, transmission, and reflectivity; 2. fluorescence, which measures the shift in the wavelength of the fluorophore, time dependence of

fluorescence emission, and energy transfer phenomena; 3. surface plasmon resonance, which measures the changes in wavelength, intensity, and the phase or angle of incidence; 4. chemiluminescence, which measures characteristic light from a reaction product prepared by oxidation of a luminol reactant; 5. Raman spectroscopy, which measures vibrational energy states; and 6. Interferometry, which measure the changes in the evanescent field. The optical immunoassay has the advantages of high sensitivity and high speed and benefit from developing infrastructure. Especially, as the fluorescence immunoassay method does not require additional substrate (TMB, p-NPP, luminol) is being widely used. The fluorescence immunoassay can be carried out by one of two methods: by conjugating the fluorophore or the quantum dot to the antibody. Of these two, the fluorophore-based method is widely used.

The representative advantage of immunoassay over other binding assays is its low detection limit and high analyte selectivity. On the other hand, its representative disadvantages are that it is greatly influenced by antibody activity and its cross reactivity with the structural analogs of the target analyte [11]. As indicated by Prof. B. M. Spiegelman [12] and Prof. A. J. Wagers [13], immunoassays using antibodies have become controversial, so much so that an article named 'Blame it on the antibodies' was published in Nature 2015. Although errors due to incorrect molecular recognition may arise with use of antibodies in immunoassays, no other substitute binding has been developed, and the immunoassay remains one of the preferred methods for biological sample analysis [14].

1.2. Planar array and suspension array

The quality and average expectancy of human life have increased with rapid advancements of modern science. In terms of disease diagnosis, specific test items have also increased with the advancement of science and technology. For example, there are over 200 test items (Table 1), including chemicals, DNA, lipid protein, and cells in a blood test [15], and early diagnosis is critical for disease prevention/treatment [16, 17].

Table 1. Sorted by category of blood analysis

	category	# of test
1	Ions and trace metals	17
2	Acid-base and blood gases	9
3	Liver function	9
4	Cardiac marker	9
5	Lipids	6
6	Tumour markers	9
7	Endocrinology	29
8	Vitamins	8
9	Toxins	2
10	Hematology	31
11	Immunology	25
12	Other enzymes and proteins	7
13	Other electrolytes and metabolites	12

Rapid, accurate, low-cost, and efficient detection and quantification of various disease markers from a limited amount of samples is the hot topic of interest in

analytical chemistry. The conventional immunoassay format of ELISA requires about 500 ng of capture antibody and 50~100 μL of a sample to analyze one specimen. As a result, an array type binding assay technology has been developed as a miniaturized, parallel binding assay for multiplexed detection [18]. The first multiplexed immunoassay was developed by L. G. Feinberg in 1961 for microspot test of antibody-antigen reaction in the thin agar films on the cover glass [19]. Since then, various attempts have been made, but the main approach can be divided into 2 general methods: the use of 2D planar micro arrays or 3D suspension array.

A 2D planar array is an assay that captures molecules immobilized in microspots (diameter < 250 μm), with several thousand spots exist per square centimeter [20]. The individual microspots are located hundreds of micrometers apart to prevent mutual contamination, and may immobilize different capture molecules. DNA chip and Protein chip are examples of 2D planar arrays, often referred to as a planar array or a microarray [21]. The protocol of a 2D planar array is similar to that of conventional ELISA, and generally scans fluorescence or chemiluminescent signals. For multiplexed detection, the different capture molecules must be located at nearby spots and the array needs to remember the immobilized capture molecule at each spot. When the X and Y locations are memorized in a 2D planar array for multiplexed detection, it is easier to remember the locations of the capture molecules, which is a comparatively easier barcoding method than 3D suspension array.

A 3D suspension array is an analytic system that suspends a few micrometer-

sized microspheres (particles or beads) of the immobilized capture molecules in a solution, and reacts them with an unknown sample to detect the signals from these particles. The suspension array has the following advantages over planar array. First, the total assay time (TAT) is shorter and a smaller sample volume is required. As the Micrometer sized particles have fast diffusion and smaller steric hindrance with their high surface to volume ratio, compulsory-mixed by external force is possible. Furthermore, a planar array must set adjacent spots apart by a fixed distance to prevent their cross contamination, creating a dead surface that consequently increases the area contacted by the sample solution. Therefore, the suspension array requires shorter total analysis time compared to the planar array, with a smaller sample volume. Second, it has greater sensing flexibility with the different capture molecules that can be mix-and-matched at different combinational at will. Third, the suspension array can replicate each target molecule from hundreds to thousands in the single experiment, offering greater reproducibility and high precision measurements. Fourth, it is cost-effective because of the reduced TAT and improved reproducibility and precision by performing only one experiment [20]. Unlike a 2D planar array, a 3D suspension array has suspended micrometer-sized particles that move while in solution, requiring barcoding for individual particles. The most widely used barcoding method is the optical one, which uses an organic dye [22], quantum dots [23], IR [24], or a Raman probe [25]. Chemical [26], graphical [27], electronic [28], and physical methods [29] are also used.

A planar array obtains signals by scanning, but a suspension array obtains

information using flow cytometry. Flow cytometry hydrodynamically focuses the suspended particles in a solution and passes a beam of light (usually laser light) of single wavelength through the suspension for the analysis. Coulter counter and fluorescence-activated cell sorter (FACS) are representative analytical methods of flow cytometry. Since the first report of flow cytometry in the 1960s, it has been used in a variety of areas, and has become an essential technique in the diagnosis of health disorders [30]. A conventional Coulter counter or FACS has the disadvantages of being expensive and very large. To compensate for these disadvantages, microfluidic chip based flow cytometry has been introduced. J. M. Ramsey distinguished 1- and 2 μm particles through electrokinetic focusing in a microchip and reported a throughput of 34 particles [31]. T. D. Chung *et al.* distinguished white blood cells and red blood cells using a microfluidic chip and direct current (DC) impedance [32], and in 2010, developed a microflow-cytometry system that could simultaneously detect particle size by DC impedance and fluorescence by laser [33]. Recently, a mixed planar array system has been reported, which can lithographically build a wall to immobilize the particles while scanning to detect signals [34].

1.3. Microspheres

Polymer particles, such as poly(methyl methacrylate) (PMMA), polystyrene (PS), or silica particles of 1~100 μm (mostly 2~15 μm) are generally used in 3D suspension array systems. Polymer or silica particles are separated by centrifugation, but magnetic particles, which encapsulate magnetic pigments such as iron oxide and

nickel particles or whose surfaces have been introduced with a magnetic pigment, are widely used. Presently, microspheres are moving beyond the academic field (Figure 1) of experimentation and are being widely used commercially. These types of microspheres are being widely used in clinical diagnostics, molecular assays/cellular assays (drug targeting, cell isolation and purification, nucleic acid or protein purification and detection) [35].

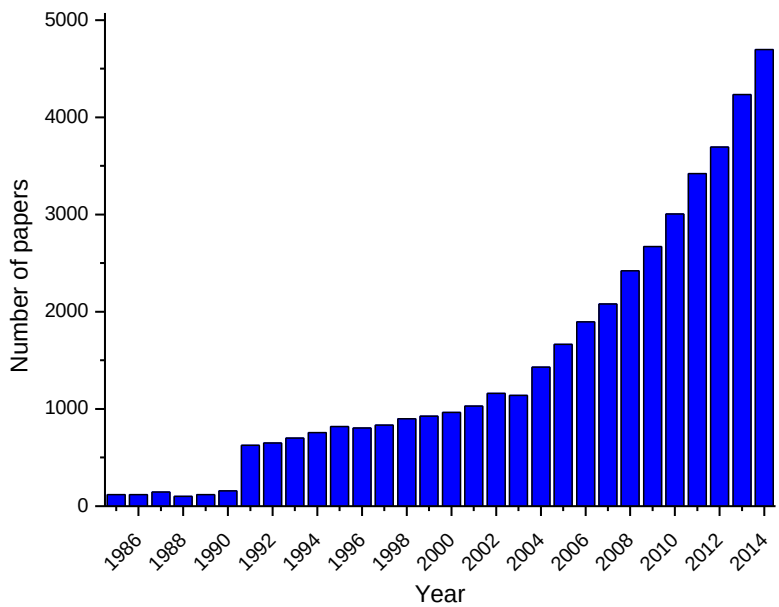

Figure 1. Number of papers published in each year between 1985 and 2014 in which terms microsphere and/or microspheres were used, according to the ISI Web of Knowledge scientific base search.

Many companies sell microspheres or microsphere-related products. For commercially available microspheres, certain beads builders sell naked beads (Table 2); however, most of the time, they sell surface-functionalized or modified beads, while also providing experimentation services (Table 3) [36].

Table 2. List of commercialized beads builders.

Company	Products	Location
Dynal Biotech Inc. → Thermo	Polymer	Norway
Merck Estabor → Millipore	Polymer/Silica	France
Seradyn Inc. →Thermo	Polymer	USA
Bnag's Lab.	Polymer/Silica	USA
Luminex Corp.	Polymer	USA
Immunico Corp. → Johnson&Johnson/Veridex	Polymer/Silica	USA
Spherotech Inc.	Polymer/Silica	USA
Advanced Magnetics Inc.	Polymer	U.K.
CPG Inc. → Millipore	Polymer	USA
Promega	Polymer	USA
Ferrofluidics Corp.	Polymer	USA
FeRx Inc.	Polymer	USA
Miltenyi Biotec	Polymer	Germany
PolyMicrospheres Inc.	Polymer	USA
Chemicell	Polymer/Silica	Germany

Bangs laboratories, Inc., established in 1988, provides 1–25 μm PS, PMMA, or SiO_2 particles whose surface have been aminated or caboxylated, or decorated with a certain antibody or protein [37]. Dynabeads, widely known as Thermo Fisher

Scientific Company, sells various products such as iron oxide type magnetism introduced 1, 2.8, 4.5 μm sized PS particles conjugated with glycidyl ether and having proteins on their surfaces [38]. The US microspheres-Nanospheres Company sells sub-micrometer sized particles of gold, silver, aluminum oxide, titanium oxide, silicon oxide and 1–100 μm particles of PS, PMMA, and SiO_2, as well as surface-functionalized products [39].

Table 3. List of commercialized beads products and services.

Company	**Products & Services**	**Location**
Marligen Biosciences	Transcription Factors	Maryland, USA
Panomics	mRNA, RNAi, Immunoassays	California, USA
Radix BioSolutions Ltd.	DNA Hybridization, Immunoassays	Texas, USA
Applied Cytometry Systems	Software & Assay Development	California, USA
Bio-Rad Life Science	Bio-Plex: Instruments, Cytokines, Isotyping, etc.	California, USA
Cayman Chemical Company	Cancer, Nitric Oxide, Apoptosis, etc.	Michigan, USA
Cogenics	Genotyping	North Carolina, USA
Eva Technologies Corp.	Autoimmunity, Cancer, etc.	Alberta, Canada
Exiqen	Gene Expression	Denmark
Expression Analysis	RNA Profiling & Genotyping	North Carolina, USA
INDOOR Biotechnologies, Inc.	Allergy	Virginia, USA
Invitrogen	Cytokines, Signal Transduction, Neuroscience, etc.	California, USA
Marligen Biosciences, Inc.	Genotyping & mRNA	Maryland, USA
Millipore Corp.	Cytokines, Apoptosis, Cardiac, Endocrine, etc.	Missouri, USA
MiraiBio	Equipment, Software & Materials	California, USA
Novagen	Cellular Signaling & Cancer	Wisconsin, USA
Panomics	Cellular Signaling, Cytokines, etc.	California, USA
PerkinElmer	Drug Discovery	Massachusetts, USA
QIAGEN	Instruments, Reagents & Cell Signaling	California, USA

R&D Systems, Inc.	Cytokines, MMP's, etc.	Minnesota, USA
Rules Based Medicine	Assay Services	Texas, USA
Wageningen University and Research Center	Plant pathogenic virus	The Netherlands
Abbott Molecular Inc.	FISH	Illinois, USA
Asuragen	Signature, Genetic Testing, Oncology	Texas, USA
BMD	Autoimmune & Infectious Disease	France
Bio-Rad Diagnostics	Autoimmune, etc.	California, USA
Celera Diagnostics	Infectious Disease &Cystic Fibrosis	California, USA
MiraiBio	Equipment, Software & Materials	California, USA
EraGen Biosciences	Genetic Analysis	Wisconsin, USA
Fisher Healthcare	Prima	Texas, USA
Focus Diagnostics	Assay Services	California, USA
INOVA Diagnostics, Inc.	Autoimmune Disease	California, USA
ImmuneTech	Allergy	California, USA
InnoGenetics NV	Neurodegeneration	Belgium
Inverness Medical Professional Diagnostics	Autoimmune Disease	New Jersey, USA
MICROBIONIX GmbH	Assay Services & Assay Development	Germany
Multimetrix GmbH	Infectious disease, Inflammation, Coagulation, etc.	Germany
One Lambda, Inc.	HTA Testing	California, USA
Tepnel Lifecodes	HLA Testing	Connecticut, USA
Zeus Scientific, Inc.	Autoimmune Disease	New Jersey, USA

The representative company that offers suspension arrays is Luminex Corp., established in 1996. They offer not only microspheres but also provide integrated support from signal readout devices to experimental services. Various chemical functional groups and oligomer or protein can be conjugated to a 5.6 μm size polystyrene particle, and 6.5 μm PS particles are used as magnetic microspheres [40]. Currently, 500-plex analysis is possible by swelling the polymer microspheres in an organic solvent and allowing two organic dyes of different proportions to enter the

microspheres, followed by shrinking them in an aqueous solution. Data can be acquired by flow cytometry, using the non-overlapping fluorophore wave as the target signal, and by barcoding and passing the microspheres through a fixed laser pathway. Like Luminex, Affymetrix also offers services related to microspheres that allow 100-plexed detection with an internal dye and 4–5 μm sized PS particles as the microspheres [41]. Miltenyi Biotec company offers 2, 3 μm microspheres, reagents; equipment; and total analysis service for flow cytometry and cell stimulation as a Magnetic Activated Cell Sorting (MACS) technology [42]. The Korean company Bioneer sells 1–5 μm SiO_2-based magnetic microspheres with various surface modifications [43].

In 2007, T. Nagaoka *et al.* made gold-coated microspheres on polystyrene and reported their applications. They attached gold nanoparticles to 6 μm polystyrene particles and plated them by electroless plating to form a gold layer, introducing various metal layers, such as nickel, silver and copper, on the polymers for application in electronic devices [44]. Furthermore, in 2009, they introduced a gold layer on plastic particles using a binder, describing its potential use as an anisotropic conductive film (ACF) [45]. M. E. Meyerhoff *et al.* reported the first instance of using magnetic gold microspheres for immunoassay in 2006. They introduced gold to 4.5 μm magnetic polystyrene microspheres through electroless plating, and covalently attached antibody fragments to a tosyl-activated surface; the absorbance signal was detected using alkaline phosphatase and p-NPP [46]. At the same time, M. Liu *et al.* proposed a fluorescence signal analysis system by attaching antibodies

after forming a gold layer on 100 μm PS particles [47]. In 2011, an immune-device system integrating gold microspheres with immobilized protein using self-assembled monolayers, microfluidic chip, and dielectrophoresis was reported [48]. Commercial gold microspheres can be purchased from the SEKISUI chemical corp. and the Nomadien corp. SEKISUI gold microspheres were developed for electric contact, and contain nickel inside with the surface gold layer [49]. Nomadien corp. introduced magnetism and a layer of gold on 2–15 μm polymer microspheres, and showed their potential use in detecting various biological molecules [50-54].

1.4 Viruses

Virus, a contagious particle of size less than a few hundred micrometers, replicates only inside the living cells of other organisms, and can be categorized into bacteriophages (shortened to phages), plant viruses, and animal viruses depending on the host. Early virus-related research was conducted in the fields of molecular and cell biology in the broad areas of life sciences and medicine. Recently, viruses have been used as chemical and biological sensors in material science and nanotechnology. Phages, which are used widely in sensing applications, have the following advantages. First is the well-established phage display technology. Phage display is a technique that selects the high-binding-affinity sequence by amplifying only the target-specific phage from a randomly sequenced phage library [55]. Second, they show high sensitivity and selectivity through target-specific recognition, an inherent virus function. Third, they exhibit multivalent interactions. A virus is composed of

several domain proteins, each domain having about 3000 copies. Therefore, a strong multivalence can be obtained if a target domain is given functionality [56, 57]. Fourth, they can be mass-produced in a cost-efficient manner in the host bacterial cell. Fifth, they have good chemical and thermal stability, allowing them to survive in acidic, basic, or non-aqueous media, and at temperatures up to 180 ℃. Sixth, they can be used as a template for self-assembly of uniform size and shape with a nucleation site [58].

Phages can be categorized into lytic phages, such as T4 and MS2 phages, which replicate in a bacterial cell and leave the host cell after killing it, and non-lytic phages, such as M13 and fd phages, which leave the host cell without killing it. The T4 bacteriophage, which is frequently shown in literature as having a spaceship-shaped icosahedral head and tail, has an inner diameter of 55 nm, tail length of 28.5 nm, and diameter of 19 nm. The MS2 phage, which looks like a nanosphere, has a diameter of 23–27 nm. Fd and M13 phages are nanofiber-shaped with a ~6 nm diameter and ~1 μm length. Filamentous M13 and fd phages have been the most-preferred genetically modified phages since G. P. Smith first introduced the phage display technology in 1985 [59].

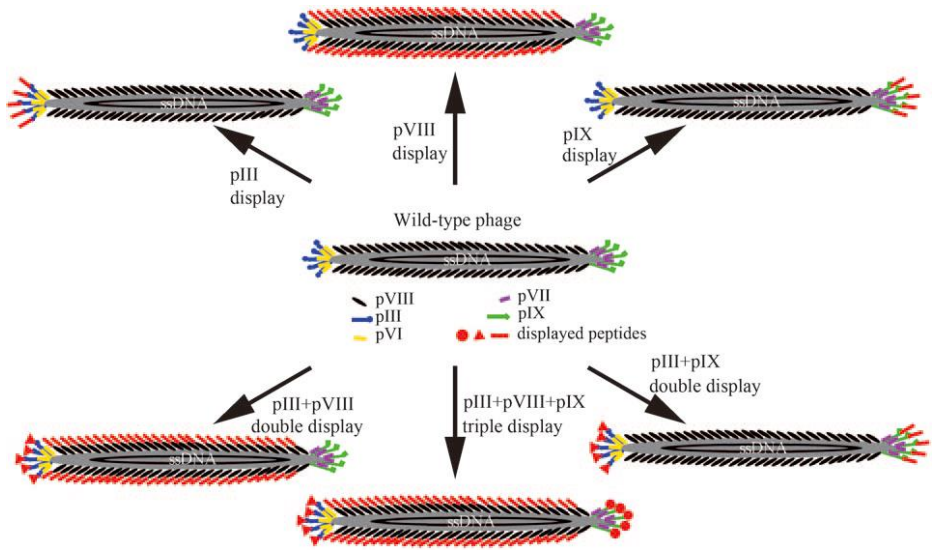

Figure 2. Structure of filamentous phage (M13 or fd) and the genetically engineered version. The phage DNA is encased in a capside made of four minor coat proteins (pIII, pIX, pVI, and pVII) located at one of the two distal ends of the phage and one major coat protein (pVIII), several thousand copies of which constitute the side wall of the phage. The landscape phaeg library was pioneered by V. A. Petrenko and G. P. Smith (adapted from reference [66]).

Of the 5 types of structural proteins that surround the internal single-strand DNA of the phages, genetic engineering techniques for the pIII and pVIII proteins have been reported most frequently, and two or more proteins can be genetically engineered simultaneously (Figure 2). For example, foreign peptides or proteins can be expressed in a certain structural protein by inserting the desired DNA sequence

in the gene of a phage vector. The yield of the structural protein with multiple copies is determined by the size and folding level of the expressed peptide; in general, a small peptide gives better expression than a large peptide.

As the filamentous phages are themselves nanoparticles, much attention has been paid not only for their sensing applications in terms of function and shape, but also as templates for nanostructure synthesis. They have been used as chemical and biological sensors [61] in a form that integrates the inherent target-recognition function of phages with the conventional methods of quartz crystal microbalance [62-64], ELISA [65-67], and optical [68, 69] and electrochemical methods [70, 71]. To use phages as a template to introduce metals or metal oxides, a nucleation site or affinity is needed; different combinations have been reported using phage display (PD) and cell-surface display (CSD) [72]. A. M. Belcher *et al.* at Massachusetts Institute of Technology conduct active research on the application of phages as a template. They reported the potential use of phage-templated nanowires as electrodes for lithium-ion batteries in their representative study published in Science in 2006 [73], with the nanowires made by expressing cobalt- and gold-nucleating motifs on phage body. J. N. Cha *et al.* detected surface-enhanced Raman spectroscopy signals after binding DNA-Raman-active nanoparticles to phages and loading the phages on silica microbeads [74]. K. T. Nam *et al.* successfully detected prostate-specific antigens using virus-probes, which were made by expressing the gold-binding peptide sequence on the phage body, integrating gold nanocubes, and immobilizing them on magnetic microbeads [75].

1.5 Purpose of this work

The major purpose of the current research was to develop a biocompatible and bio-inspired biosensor with high potential to be used for the improved analyte-solid surface interactions. In this work, we will focus on demonstrating the feasibility of our phage-decorated three-dimensional suspension array system using cardiac marker proteins, cardiac troponin I (cTnI) and myoglobin. While many assay systems based on microbeads lack quantitative mode of action, our virus-gold microshells clearly show the capability of quantitative assay.

2. Introduction

Recent outbreak of virus-based hybrid materials has enabled realization of highly selective and sensitive biosensors [58]. The benefits of the merger between virions and biosensing materials intuitively originate from the virion's capability of molecular recognition [76-80] and innate physical properties that stem from the phenotypic morphologies [81-88]. However, despite the functional advances in biosensors using virus hybrids, the detection systems largely remain in two-dimensional planar platforms, requiring relatively large sample volumes and greater time for analysis [58].

In this work, we demonstrate enhanced detection of protein biomarkers using gold-layered magnetic microspheres on which viral filaments are tethered in orientation-controlled manner. The magnetic gold microspheres, like many other typical microspheres, are compatible with flow cytometers, fluorescence activated cell sorting (FACS) systems, and conventional fluorescence microscopes, requiring minute sample volumes, and allowing statistical analysis that raises credibility [89]. Importantly, in contrast to nanoparticles, the gold microspheres are eligible for the detection of small molecule biomarkers in serum.

In biosensor development for immunoassays, preventing non-specific adsorption while providing high antibody loading is of primary importance. Since we had been experiencing a heavy non-specific binding to typical polymer beads

when using blood or serum samples, we envisioned that covering the porous and sticky surfaces of the polymer beads with gold and thiol self-assembled monolayers (SAMs) should resolve the adsorption problem. The SAM molecules, if properly chosen, are able to prevent non-specific interactions between gold surface and analytes as well as to provide functional groups for protein conjugation [90-92].

Filamentous bacteriophages, such as fd and M13, have nanostructured morphologies with contour length of ~ 1 μm and diameter of ~ 7 nm [93].

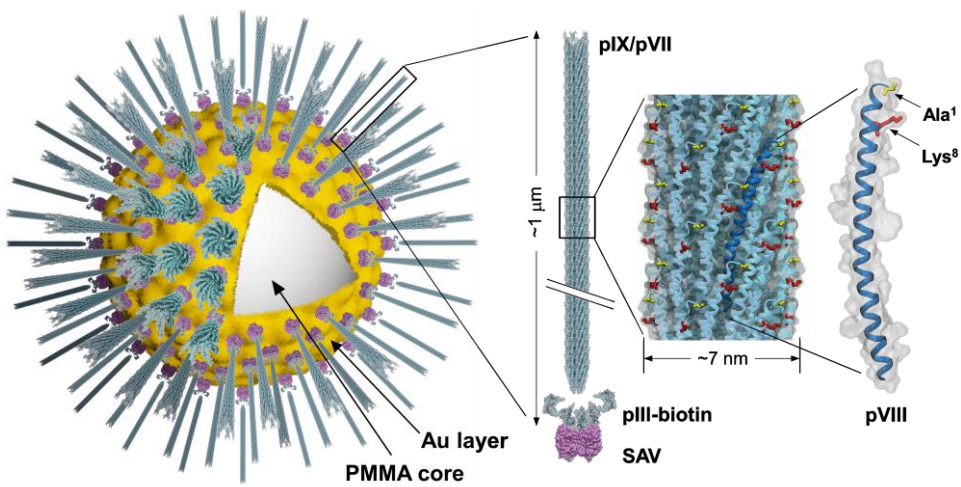

Scheme 1[i]. Schematic representation of the bioinspired virus-gold microsphere. A thin gold layer allows facile surface modifications by thiol SAMs followed by chemical conjugation of functional proteins, such as streptavidin (streptavidin,

[i] Dr. Inseong Hwang contributed to this scheme.

purple). The streptavidin-modified microspheres are decorated with pIII-biotinylated phage virions (pale blue) that have filamentous structure, resembling the surface morphology of some cells. The surface-exposed amine groups of N-terminal Ala-1 (yellow stick) and Lys-8 (red stick) of the viral major coat proteins (blue for a single pVIII unit) are used for the Staudinger ligation with primary antibodies to yield microspheres covered with high-density antibodies. Protein figures were generated using VMD [94] based on PDB code 1IFJ.

The viruses are comprised of five different kinds of structural proteins (pIII, pVI, pVII, pVIII, and pIX) that encase a single-stranded viral DNA. Among them, more than 2700 copies of the major coat protein pVIII serve for the assembly of filamentous structure with their ε-amino groups of Lys-8 and α-amino groups of N-termini being exposed, each of which have been successfully modified with macromolecules using chemical conjugation [80, 95-97]. A minor coat protein pIII, three to five copies per virion, has been dominantly used for the display of peptides and proteins (Scheme 1) [55].

The filamentous morphology of the filamentous (fd) virus provides unique opportunity to construct bioinspired architectures because the virus has similar structural dimensions to many cellular threadlike structures that leverage various cellular functions. Furthermore, in biorecognition processes, such as ligand-receptor interactions, longer and flexible tethers and polyvalency have proved to be beneficial

[98-101]. Indeed, in biological systems, neuronal cells are rich in neurites and filopodia that maximize the cellular interactions by forming synapses [102]. Leukocytes, macrophages, and some epithelial cells are covered with microvilli that facilitate cellular movement, adhesion, endocytosis, and exocytosis [103]. Similarly, some bacterial cells represent pili that help cell–cell interactions essential for mating; others have fimbriae that aid adhesion [104, 105]. Based on these observations, we reasoned that the surface of gold microspheres, once modified with nanostructured filamentous virions, would have greater surface to volume ratio, mimicking biological architectures and thus allowing high degree of conjugation with functional molecules, such as antibodies. Such an increased ratio of antibody to biomarkers, together with three-dimensional gold-SAM protected surface of microspheres and microvilli-like long virus tethers, would provide improved performance compared to conventional 2D or 3D detection systems.

3. Experimental methods

3.1. Reagents

Sulfo-N-hydroxysulfosuccinimide (Sulfo-NHS), sulfo-NHS-phosphine, NHS-PEG_{12}-azide, Streptavidin-coupled Dynabeads Myone T1 and 1-ethyl-3-[3-dimethylaminopropyl] carbodiimide hydrochloride (EDC) were purchased from Thermo Scientific (Rockford, IL). Carboxyl-terminated hexa(ethylene glycol) undecane thiol (CMT002) was obtained from Nanoscience Instruments (Phoenix, AZ). Biotin-terminated daca(ethylene glycon) ethane thiol (41156-1095) was purchased from Polypure (Oslo, Norway). Carbenicillin (Carb) and isopropyl β -D-1-thiogalactopyranoside (IPTG) were from Gold Biotechnology (St. Louis, MO). Streptavidin (SAV), bovine serum albumin (BSA), tetracycline (Tet), Tween-20, adenosine 5′-triphosphate (ATP), and cardiac troponin I (cTnI) were purchased from Sigma-Aldrich (St. Louis, MO). Plasmid pET21a-BirA was obtained from Addgene (Cambridge, MA). Magnetic gold microspheres (M-NG0501, Nomadien.com) were generated using proprietary methods including electroless plating of auric acids on proprietary magnetic poly(methyl methacrylate) (PMMA) beads (Nomadien.com) that were 15 μm in diameter. Nominal 10 μm diameter carboxylated polystyrene (PS) beads were from Polysciences (Warrington, PA). Phage vector, fd-tet with Sfi I and Not I cloning site in front of pIII, was kindly provided by Drs. Philipp Holliger and Chang-Hoon Nam. Rabbit polyclonal anti-fd (ab6188) and anti-cTnI (ab47003)

antibodies were purchased from Abcam (Cambridge, MA). Mouse monoclonal anti-cTnI antibody [19C7] was from GeneTex (Irvine, CA). Chicken Alexa Fluor 594 anti-mouse antibody (A21201), goat Alexa Fluor 610-R-Phycoerythrin (PE) anti-rabbit antibody, Alexa Fluor 594 biocytin, streptavidin conjugated with horseradish peroxidase (streptavidin-HRP), biotin, and bacterial cell lines for protein expression and phage amplification were obtained from Invitrogen (Carlsbad, CA). Myoglobin, rabbit polyclonal anti-myoglobin antibody (70-MR13), and mouse monoclonal anti-myoglobin antibody (10-M50A) were from Fitzgerald (North Acton, MA).

3.2. Fluorescence microscopy

Gold microspheres (~ 500) in phosphate buffered saline (PBS, 5 μL) were spotted on a glass slide. The fluorescence was monitored using Nikon Ti-E (Nikon, Japan) equipped with zyla sCMOS camera (Andor, Northern Ireland). At least thirty microspheres were chosen for the determination of mean fluorescence intensity (MFI) using NIS-Elements software version 4.2 (Nikon, Japan).

3.3. Field-Emission Scanning Electron Microscopy (FE-SEM)

The surface morphology of gold microspheres on a carbon tape was monitored using JSM 5410LV (JEOL, Japan) with 2 kV of acceleration voltage at the National Instrumentation Center for Environmental Management (NICEM), Seoul National University. To monitor the surface morphology of gold microspheres modified with

thiol SAM, streptavidin, and phage virions, Pt was sputtered using BAL-TEC SCD 005 sputter coater at 15 mA for 100 s.

3.4. N-SIM super resolution microscopy

Fd-tet-APpIII phage virions on streptavidin coated microspheres were detected using rabbio anti-fd antibody and anti-rabbit alexa Fluor 488 antibody. Phage decorated microspheres in PBS (5 μm) were spotted on a glass slide. The fluorescence was monitored using N-SIM super resolution microscope (Nikon, Japan) at the Boimedical Imaging Center (BIM) of Seoul National University.

3.5. Production of BirA

His-tagged BirA was prepared according to the provider's protocol with conditional modifications. Briefly, the pET21a- BirA plasmid was transformed into E. coli BL21(DE3)pLysS, plated on lysogeny broth (LB)-agar with Carb (100 μg/mL). A single colony was inoculated into LB-Carb media and was grown until the cell density reached mid-log phase when IPTG (1.0 mM) was added for induction. After overnight incubation at 37 ℃, the cells were harvested, broken by sonication, and centrifuged. The supernatant was loaded onto Co-NTA column to purify His-tagged BirA. Typically, a small-scale pilot test was performed using seven individual colonies when the best-expressing colony was used for the large-scale enzyme preparation.

3.6. Production of phages carrying biotinylation motif

The two primers, AP-F (5′-CGG CCA TGG CAG GTC TGA ACG ACA TCT TCG AGG CTC AGA AAA TCG AAT GGC ACG AAG GCT CCG GTG C-3′) and AP-R (5′- GGC CGC ACC GGA GCC TTC GTG CCA TTC GAT TTT CTG AGC CTC GAA GAT GTC GTT CAG ACC TGC CAT GGC CGG CT-3′), were annealed and ligated with fd-tet phage vector that had been digested with Sfi I and Not I. After the verification of the ligation by DNA sequencing, the phage vector was transformed into *E. coli* TG1 and grown in LB agar plate containing Tet (40 μg/mL) for 16 h at 37 ℃, the Next morning, a single colony was picked and inoculated into 3 mL of NZY liquid media with Tet (20 μg/mL) as a starter culture. For large-scale phage preparation, the starter culture was inoculated into NZY-Tet media (400 mL) and grown for 16 h at 37 ℃ with vigorous shaking. Phages were then purified by polyethylene glycol (PEG)/NaCl precipitation according to the standard protocols.

3.7. Biotinylation of phages

The purified phage virions (10^{13}) were incubated with BirA (30 nM), biotin (100 μM), and ATP (1 mM) in PBS-Mg (0.5 mL, pH 7.4 with 5 mM $MgCl_2$) for 2 h at 37 ℃. The phages were then precipitated by PEG/NaCl two times and the residual PEG/NaCl molecules were removed by buffer exchange using Centricon (MWCO = 100 kDa). The level of biotinylation was evaluated by western blot using streptavidin-HRP.

3.8. Surface modifications of gold microspheres

Gold microspheres (1 mg) was rotary incubated with thiol SAM molecules (1 mM) in 0.5 mL of ethanol for 16 h at 25℃. To the SAM-modified gold microspheres (5 μg) was added EDC (2 mM) and NHS (5 mM) in 0.5 mL of MES buffer, pH 5.0 for 30 min at 25 ℃. The beads were then washed with PBS (1 mL, pH 7.4) three times, followed by the addition of streptavidin (0.5 mg) in PBS (50 μL). The streptavidin-modified microspheres were treated with PBS-BT (PBS with 1% BSA, 0.1% Tween-20, pH 7.4) for 30 min and the streptavidin loading was verified using biocytin-Alexa Fluor 594.

3.9. Optimization of phage loading onto gold microspheres

A range of biotinylated phage virions were rotary incubated with streptavidin-modified gold microspheres (5 μg) in PBS-BT (50 μL) for 16 h at 25 ℃. As a negative control, wild-type fd-tet virions were used. After washing three times with PBS, the beads were treated with anti-fd rabbit IgG (37 ng) in PBS (50 μL) for 1 h at 25 ℃. After washing, the loading of phage virions were visualized by incubating with anti-rabbit Alexa Fluor 610-R-PE antibody (100 ng) in PBS (50 μL) for 1 h at 25 ℃, followed by the monitoring with a fluorescence microscope.

3.10. Optimization of staudinger ligation

Streptavidin-modified beads (5 μg) were incubated with varying amount of sulfo-

NHS-phosphine in PBS (0.5 mL) for 1 h at 25 ℃, which were used as a positive control. To build virus-immobilized beads, the streptavidin-modified beads were further incubated with 1.0×10^{10} of biotinylated phages in PBS-BT (50 μL) for 16 h at 25 ℃, washed three times with PBS-BT and three times with PBS, followed by an incubation with a range of Sulfo-NHS-Phosphine in PBS (0.5 mL) for 1 h at 25 ℃. For the Staudinger ligation, primary antibody from mouse (100 μg) was incubated with NHS-PEG_{12}-azide (0.1 and 1.0 mM) in of PBS (0.1 mL) for 1 h at 25 ℃, followed by overnight dialysis against PBS. The phosphine-treated streptavidin- and virus-gold microspheres (5 μg) were ligated with the azide-modified mouse antibody (0.5 μg) in PBS for 4 h at 37 ℃. The resulting beads were then washed three times with PBS-BT, followed by the incubation with anti-mouse Alexa Fluor 594 antibody for the fluorescence microscopic analysis. As a negative control, anti-mouse Alexa Fluor 594 antibody was directly treated with streptavidin- and virus-beads without azide-modified antibody and the background signals, if any, were subtracted.

3.11. Cardiac marker assays

Initially, the streptavidin- and virus-gold microspheres (5 μg) were treated with sulfo-NHS-phosphine (0.5 mM) in PBS (0.5 mL) for 1 h at 25 ℃, followed by the ligation with rabbit polyclonal anti-cTnI capture antibodies (0.5 μg) that had been incubated with NHS-PEG_{12}-azide (100 μM) in PBS (50 μL) for 4 h at 37 ℃. The resulting beads were then washed three times with PBS-BT and were mixed with cTnI (0.02, 0.2, 2, and 10 ng/mL) or myoglobin (0.02, 0.2, 2, 10, 40, and 100 ng/mL)

in PBS (0.5 mL) for 1 h at 25 ℃. For the detection of cTnI in human serum, PBS was replaced with cTnI-spiked human serum (0.02, 0.2, 2, and 10 ng/mL in 0.5 mL). The beads were then washed, incubated with mouse monoclonal anti-cTnI detection antibody [19C7] in PBS (500 ng, 50 μL) for 1 hr at 25 ℃, and visualized with anti-mouse Alexa Fluor 594 antibody (500 ng). For the determination of background signals, the assay was performed using the same conditions without marker proteins.

4. Results and Discussion

4.1. Characterization of magnetic gold microshells

Beads that are used in suspension arrays for bio-analysis are of low density and most of them use polymer microspheres, which are amenable to surface modification. However, these beads are not free from non-specific adsorption, which is a problem not only because it leads to adsorption of non-specific species into the microsphere surface, but also because of the introduction of these species into the polymer microsphere core. Therefore, in this study, we used gold microshells from Nomadien Corp. (www.nomadien.com), which consist of a thin gold layer that forms a metal barrier that blocks contact between the polymer core and external solution fundamentally while easily facilitating surface modification. Iron oxide was introduced into the poly(methyl methacrylate) (PMMA) surface to make the beads magnetic, and finally a gold layer was added using electroless plating (Figure 3a). The gold layer was approximately 200 nm thick, as verified by TEM (Figure. 3c), and its density was 2.64 g/mL.

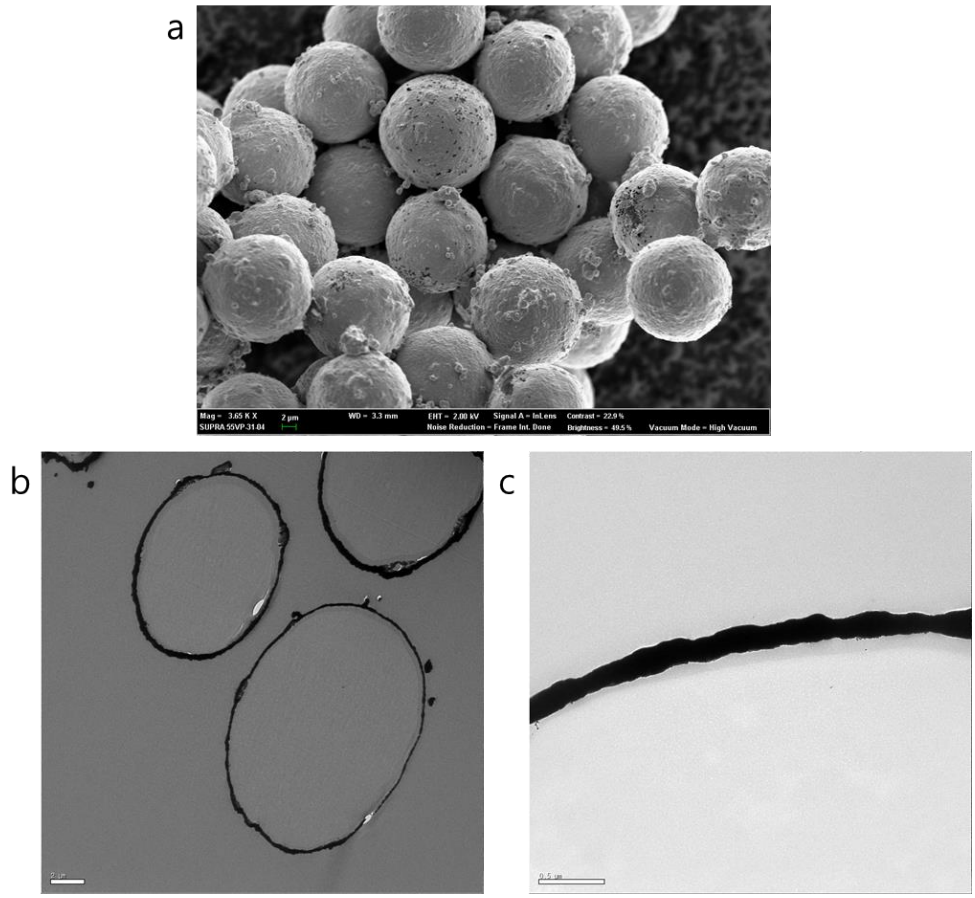

Figure 3. (a) SEM image of iron oxide embedded 15 μm magnetic gold microshells. TEM images of magnetic gold microshells (b) and (c). As shown in (c), the thin gold layer was less than 200 nm thick.

4.1.1. Testing the physical and chemical stability of gold microshells

To measure the physical and chemical stability of the gold microshells, a 5 μg gold microshell was added to ethanol, dimethyl sulfoxide, N,N-dimethylformamide or 1,4-dioxane solution. This was followed by sonication for 30 minutes and incubation for a further 15 hours.

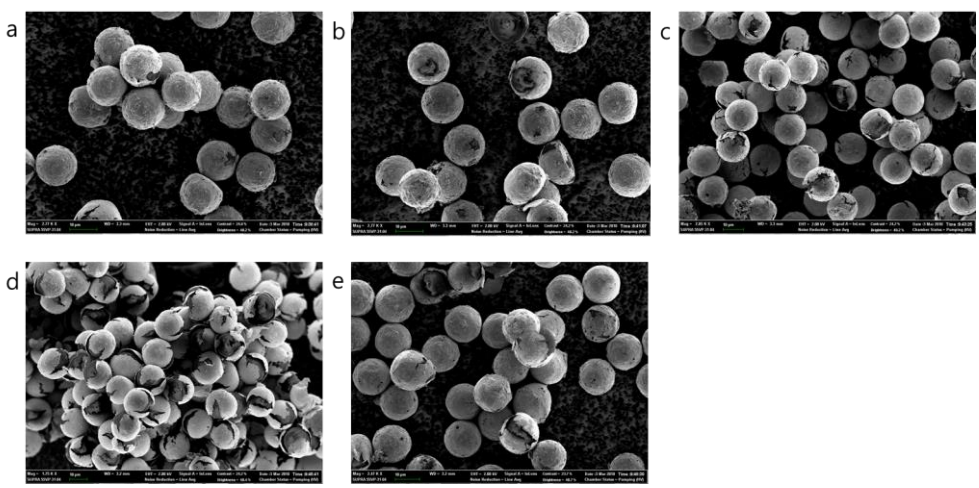

Figure 4. Solvent test of gold microspheres. SEM images of gold microshells that were put into (a) PBS buffer, (b) ethanol, (c) dimethyl sulfoxide, (d) N,N-dimethylformamide, or (e) 1,4-dioxane, followed by 30 minutes of sonication and a 16 h incubation at 25 ℃.

As shown in Figure 4, separation of the gold layer was observed as a swelling of the polymer microsphere in the organic solution. Separation of the gold layer was also observed when sonication was performed for more than 30 min. We did not observe cracking of the gold layer in the water and ethanol solution (Figure 4a-b). Thus, we confirmed that the gold layer is stable in an ethanol solution and remain stables even after up to three minutes of sonication.

Next, we prepared SAM-protected gold microspheres using carboxyl-terminated hexa(ethylene glycol) undecane thiol, followed by protein conjugation using 1-ethyl-3-(3-dimethylaminopropyl)-1-carbodiimide hydrochloride (EDC) and N-hydroxysuccinimide (NHS). The gold-layered microspheres were stable in ethanol for 16 h, enough time for SAM formation. The bead system facilitated chemical conjugation of protein on the SAM-modified gold microspheres using EDC-NHS in that the unreacted excessive EDC and NHS could be easily washed out. When gold microshell powder was added to the solution, the gold-gold affinity increased, resulting in aggregation (Figure 5a). However, because the SAM-protected gold microshells have a high affinity for gold-thiol, they formed single beads (Figure 5b). The SAM-protected gold microshells were well dispersed in the solution (Figure 5c) and could be collected using a magnet after 30 seconds (Figure 6d).

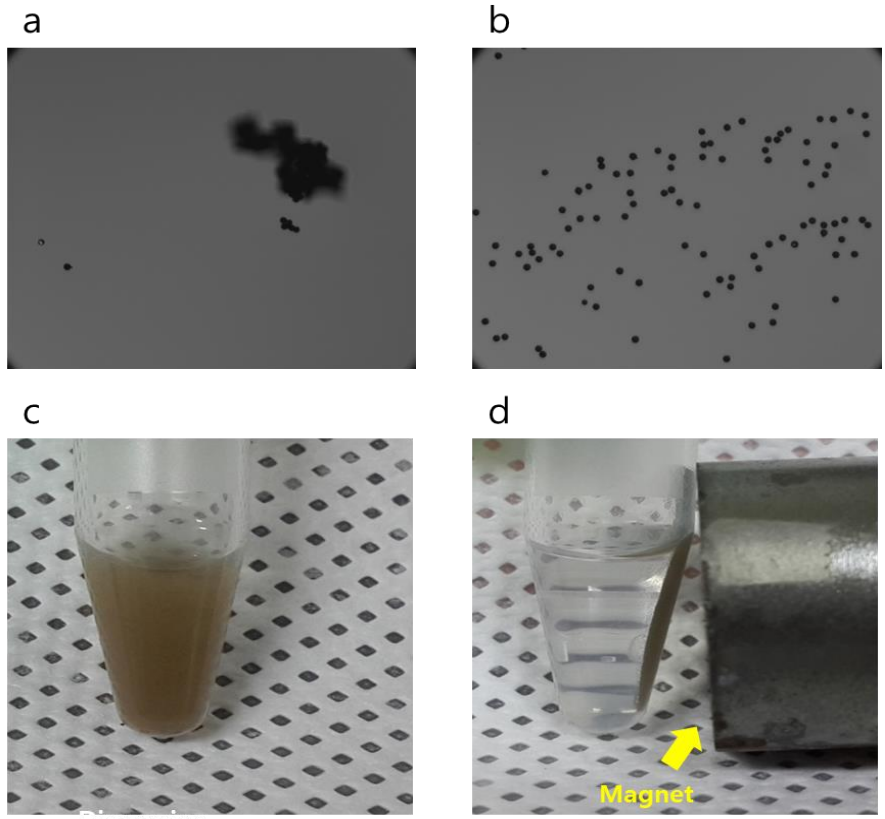

Figure 5. (a) Optical image of the gold microshell before the SAMs were formed (b) Optical image of the gold microshell after the SAMs were formed (c) Dispersion state in the solution after the SAMs were formed (d) Image at 30 seconds after a magnet was placed beside the tube.

To investigate the effect of temperature on SAM formation, SAM-modified gold microshells were incubated for 24 hours at either 4 ℃ or 25 ℃ and then

incubated with Alexa 594 conjugated biocytin at 4 ℃, 25 ℃ or 40 ℃. As shown in Figure 6, the fluorescence values for all samples were not significantly different within the error range. This result indicates that there was no desorption of SAM molecules at either 4 ℃ or 25 ℃ and there was no effect of temperature on streptavidin and biocytin-Alexa 594.

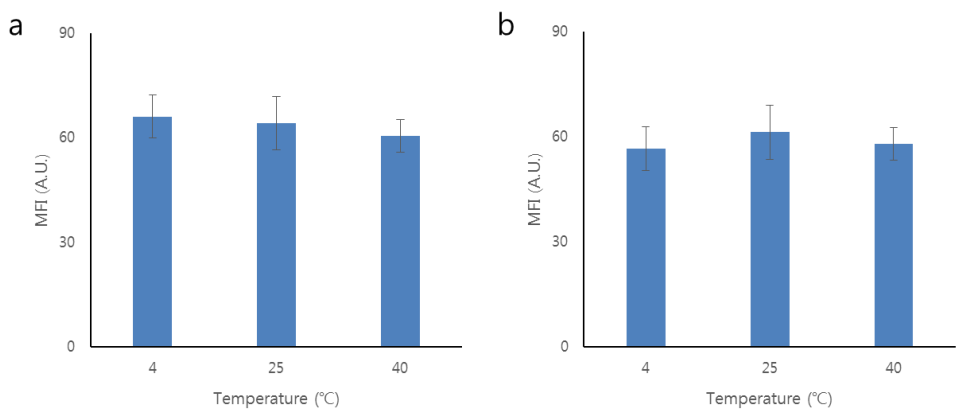

Figure 6. Verification of the stability of SAM-modified gold microshells. SAM-protected gold microshells were incubated in phosphate-buffered saline (PBS) buffer at (a) 4 ℃ or (b) 25 ℃ for 24 hours. Each of (a) and (b) samples was incubated at 4 ℃ , 25 ℃ , 40 ℃ for 24 hours and then treated with streptavidin and biocytin-alexa594 for 1 hour at 25 ℃ to observe fluorescence. Biocytin-Alexa Fluor 594 dye was used for the determination of mean fluorescence intensity (MFI).

4.1.2. Protein immobilization of gold microshells

Having verified the stability of the thiol SAMs-treated gold microshells, we wanted to determine whether the protein could be incorporated into them. After activating the carboxyl-terminated gold microshells using EDC/NHS, the primary antibody was covalently attached and fluorescence was observed using an alexa488 conjugated secondary antibody (Figure 8a). As shown in Figure 7c, green fluorescence was observed on the gold microshells, indicating that the protein had successfully attached.

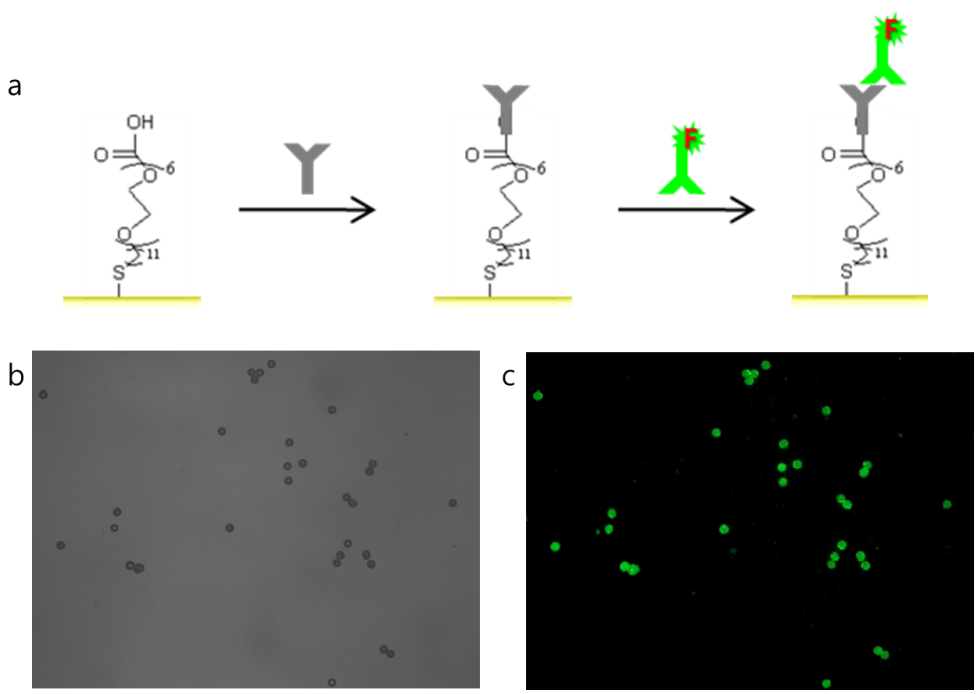

Figure 7. (a) Schematic representation of antibody immobilization on carboxyl-

terminated gold microshells. After the primary antibody was attached to the surface of the gold microshells using EDC/NHS, the reaction was observed via fluorescence with an alexa488 conjugated secondary antibody. (b) DIC image. (c) Fluorescence image.

To optimize protein immobilization on the gold microshells, we tested different numbers of gold microshells, antibody concentrations, working volumes, and reaction times. Full-length IgG antibodies have a molecular weight of 150 kDa and a size of 3 nm × 15 nm × 15 nm, and we assumed their area as 2 nm × 4 nm. Given the three-dimensional curvature of the microspheres, the degree of freedom of polyethylene glycol and the size of a single chain fixed at the surface, we estimated that 5 μg of 15 μm sized gold microshells would require 24 ng of antibody. The following conditions were fixed: 5 μg gold microshells, 500 μL working volume, 1 h reaction time, and 2 μg secondary antibody. Only the amount of primary antibody was changed, and the degree of protein attachment was determined by the level of fluorescence (Figure 8a). A fluorescence value for the ratio of experimental value to theoretical value of the antibody was determined (Figure 8c), and with the use of approximately more than 20 times the amount of antibody, saturated fluorescence was found such that 500 ng used with 5 μg of gold microshells was sufficient. Thus, results from this experiment indicate that when proteins were fixed and secondary antibody was used, 0.5 μg of protein was used in 5 μg gold microshells.

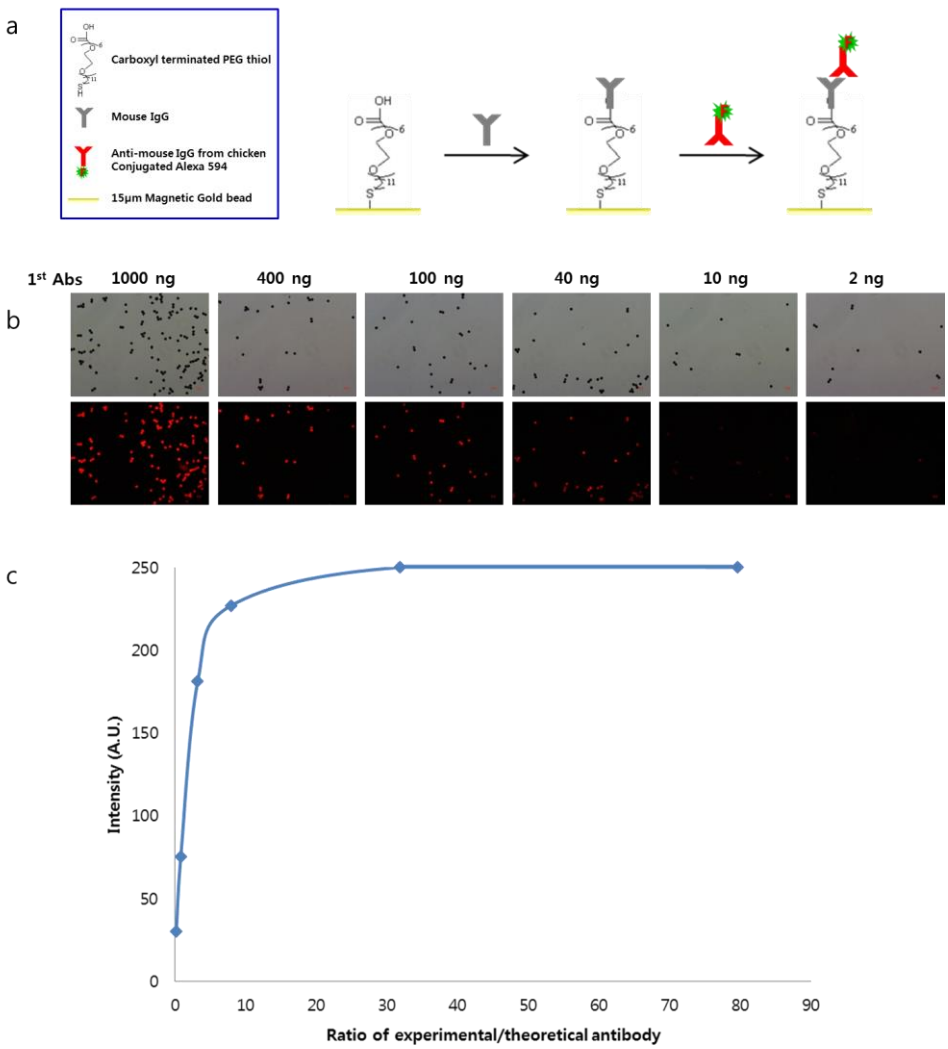

Figure 8. Optimization of antibody loading on gold microshells. (a) Schematic representation of antibody immobilization on thiol SAM-decorated gold microshells. (b) DIC and fluorescence images with different amounts of primary antibody, and a fixed amount of secondary antibody. (c) Fluorescence intensity according to the ratio of experimental to theoretical antibody.

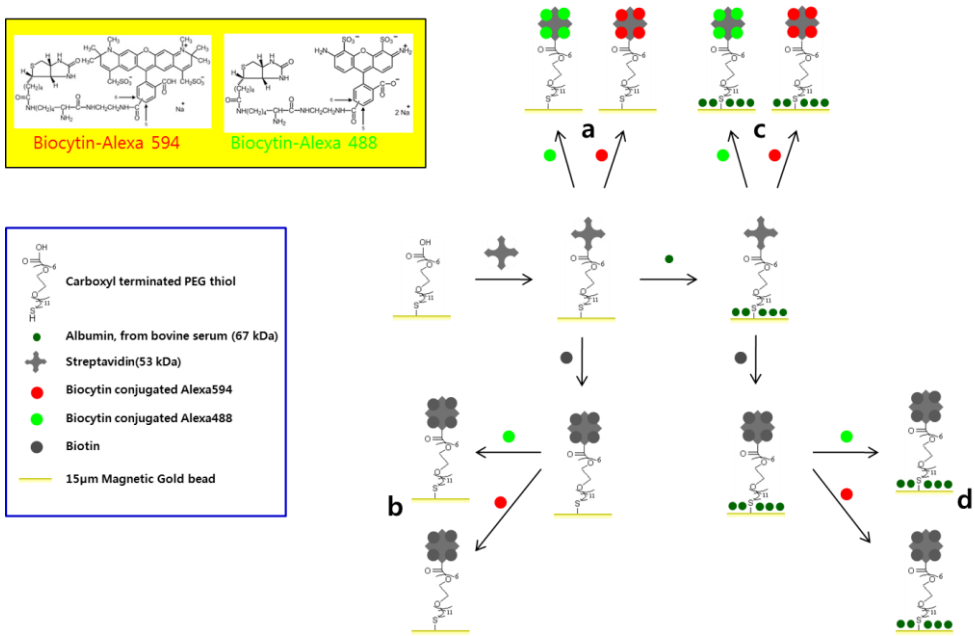

Scheme 2. Schematic representation of streptavidin immobilization on gold microshells to determine the quenching effect. (b) and (d) are a control experiment after pretreatment with free biotin. (a) and (b) are pretreatments without albumin.

Next, we evaluated streptavidin conjugation using biocytin-Alexa Fluor 594 and biocytin-Alexa Fluor 488 (Scheme 2). When the beads were pre-treated with free biotin, no fluorescence was observed after incubation with fluorescent biocytin (Figure 9b and d). In contrast, we observed strong fluorescence signals when the beads were directly incubated with the fluorescent biocytin (Figure 9 Lower panel a, c). Unexpectedly, no green fluorescence was observed following incubation with

biocytin-Alexa Fluor488 (Figure 9 Upper panels a, c). This could be because the green fluorescence was quenched by the gold because there is some overlap between the maximum absorption wavelength of the absorption spectrum in the gold visible light region and the green region. Thus, we repeated the experiments only using red based fluorescence (biocytin-Alexa 594) and were able to observe fluorescence on the beads (Figure 9). In addition, in bio-analysis experiments, and in particular those involving blood, it is possible that proteins in the serum, such as albumin, could be a problem when using the polymer microspheres. However, we showed that there was no significant difference in fluorescence values following pretreatment with albumin (Figure 9a and c, lower panel).

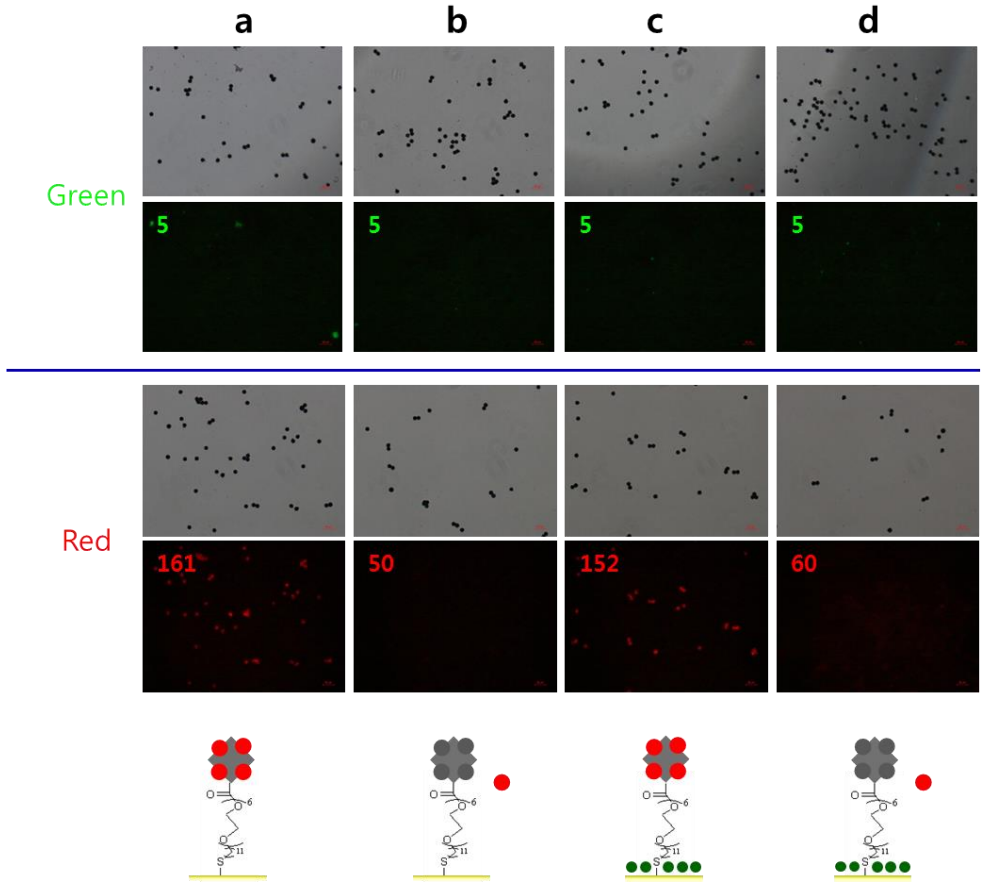

Figure 9. Results of streptavidin immobilization on gold microshells. In (a) and (c), experiments using biocytin-Alexa 488 (upper panels) did not show fluorescence due to quenching whereas biocytin-Alexa 594 (lower panels) showed strong fluorescence. (b) and (d) indicate pretreatments with free biotin, and no fluorescence was observed.

4.1.3. Sandwich immunoassay of antibody-decorated gold microshells

Using antibody-decorated gold microshells fixed directly with SAM molecules, a spike test of cardiac troponin I was conducted in human serum. A polyclonal antibody was covalently attached to the gold microshell using EDC/NHS and a sandwich-type immunoassay was performed after detecting a biomarker from the human serum (Scheme 3). For the control experiments, a carboxyl-terminated polymer microsphere was used and conditions without a biomarker or without a monoclonal antibody were compared to determine the level of fluorescence caused by non-specific binding.

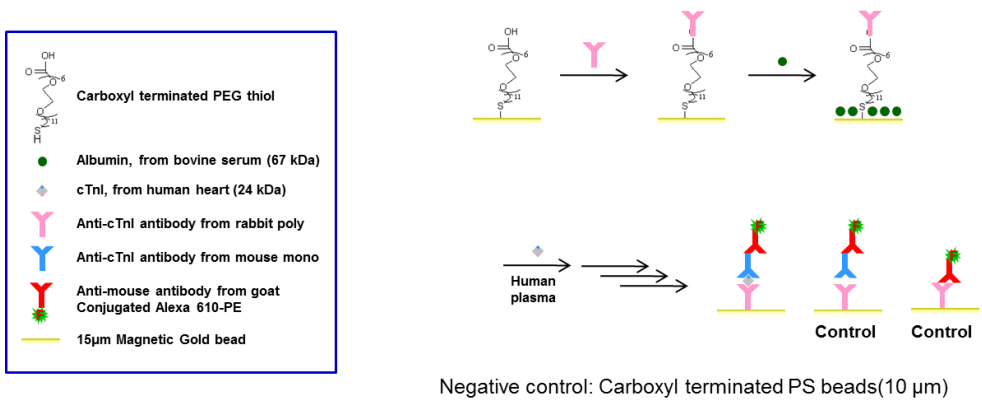

Scheme 3. Schematic representation of the 100 ng/mL cardiac troponin I assay in human serum.

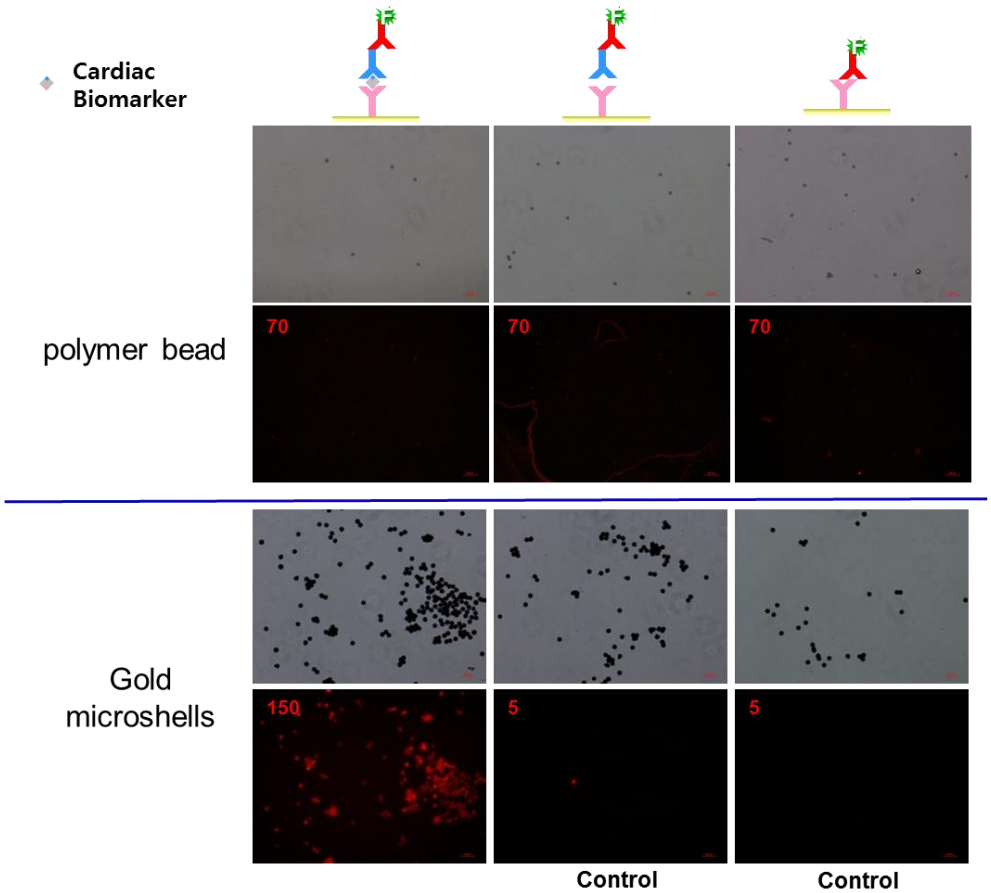

Figure 10. Detection of cardiac troponin I in human serum.

We verified that the mean fluorescence intensity (MFI) was approximately 150 for the gold microshells when 100 nm/mL cardiac troponin I was spiked in human serum. For polymer microspheres, high background fluorescence of 70 MFI was measured. This value was similar to that of a control sample in the absence of cardiac troponin I due to non-specific adsorption of secondary antibody. Gold microshells

in the absence of cardiac troponin I had a MFI value of approximately 5, which indicated significantly low non-specific adsorption. We inferred that this was due to the effect of the polyethylene glycol in the thiol SAM molecule and a thin gold layer that forms a metal barrier and blocks contact with the polymer core. Our colleague, S. R. Kwon, discovered how to prevent non-specific adsorption effectively using the same magnetic gold microshell and PEG-thiol SAM molecules that we used through MALDI analysis [106]. S. R. Kwon *et al*. shows the MALDI-TOF mass spectra for commercial polymer microspheres and for the magnetic gold microshells used in our experiments. A human serum albumin peak of non-specific adsorption was detected at 33 and 66 kDa , but was not detected with magnetic gold microshells. The detection ability of Myoglobin, which is a target biomarker, showed that the magnetic gold microshells had the best result. Based on the above results, polyethylene glycol and the metal barrier are both effective at suppressing non-specific adsorption.

4.2. Preparation and characterization of engineered phage virions

To prepare microshells covered with threadlike nanostructured surface, we employed fd-tet phage virus that has intriguing morphology similar to cellular microvilli-like edifice. A 14-mer bacterial biotin acceptor peptide (AP), GLNDIFEAQKIEWHE [107], was introduced using SfiI and NotI cloning sites in front of pIII of fd-tet (Figure 11) [108].

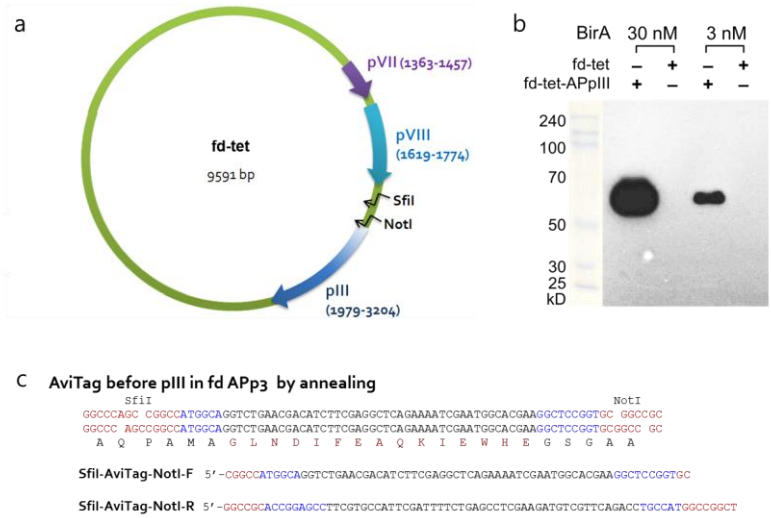

Figure 11. (a) Phage vector map, fd-tet with SfiI and NotI cloning site in front of pIII. (b) Wild-type fd-tet and AP-representing fd-tet-APpIII virions (10^{13}) were treated with BirA, followed by western blot visualized using streptavidin-HRP. (c) The two primer, SfiI-Avitag-NotI-F and SfiI-Avitag-NotI-R, were annealed and ligated with fd-tet phage vector (a) that had been digested with SfiI and NotI.

Since the ε-amino group of Lys, a specific biotinylation site within the AP tag, is vulnerable to chemical modification by NHS for the subsequent Staudinger ligation, we tried in vivo biotinylation of phages by endogenous biotin ligase BirA that recognize AP in bacterial cells [107]. The degree of in vivo biotinylation, however, was minute, making us to purify BirA and biotinylate the virions in vitro

[109]. When we incubated AP-containing phage (fd-tet-APpIII) with BirA, distinct bands (~60 kDa) appeared in a western blot using streptavidin-HRP (Figure 11b) and we were able to successfully visualize negatively stained virions using uranyl acetate (Figure 12).

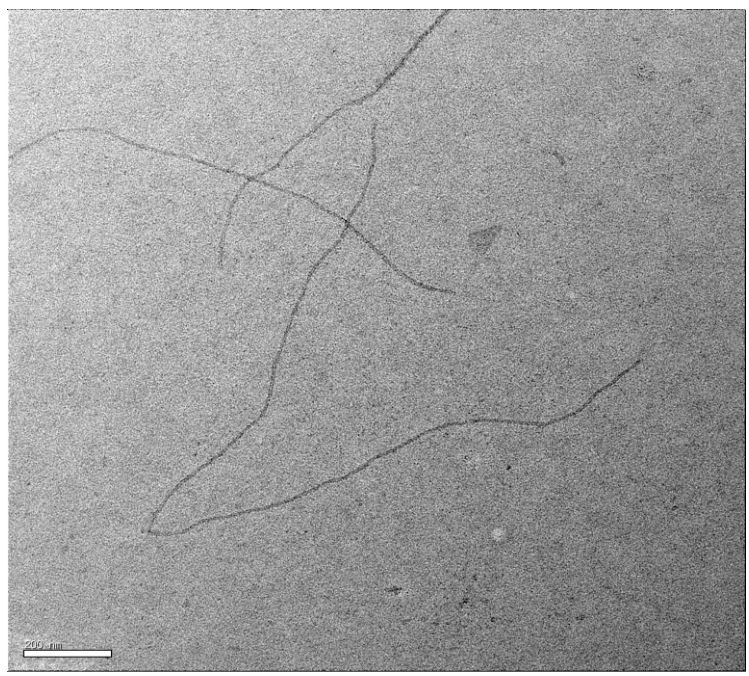

Figure 12. TEM image of PEG/NaCl-purified fd-tet-APpIII phage after 2% uranyl acetate staining. Scale bar = 200 nm.

4.3 Evaluation and optimization of virus-decorated gold microshells

We then briefly evaluated the loading of virions on streptavidin-gold microspheres and found saturated fluorescence signals using 1.0×10^{10} virions and 5 μg of streptavidin-gold microspheres (Figure 13). Given that the apparent diameter of terminal N1-N2 domain of pIII is ~6 nm and the tail part of the fd virus is composed of three to five copies of pIII [110], one virion may be ensconced in an area of ~8.5×10^{-17} - 1.4×10^{-16} m^2. Since 5 μg of gold microspheres corresponds to ~1,000 beads, the total surface area of the beads is ~7×10^{-7} m^2 on which ~$5\text{-}8 \times 10^9$ of virions can be accommodated without gaps in theory.

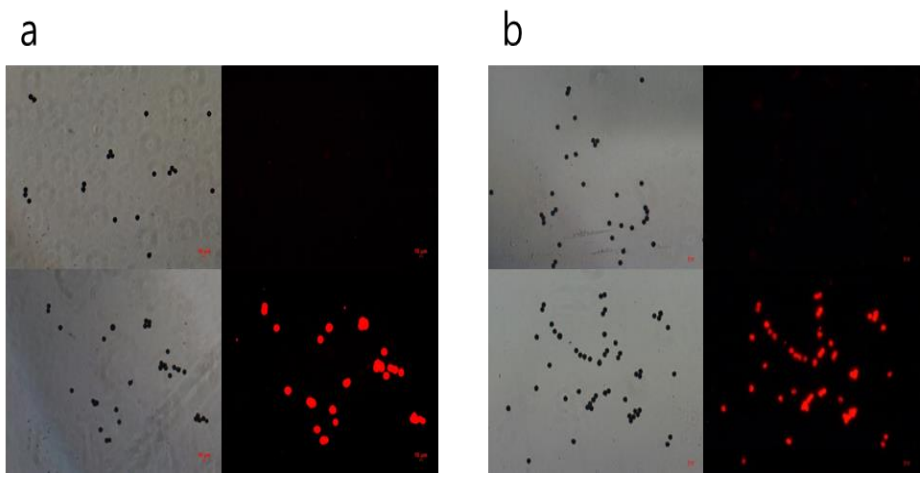

Figure 13. BirA-treated fd-tet (upper panel) and fd-tet-APpIII (lower panel) phage virions (1.0×10^{10}) on streptavidin-SAM gold microspheres were detected using (a) Alexa Fluor® 610 Succinimidyl Esters, (b) rabbit anti-fd antibody and anti-rabbit Alexa Fluor® 610-R-PE antibody.

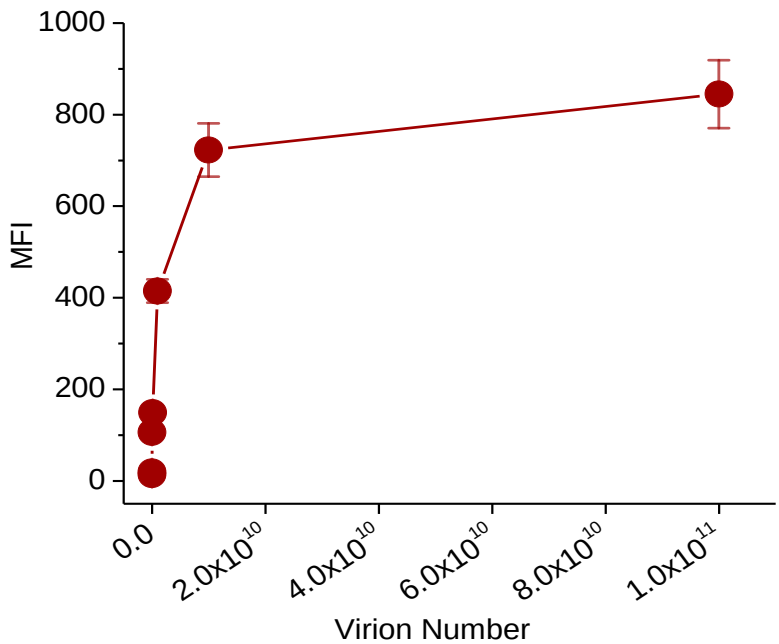

Figure 14. Optimization of surface modifications of gold microspheres with streptavidin and phage virions. Various amount of biotinylated phage virions were used for the titration of virus loading with the same reaction conditions as in Figure 13 (b).

Indeed, when we titrated the loading of virions on the microspheres, the fluorescence intensity began to plateau from 1.0×10^{10} virions near the theoretical value (Figure 14). Thus, we used 1.0×10^{10} virions to maximize antibody loading for subsequent immunoassays, while keeping the efficiency in phage preparation.

4.4 Visualization of virus-decorated gold microshells

We next compared the surfaces of gold microspheres before and after the phage immobilization. Figure 15a and b are the FE-SEM images of bare gold microspheres that reveal gold granules layered on the surface of microspheres. After thiol SAM formation, gold surface maintained the overall roughness similar to the bare gold surface (Figure 15c). By contrast, streptavidin-modified surface exhibited tiny pimples, believed to be Pt-coated streptavidin, added on the gold granular blocks (Figure 15d and Figure 16a). Furthermore, in the case of virus-modified surface, we could clearly identify the virion fibers on the streptavidin layer with the increased thicknesses of 10~15 nm due to the sputtered Pt (Figure 15e and Figure 16b). The virion strands appeared to lie down because of the dry conditions and Pt sputtering required for the FE-SEM operation.

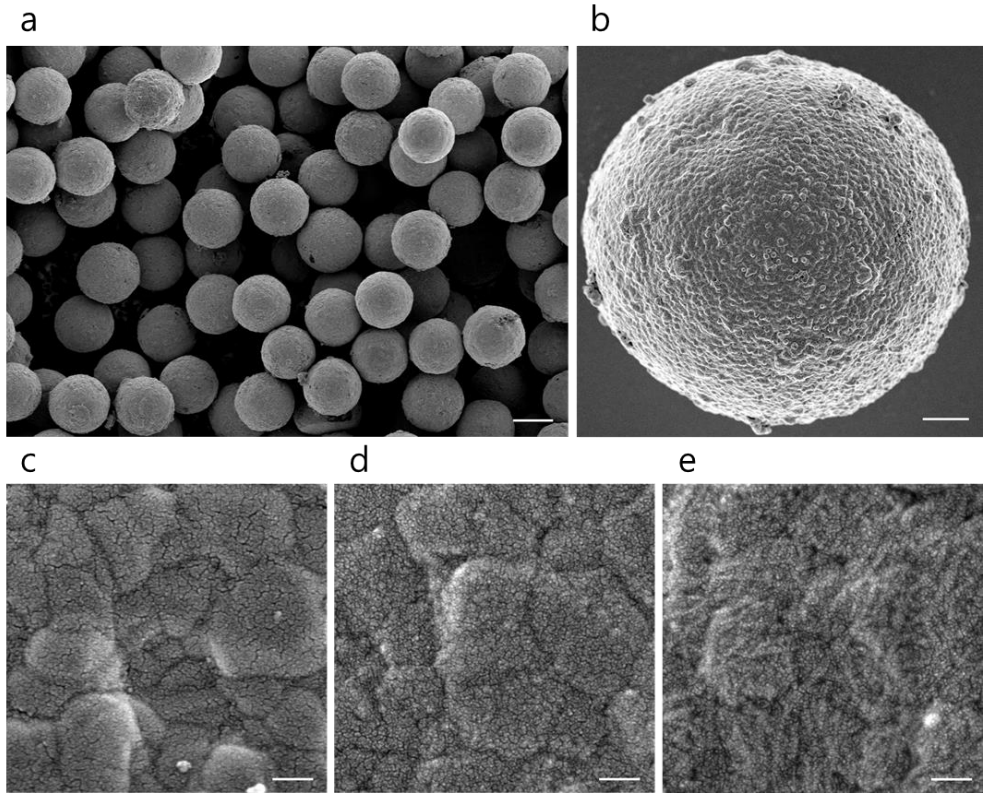

Figure 15. (a) SEM image of bare magnetic gold microspheres (scale bar = 10 μm). (b) Magnified image of gold microspheres reveals the morphology of gold layer (scale bar = 2 μm). Pt-sputtered surface morphology of the beads that had been modified with carboxyl-terminated hexa(ethylene glycol) undecane thiol SAM (c), then conjugated with streptavidin (d), and finally with pIII-biotinylated fd-tet phage virions (e). Scale bars for (c)-(e) = 100 nm.

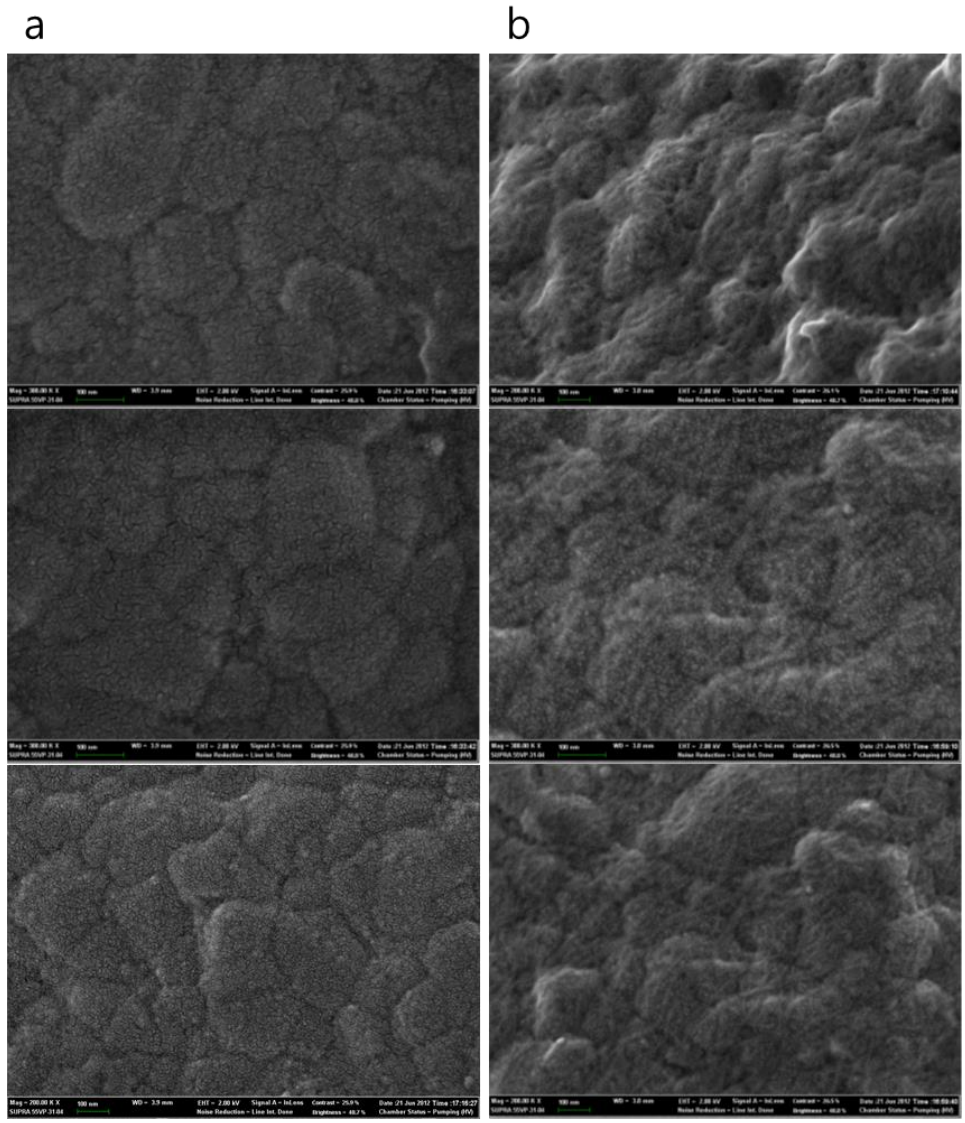

Figure 16. (a) SEM images of independent areas of streptavidin-modified gold microshells with Pt sputtering. (b) SEM images of independent areas of streptavidin-gold-microshells treated with phage virions at various magnifications with Pt sputtering.

The presence of virus on the streptavidin-decorated gold microshells was verified via FE-SEM imaging, however the actual location of the virus in the solution was not known. To determine this, we used Alexa Fluor® 488 Succinimidyl ester, which is an amine-reactive dye and introduced fluorescence to the primary amine of the protein fixed at the bead in order to visualize the location of the virus in the solution. In contrast to streptavidin-coated beads in the absence of virus, the virus-decorated beads were well established within the three-dimensional space (Figure 17). As such, fixation using a virus rather than fixing an antibody directly onto the bead will increase the availability of the antibody and ultimately increase the frequency of ligand-receptor interactions.

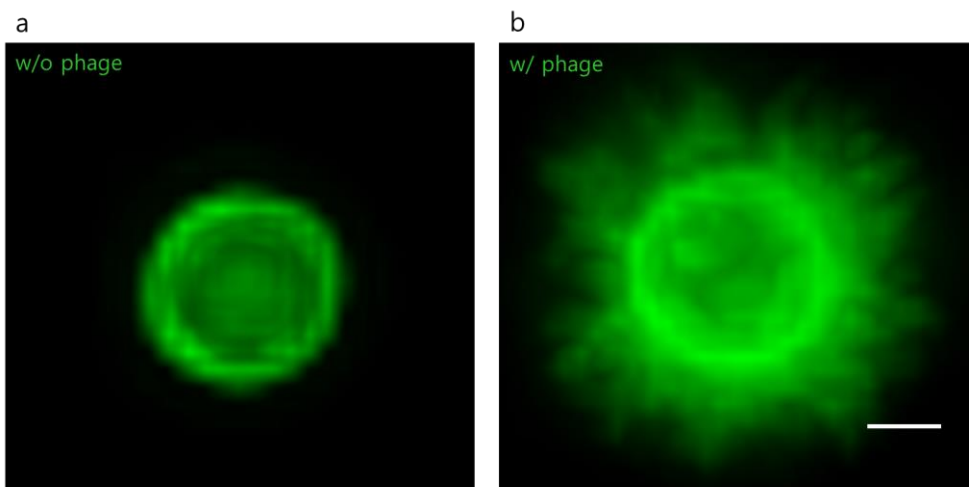

Figure 17. 3D N-SIM super resolution image from a 100 nm Z-stack step size and 0.1 reconstruction factor. w/o phage (a) and w/ phage (b) (scale bar = 1 μm) at 1 μm streptavidin-coated microsphere.

4.5 Optimization of the Staudinger ligation

Staudinger ligation, an extended version of classical Staudinger reaction, has been rediscovered by Saxon and Bertozzi [111]. Among several bioconjugation techniques, the Staudinger ligation has garnered much interest in that it has highly chemoselective and bio-orthogonal conjugation mechanism (Scheme 4). Consequently, the Staudinger ligation has been deployed not only to label glycans, lipids, nucleic acids, proteins, and cell surface, but also to manufacture glycopeptides, microarrays, and biopolymers. To keep the intact filamentous structure of the virions on microspheres, conjugation reactions should be devoid of intra- and inter-molecular crosslinking of the virions, while not interfering with a directional binding of virion tips to microspheres. To that end, we selectively biotinylated pIII parts for the orientation-controlled immobilization of fd virions and thereby used the Staudinger ligation, a bioorthogonal and chemoselective crosslinking between azide and phosphine, for the ligation of phage virions and antibodies (Scheme 4).

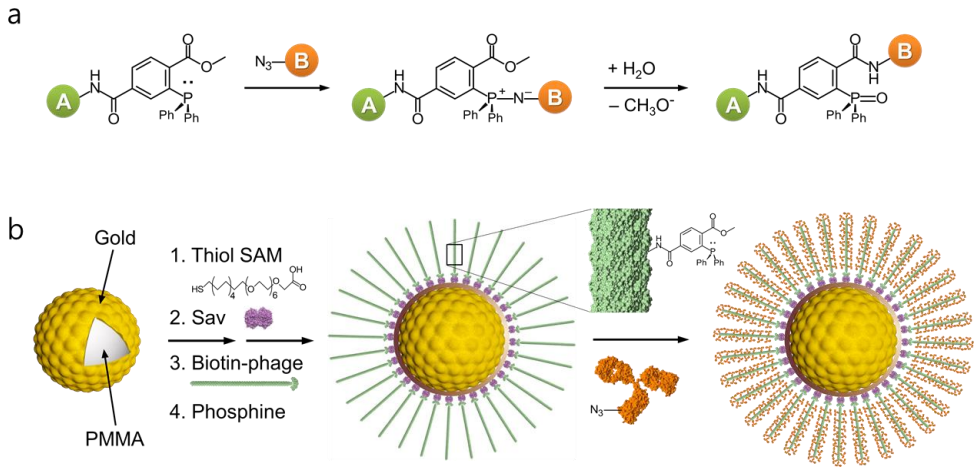

Scheme 4[ii]. Schematic representation of the fabrication of bio-inspired virus-gold microsphere. (a) The Staudinger ligation (azide-phosphine conjugation) between phosphine-activated A and azide-labeled B. An aza-ylide intermediate (middle) converts to a stable covalent amide bond (right). (b) A thin layer of gold allow facile surface modifications by thiol SAM followed by chemical conjugation of streptavidin. The resulting streptavidin-modified microspheres are decorated with pIII-biotinylated phage virions that have filamentous structure, resembling the surface morphology of specific types of cells. The surface-exposed anime groups of N-termini of the viral major coat proteins are conjugated with phosphine and mixed with azide-modified primary antibodies to yield microspheres covered with high-density antibodies via bioorthogonal Staudinger ligation (figures shown cross-sectional area of virions layer and not drawn to scale).

[ii] Dr. Inseong Hwang contributed to this scheme.

We then optimized antibody labeling with either amine-reactive NHS-PEG_{12}-Azide or Sulfo-NHS-Phosphine. In our experimental conditions, antibody precipitated after incubation with Sulfo-NHS-Phosphine probably because of the increased hydrophobicity stems from the phenyl groups of phosphine. On the contrary, no antibody precipitate was found with NHS-PEG_{12}-Azide, and no visible changes of streptavidin- and virus-beads were observed after labeling with Sulfo-NHS-Phosphine; streptavidin is already fixed on the beads, allowing no further aggregation, and phages are rich in surface charges that negate the effect of increased hydrophobicity. After ligation of the azide-modified primary antibody and the phosphine-modified beads, we stained the beads with fluorochrome-labeled secondary antibody and measured the fluorescence intensity of the beads.

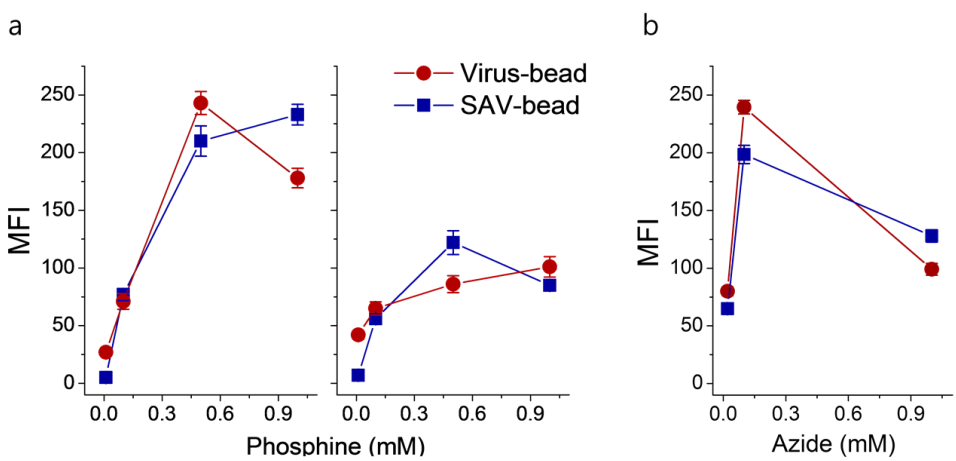

Figure 18. Optimization of Staudinger ligation using mouse antibody. (a) Gold microspheres, covered with streptavidin or phage virions, were treated with four

different concentrations of Sulfo-NHS-Phosphine, while mouse antibody were incubated with 0.1 mM and 1.0 mM NHS-PEG_{12}-Azide. (b) streptavidin or phage-covered gold microspheres were incubated with fixed concentration of phosphine (0.5 mM), while the concentration of azide varied. Anti-mouse Alexa Fluor 594 antibody was used for the determination of mean fluorescence intensity (MFI).

We found that the optimum concentration of phosphine was around 0.5 mM with 100 μM azide where, among others, the virus-tethered beads exhibited the highest fluorescence intensity (Figure 18a). The efficiency of antibody loading decreased at higher concentration of azide (1.0 mM) probably because of the limited access of secondary antibody to buried epitopes of the primary antibody. Lower amount of azide (20 μM) did not seem to push efficacious Staudinger ligation (Figure 18b). However, we cannot rule out the possibility that the lower the level of azide modification, the better the antibody activity.

4.6 Sandwich immunoassay of cardiac biomarkers

To demonstrate the effect of long virus threads, after antibody loading we compared the biomimetic virus-beads with streptavidin-coated beads in terms of antibody activity against cardiac marker proteins, cardiac troponin I (cTnI) and myoglobin.

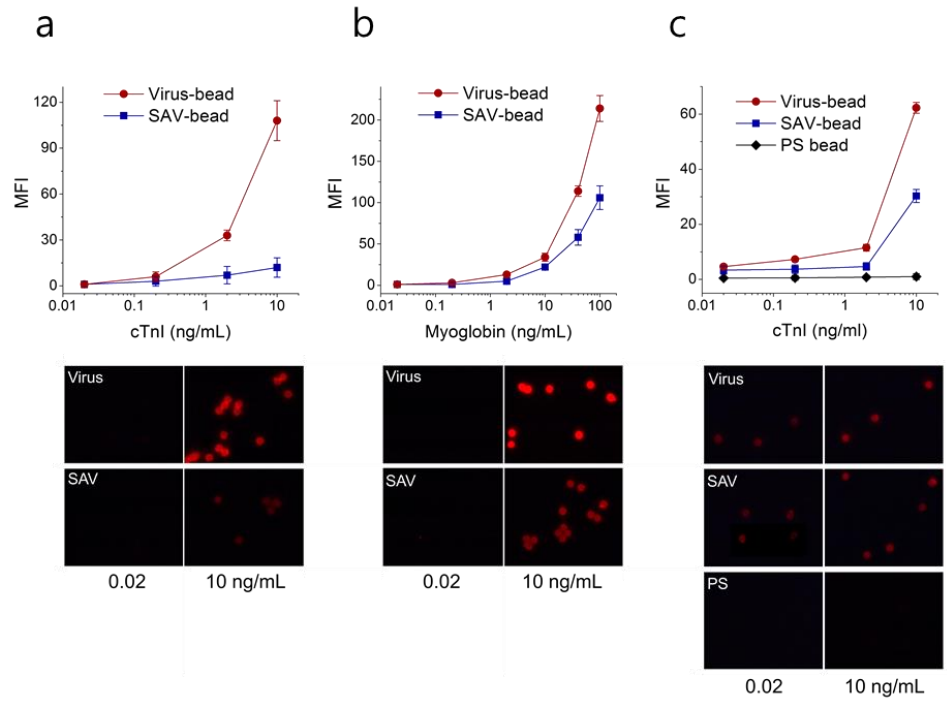

Figure 19. Sandwich immunoassay profiles (top) and representative fluorescence images of each functionalized microspheres corresponding to the w/o initial and final concentrations (bottom) tested for cardiac marker proteins. A range of cTnI in PBS (a), myoglobin in PBS (b), and cTnI in serum (c) were detected using virus- and streptavidin-gold microspheres (a and b), as well as polymer microspheres (c).

We focused on the low range of cTnI and relatively higher range of myoglobin concentrations on the basis of clinical applications [112]. In immunoassays using cTnI- and myoglobin-spiked PBS, virus-decorated gold microspheres showed markedly enhanced signals compared to streptavidin-modified gold microspheres (Figure 19a and b). We could detect as low as 0.2 ng/mL of cTnI and myoglobin using virus-beads. The signals from streptavidin-beads lingered with the background until the concentration reached 2.0 ng/mL of cTnI and myoglobin. The effect of virions was more dramatic in the higher range of cTnI concentration with up to 9-fold increase in fluorescence signal at 10 ng/mL, while the effect of virions on myoglobin showed 2-fold increase within the concentration range tested. The difference in fold increase may originate from the intrinsic variances of antigens, such as size, structure, and binding constant to primary antibodies. Note that the difference in assay performance is greater than the one in the antibody loading between the streptavidin- and virus-beads (see Figure 19). Furthermore, the effect of viral fibers stands out when the amount of captured antigens, and thus the detection antibodies in sandwich assay, is limiting. Therefore, the enhanced sensitivity of the virus-beads may be ascribed to the greater amount of antibody and the long and flexible virus filaments that increase receptor-ligand interactions.

The preventive role of SAM-gold layer for nonspecific adsorption was marked in immunoassays using serum samples that were spiked with cTnI. Interestingly, both the virus- and streptavidin-beads detected as low as 20 pg/mL of cTnI (Figure 19c), while the streptavidin-beads exhibited partial improvement at higher

concentration of cTnI (10 ng/mL) with two fold lower sensitivity than the virus-beads. Importantly, we observed concentration-dependent increase of fluorescence signals at lower range of cTnI only in the case of virus-beads. By contrast, typical carboxylated polystyrene (PS) beads, on which antibodies were conjugated with EDC-NHS chemistry, failed to produce any signals throughout the range tested in serum, although the beads were able to detect cTnI in PBS (Figure 20).

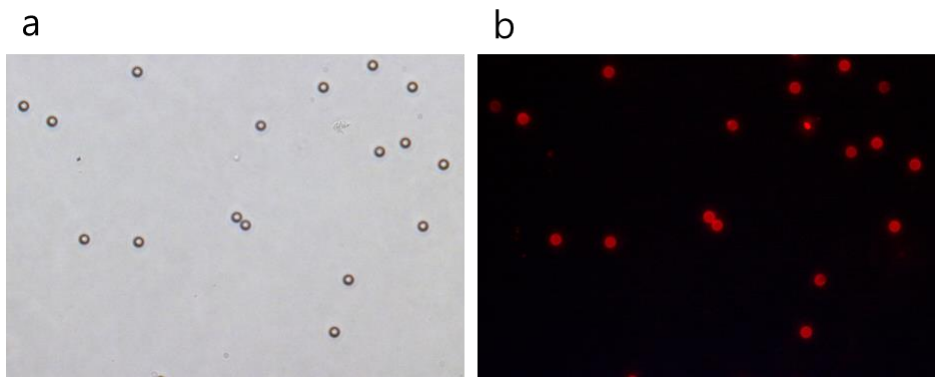

Figure 20. Immunoassay of cTnI in PBS buffer (10 ng/mL) using 10 μm-diameter polystyrene beads whose surfaces were modified with an anti-cTnI antibody using EDC/NHS chemistry. (a) DIC image. (b) Fluorescence image.

The reason why the sensitivity for cTnI in serum should increase remains obscure, although the results suggest that the dense antibodies on phage tentacles and the SAM-gold protection layer synergistically enhance the sensitivity for the lower range of marker proteins.

5. Conclusion and Perspective

In cellular systems, threadlike protruding structures have been evolved to sustain efficacious cellular functions, such as cellular uptake of small- and large molecules, cellular adhesions to biological and non-biological matrices, cell-cell interactions, and ligand-receptor interactions. Inspired by the cellular morphology and by the additive effect of long tethers on receptor-ligand interactions, we decorated SAM-protected gold microspheres with filamentous virions that mimic microvilli-like biological architectures. The SAM-protected virus-gold microspheres showed extremely low non-specific bindings, enhanced capacity of antibody loading, and superior performance in analyte-solid surface interactions when compared with bare polymer beads and non-viral streptavidin-gold beads. The gold-protected and virus-tethered microbeads that resemble biological architectures will open up new possibilities for developing biocompatible and bio-inspired solid surfaces for the improved analyte-solid surface interactions. The microsphere, which is the key to the multiplex suspension array, can be replaced with the virus-decorated gold microshells we developed. This is applicable to the entire field of in-vitro diagnoses and feasible for point-of-care testing (POCT) in combination with microfluidics. Also, since gold microshells with a thin gold layer themselves conduct electricity, they could be used in electrical connections in printed circuit boards or connections among semiconductor elements.

Part 2

Cell-solid surface interaction:

Purified synaptic cell adhesion molecules for induced artificial synapse and bioanalysis

1. Introduction

A neuron is the main cell constituting the nervous system. Unlike other cells, it can transfer electrical signals, and can be classified into various types according to location and function. A typical neuron is composed of the cell body, called a soma, the signal receptors, called dendrites, and the main channel of signal transmission, called an axon. In the nervous system, neuron-to-neuron communication occurs by electrical or chemical signals passing through the neuron junctions (synapses). A typical synapse consists of a connection between the axon of one neuron and a dendrite or soma of another. The electrical signals are transmitted by the presynaptic axons and are transformed into chemical signals (neurotransmitters) in synapses where the probability of the transmission of the electrical signals to postsynaptic dendrites is determined by the types of the neurotransmitters. Excitatory synapses allow postsynaptic transmission of electrical signals, inhibitory synapses block postsynaptic transmission of the signals.

In-depth analysis of the signal transmissions between the axon and synapse reveals that they are ultimately a local movement of chemical species, and such changes in their electrochemical potential allow external stimulation or measurements of signals within the cell. Currently, in most studies, excluding the patch clamp method, neuronal cells are simply developed on or near a solid electrode surface to receive cellular signals.

E.G. Gray elucidated the structure of a synapse using an electron microscope in

1959 [113]. Synapses are ~1 μm in diameter with an intercellular space called synaptic cleft, which is ~20 nm wide, and their formation requires mutual pairing between cell adhesion molecules (CAMs). Synaptic CAMs are proteins localized on the cell surface that adhere to the pre- and post- synaptic terminals and increase the mechanical stabilization of the synapse, while modulating its structure and function. Generally, synaptic CAMs consist of 3 domains: the intracellular domain that interacts with intracellular scaffold proteins, the transmembrane domain, and an extracellular domain that interacts with other Synaptic CAMs. Several families of Synaptic CAMs have been discovered [114], including neuroligins (NLs), neurexins (Nrxs), Slit and Trk-like family (Slitrks), netrin-G ligand proteins (NGLs), leucine-rich repeat transmembrane neuronal proteins (LRRTMs), neural cell adhesion molecules (NCAM), L1-cell adhesion molecules (L1-CAMs), synaptic adhesion-like molecules (SALMs), etc (Table 4).

Most attempts in the formation of artificial synapses started from the year 2000 when seminal experiments were reported on stable synaptic junctions between non-neuronal cells expressing synaptic CAMs and cultured neuronal cells [115, 116, 121]. Recently, the purified synaptic CAMs were immobilized on a solid surface to induce artificial synapses [117, 118].

Table 4. Locations and functions of selected cell adhesion molecules [114].

Molecules	Synaptic location	Pairing	Function
NLs	post	Nrxs, PSD-95	Excitatory synapse formation (NL1)
Slitrks	post	PTPδ	Inhibitory synapse formation (Slitrk3)
NGLs	post	PTPσ, etc	Maintain excitatory synaptic current (NGL3)
LRRTMs	post	Nrxs	Excitatory synapse formation
Nrxs	pre	NLs, LRRTMs	Induce post-synaptic differentiation (β-Nrx)
L1-CAMs	pre	-	Decrease of inhibitory synaptic response (L1)
SALMs	both	NMDAR, etc	Control of excitatory synapse maturation (SALM2)

pre, pre-synaptic; post, post-synaptic; both, pre- and post-synaptic; PSD-95, post-synaptic density-95; PTPδ, protein tyrosine phosphatase δ; NMDAR, N-Methyl-D-aspartate receptor.

Among other synaptic CAMs, NLs and Nrxs are the most studied proteins; rats and mice have three genes encoding NLs, whereas humans have five. Previously in 1995, Südhof *et al*. first purified NL1 using affinity chromatography with immobilized Nrx-1β [119], and the complete paired structure of NL1 and Nrx-1β was revealed in 2007 [120]. Scheiffele *et al* expressed NLs in HEK-293 cells, co-cultured them with neuronal cells [121], and discovered that NL1 triggers pre-synaptic development. Similarly, Südhof *et al*. transfected NL1 derivatives into COS

cells and showed that this induced the formation of an artificial synapse [122]. Furthermore, Groves and coworkers immobilized a glycosylphosphatidylinositol (GPI)-linked NL1 ectodomain on silica microbeads covered with supported lipid bilayer (SLB) membrane, and confirmed the synaptogenic activity of the GPI-anchored NL1 ectodomain [118]. On the other hand, Colman group used poly-D-lysine (PDK)–coated polymer beads to induce the formation of artificial synapses without using synaptic CAMs [123]. Recently, research is being actively conducted on various synaptic CAMs and induced artificial synapses, but the function and mechanisms of these are yet to be completely revealed.

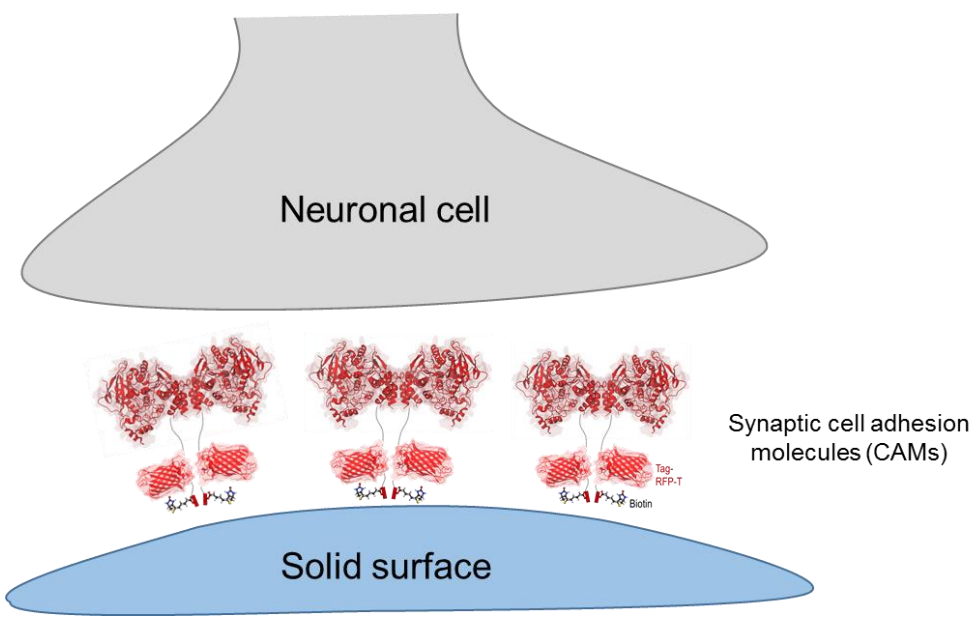

Scheme 5. Schematic representation of artificially induced neuronal cell-solid surface interfaces.

Unlike the detection of delocalized analytes in solutions, the detection of extremely local neuronal signals (e.g., electrical signal or neurotransmitter) needs sophisticated regulation of distances between an electrode surface and cells. Studies have so far only stochastically localized the cells on a solid surface, which causes a loss in sensitivity, selectivity, and reproducibility. If we allow the cells to meet electrodes through the synaptic connections, we not only ensure the reproducible physical geometry of the cell-electrode interfaces, but also have the possibility to measure neurotransmitters otherwise impossible (Scheme 5). Therefore, it is expected that the synaptic CAMs, which were developed to induce artificial synapses on a solid surface, will allow us to consistently position the neuronal cells evenly, thereby providing reproducible and selective signal exchanges. Furthermore, the induced artificial synapses using synaptic CAMs will ultimately provide the foundation for the systematic study of interactions between the solid surface and the cells, as well as the understanding of the information processes in neural networks.

To understand and mimic neuronal network behavior, the ability to monitor, and thus distinguish between, the excitatory and inhibitory signals is essential. In biological systems, excitatory and inhibitory synapses are determined by synaptic CAMs [124, 125]. Notably, chemical conjugation of NL1 on polystyrene beads, despite their capability of adhering to Nrx-expressing cells, failed to induce presynaptic differentiation, suggesting that NL1 requires fluidic lipid bilayer environment for its activity [117]. As a consequence, the use of synaptic CAMs such as NL1 to build artificial synapses has been blocked by the lipid membranes that

create a huge insulating barrier between neurons and the signal recording materials, e.g., electrodes. When it comes to direct recording of neuronal signals via artificial synapses induced by synaptic CAMs, an electrode is expected to act as a 'fake' postsynaptic bouton, and thus the requirement of lipid bilayer on the electrode is a significant challenge. NL isoforms (NL1, 3, and 4) are well-known to induce the formation of excitatory (glutamatergic) presynapses, while NL2 and recently found Slitrk3 inhibitory (GABAergic) presynpases [126-129]. As synaptic CAMs for inhibitory synapses are quite rare, unprecedented specificity to inhibitory synapses of Slitrk3 is of importance [130, 131].

Here, we demonstrate functional interactions of fluorescent and biotinylated synaptic CAMs with cultured hippocampal neurons, independent of SLB media. The fluorescence tag should aid in establishing stable cell lines, and thus mass production, quantification, and tracking of synaptic CAMs on a given artificial substrate.

2. Experimental Methods

2.1. Materials

Plasmids encoding cholinesterase-like domain (CLD) of neuroligin-1 (NL1) followed by GPI anchoring motif (pNICE-HA-H6-NL1-GPI) and full length NL1 and NL2 (pNICE-HA-H6-NL1 and pNICE-HA-NL2) were a generous gift from Peter Scheiffele. A plasmid carrying EYFP-tagged full length NL1 (pNICE-YFP-NL1) was a kind gift from Ann Marie Craig. A plasmid encoding full length Slitrk3, pGW1-Slitrk3, was a kind gift from Jaewon Ko. A plasmid expressing TagRFP-T (pcDNA3-TagRFP-T) was kindly provided by Roger Y. Tsien. BirA expressing plasmids pDisplay-BirA-ER (Addgene plasmid #20856) and pET21a-BirA (Addgene plasmid #20857) were provided by Alice Ting. pAd:CMV-rtTA-IRES-BirA was a gift from William Pu (Addgene plasmid #31375).

Carbenicillin (Carb) was from Gold Biotechnology (St. Louis, MO). Streptavidin, bovine serum albumin (BSA) (A3059), adenosine 5'-triphosphate (ATP), polyethyleneimine (Mw: 25,000), Kanamycin sulfate, and G418 (Geneticin) were from Sigma-Aldrich (St. Louis, MO). QIAprep Spin Miniprep, QIAGEN Plasmid Plus Midi, QIAquick Gel Extraction, Phusion DNA polymerase, and Ni–NTA resin were obtained from Qiagen (Seoul, Korea). Restriction enzymes and T4 ligase were obtained from New England Biolabs (Ipswich, MA). Alexa-labeled secondary antibodies, bacterial cell line DH10B, mammalian cell line HEK293-H,

HEK-293, streptavidin conjugated with horseradish peroxidase (streptavidin-HRP), Opti-MEM® I Reduced Serum Medium, Biocytin-Alexa 594, D-biotin, and Dynabeads® M-280 Streptavidin were obtained from Life Technologies (Invitrogen, Carlsbad, CA). Goat NL1 polyclonal antibody (sc-14084) was from Santa Cruz Biotechnology, Inc. (Santa Cruz, CA)

2.2. Molecular biology

2.2.1. Y-NL1-G

pNICE-YFP-NL1 was cut by KpnI and NotI to remove the predicted O-glycosylation motif (OG), transmembrane domain (TMD), and cytosolic domain of NL1 was replaced by GPI linker from pNICE-HA-H6-NL1-GPI by cutting with the same enzymes, yielding pNICE-YFP-NL1-GPI.

2.2.2. Y-NL1

The GPI portion of the pNICE-YFP-NL1-GPI was replaced with GS-linker (PHLHNLDI639 GGGSGGGSEGGGSGGGSGGGSEGGGSGG) fused with a 14-mer biotin acceptor peptide (AP or AviTag, GLNDIFEAQKIEWHE). First, pNICE-YFP-NL1-GPI and the staggered PCR product (primers N38, N39, N40 and N41) were digested with KpnI and NotI and ligated together. To aid purification, His×8 encoding primers, N43 and N44, were annealed and introduced in front of the YFP sequence using a single PvuI site, yielding pNICE-H8-YFP-NL1-AP (encoding Y-NL1).

2.2.3. R-NL1

TagRFP-T was PCR amplified from the pcDNA3-TagRFP-T plasmid using primers N48 and N49, cut by PvuI and SalI, and ligated with pNICE-H8-YFP-NL1-AP that had been digested with the same restriction enzymes, resulting in pNICE-H8-RFP-NL1-AP (encoding R-NL1).

2.2.4. NL1-R

First, we replaced the GPI tag of pNICE-HA-H6-NL1-GPI with a new GS linker containing additional cloning sites, PvuI and SalI, and AP tag (PHLHNLDI639GGGSGGGSEGGGSGGGSGGGSEG-RS(PvuI)GVD(SalI)-(AP)). The GS linker was synthesized using primers N38, N39, N50 and N41 by staggered PCR, cut by KpnI and NotI, and ligated with pNICE-HA-H6-NL1-GPI that had been cut by KpnI and NotI, yielding pNICE-HA-H6-NL1-GS-PS-AP. The TagRFP-T PCR product obtained from primers N48 and N49 and pNICE-HA-H6-NL1-GS-PS-AP were then digested with PvuI and SalI, followed by a ligation to give pNICE-HA-H6-NL1-H8-RFP-AP (encoding NL1-R).

2.2.5. NL2-R

NL2 was amplified from pNICE-HA-NL2 using primers N55 and N56. The GS linker was PCR amplified from pNICE-HA-H6-NL1-H8-RFP-AP using primers N103 and N104. The pNICE-HA-H6-NL1-H8-RFP-AP was but by BamH I and SalI and served as a vector for three-piece Gibson assembly.

2.2.6. SL3-R

Ectodomain of Slitrk3 was copied from pGW1-Slitrk3 using primers N83 and N74-2 and cut by HindIII and KpnI. The GS linker fused with H8-RFP, GT(KpnI)GSGGGSEGGGSGGGSGGGSEG-RS(PvuI)-(H8-RFP)-VD(SalI)-(AP), was PCR copied from pNICE-HA-H6-NL1-H8-RFP-AP using N38-2 and N41 and cut by KpnI and NotI. The pNICE-HA-H6-NL1-GS-AP was cut by HindIII and NotI and served as a vector for three-piece ligation, finally giving pNICE-SL3-H8-RFP-AP encoding SL3-R. To screen linker sequences, pNICE-SL3-H8-RFP-AP was cleaved by KpnI and PvuI where other linkers with various lengths were inserted. The active SL-R was obtained using annealed primers N106 and N107, yielding GT(KpnI)GSGGGSEGRS(PvuI)-(H8-RFP)-VD(SalI)-(AP).

Bicistronic synaptic encoding of postsynaptic CAMs and BirA: To make a bicistronic expression vector that allows a simultaneous expression of BirA-ER with the postsynaptic CAMs, the internal ribosome entry site (IRES) followed by BirA-ER gene was introduced (Figure 21). The pNICE-(HA-H6)-CAM-H8-RFP-AP (CAM = ectodomain of NL1, NL2, or Slitrk3) were cleaved by NotI to insert IRES-BirA that was amplified from pAd:CMV-rtTA-IRES-BirA using primers N86 and N87 and cut by NotI, generating pNICE-CAM-RAP-BirA after ligation.

Bacterial expression and purification of bacterial BirA biotin ligase was conducted using pET21a-BirA plasmid. The major primers used in this study are listed in Table 5.

Table 5. Primers used for the generation of protein NL1-R. Sequences underlined are crossover area for the staggered PCR.

Primer name	DNA oligomer sequence from 5' end (length)
N38_KpnI-AP-1F	ggcggt***GGTACC***TCATCTGCATAATCTCAATGACATTGG CGGCGGCAGCGGCGGAGGCAGCGAGGG (66)
N38-2_KpnI-GS-F	ggcggt ***GGTACC***GGCAGCGGCGGAGGCAGCGAGGG (35)
N39_AP-2R	GCCCTCGCTGCCGCCTCCGCTGCCGCCTCCGCTGCC TCCGCCCTCGCTGCCTCCGCCGCT (60)
N40_AP-3F	GCGGAGGCGGCAGCGAGGGCGGAGGCAGCGGCGG CGGCCTGAACGACATCTTCGAGGCCC (60)
N41_AP-NotI-4R	ggcagc***GCGGCCGC***TTACTCGTGCCACTCGATCTTCTG GGCCTCGAAGATGTCGTTC (57)
N50_AP-PvuI-SalI-3F	GCGGAGGCGGCAGCGAGGGC***CGATCG***GGT***GTCGA C***GGCCTGAACGACATCTTCGAGGCCC (60)
N43_H8-PvuI-F	***CG***CACCATCACCACCACCACCATCACCGAT (30)
N44_H8-PvuI-R	CGGTGATGGTGGTGGTGGTGATGGTG***CGAT*** (30)
N49_PvuI-H8-TagRFP-F	ggc***CGATCG***CACCATCACCACCACCACCATCACATGG TGTCTAAGGGCGAAGAG (54)
N48_EK-SalI-R	gccacc***GTCGAC***CTTGTCGTCGTCGTCCTTGTACAGCT CGTCCATGC (47)
N55_NL2-BamHI-F	GTGTGGTCCACAGG ***GGATCC*** (20)
N56_NL2-631-639-R	TCTGTGTGCAGGTTGTGCAGGTG (23)
N74-2_Slitrk3-Ecto-KpnI-R	accgcc***GGTACC***GCCCCCAGGAGGAGAAAACTC (33)
N83_pGW1-HindIII-F	CACCGTCCTTGACACG***AAGC*** (20)
N86_NotI-IRES-F	ct***GCGGCCGC***cgagcatagtcatctagcacaatTCCGCCCCTCTCC

	CTCCCCCCCCCCTAA (61)
N87_BirA-ER-NotI-R	ga***GCGGCCGC***TCACAGCTCGTCCTTTGAACCcccagatc cagatgtagacccTTTTTCTGCACTACGCAGGG (72)
N103_NL2-631-639-F	CTGCACAACCTGCACACAGAGGGCGGCGGCAGCG G (35)
N104_SalI-AP-R	CGAAGATGTCGTTCAGGCC***G*** (20)
N106_SL3-shortGS-F	***C***GGCAGCGGCGGAGGCAGCGAGGGC***CGAT*** (29)
N107_SL3-shortGS-R	***CG***GCCCTCGCTGCCTCCGCCGCTGCCG***GTAC*** (31)

2.3. Stable cell lines

For the initial screening of synaptogenic activity of NL1 ectodomains, 24 μg of each NL1-encoding plasmid DNA (pNICE-H8-YFP-NL1-AP, pNICE-H8-RFP-NL1-AP, and pNICE-HA-H6-NL1-H8-RFP-AP) was added to the 1.5 mL of Opti-MEM I Reduced Serum Media. Likewise, 60 μl of 1.0 mg/mL PEI solution was added to the 1.5 mL of Opti-MEM solution. After 5 min incubation at 25 ℃, the two solutions were mixed at room temperature for 30 min and added to HEK293 cells grown to ~20% confluence in a culture dish of 10 cm diameter at 37 ℃. The DMEM medium was replaced after 4 h incubation. After three days, the cells were treated with G418 with final concentration of 0.8 mg/mL. The G418 treatment was repeated with fresh medium after two days. After two weeks, single colonies with brightest fluorescence signals were picked and seeded on a 24-well plate. Among them, the best fluorescent

colonies were repeatedly selected until only one colony was left and seeded on a culture dish of 10 cm diameter for the subsequent passage. The established stable cell line was kept in DMEM medium containing 100 μg/mL G418.

2.4. Preparation of biotinylated synaptic CAMs

Plasmid pDisplay-BirA-ER (24 μg) in 1.5 mL of Opti-MEM solution was mixed with 1.5 mL of Opti-MEM solution containing 60 μg of PEI for 20 min at 25 ℃. The mixture was added to the established HEK293-H stable cell lines at ~20% confluence in a culture dish of 10 cm diameter. After 4 h incubation, the DMEM medium was replaced with a fresh one containing 100 μg/mL G418 and 10 μM biotin. The in vivo biotinylated synaptic CAM was allowed to secrete into culture medium for three days at 37 ℃. Then, 10 mL of the medium was saved and the whole cells were transferred to a culture dish of 15 cm diameter and filled with 30 mL of DMEM containing 100 μg/mL G418 and 10 μM biotin. After another three days, the culture media were combined and subjected to column purification using 2 mL of Ni-NTA resin according to the manufacturer's protocol. The three 1 mL elution fractions were subjected to fluorescence analysis using Synergy Mx fluorescence microplate reader (BioTek, Seoul, Korea).

For in vitro biotinylation, the stable cell line was grown without BirA transfection. To the 1 mL of column elution fraction showing the highest fluorescence signal was added 5 mM $MgCl_2$, 1 mM ATP, 0.1 mM biotin, and 30 nM BirA enzyme as final concentration and shake incubated for 2 h at 37 ℃. The level

of in vivo and in vitro biotinylation was analysed via western blot using streptavidin-HRP or using goat or mouse anti-NL1 antibody and HRP-conjugated secondary antibody. The purity of NL1 was analysed by SDS-PAGE with silver staining

2.5. Immunocytochemistry

Cells were fixed using formaldehyde (4%) for 25 min and rinsed three times with PBS (100 mM, pH 7.4). The cells were then incubated in blocking solution (PBS containing 4% BSA and 0.1% Triton X-100) for 30 min, followed by incubation in primary antibodies diluted in TBS (Tris-buffered saline, pH 7.4) containing BSA (0.5%) and Triton X-100 (0.1%) overnight at 4℃. The samples were then washed three times with TBS and the fluorescent secondary antibodies were applied for 1 h at room temperature in TBS containing BSA (0.5%). The samples were washed again three times with TBS and once with DDW, and stored in VECTASHIED Mounting Medium with DAPI at -80℃ until microscopic examination. Fluorescence images were taken with a Zeiss LSM710 confocal laser scanning microscope equipped with ZEN 2009 software at the National Center for Inter-university Research Facilities (NCIRF) at Seoul National University.

3. Results and Discussion

3.1. Construction of labelled NL1 ectodomains

To generate type-specific artificial dendrites, ectodomains of NL1 (48-639), NL2 (15-614), and Slitrk3 (28-649) were exerpted from their full sequences (Scheme 5). NL1 ectodomain was determined by the crystal structure of NL1/Nrx-1β complex that reveals Leu636 as the end of the α-helix required for NL1 dimerization [120, 132]. Indeed, NL1 (46-638) was the minimum domain functionally secreted to the culture medium, whereas NL1 (46-626) and NL1 (46-633) were not [133]. Intriguingly, the functional GPI-anchored NL1 contains Leu48-Pro631 [117, 125, 134], lacking several C-terminal amino acids required for the formation of α-helix bundle. Since the GPI motif linked to NL1 (48-631) begins with KLLSATA that has high α-helical propensity [135], the overall dimeric structure of GPI-anchored NL1 may have remained unaltered despite the absence of 631-638 helical residues. Ectodomain of NL2 (15-614) was determined by sequence homology with NL1. The border of Slitrk3 ectodomain was conservatively set further away from the C-terminal Leu-rich repeat domain (LRR-CT), seven residues before the transmembrane domain (TMD) (Scheme 6).

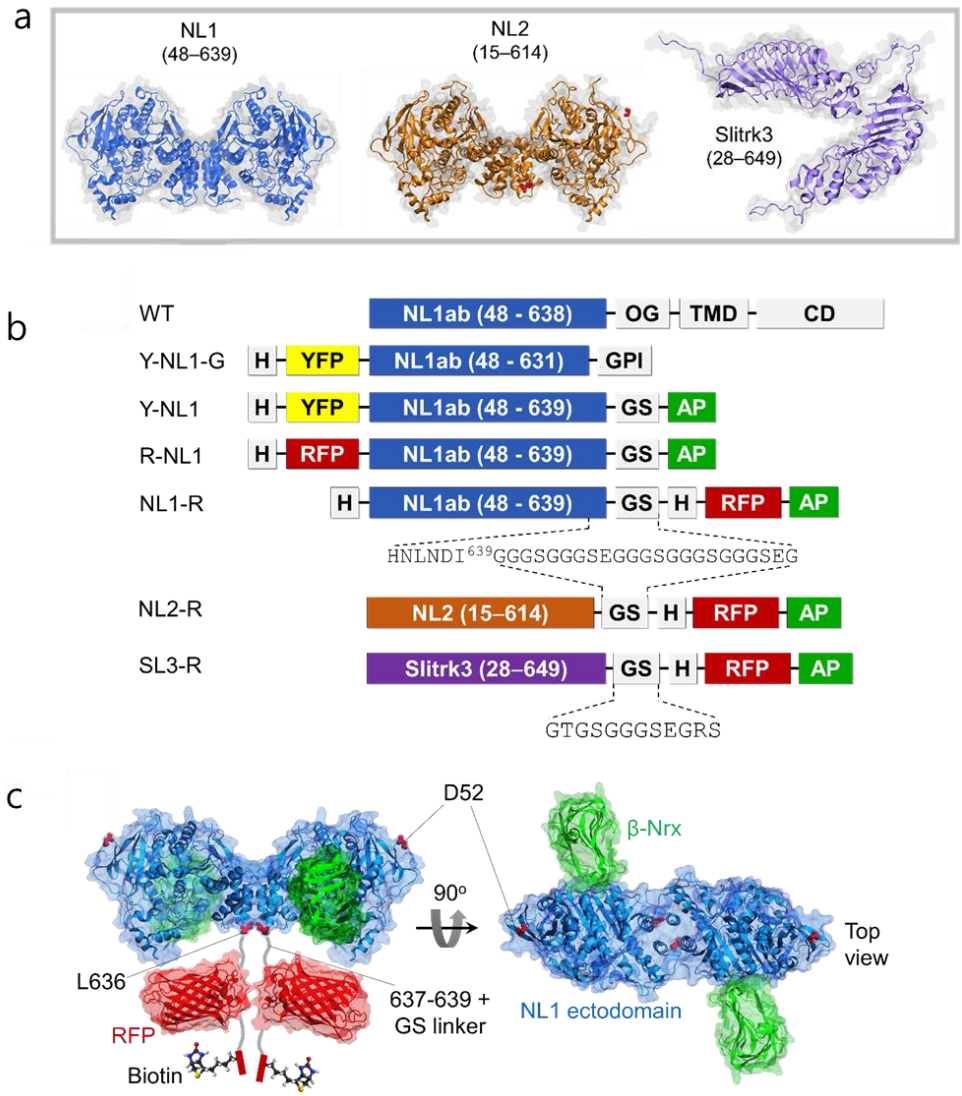

Scheme 6[iii]. (a) Schematic structure of artificial synapse displaying postsynaptic NL1 homodimer (NL1-R), NL2 homodimer (NL2-R), and Slitrk3 (SL3-R). The

[iii] Dr. Inseong Hwang contributed to this scheme.

structures were modeled after NL1 (PDB ID, 3BIX) [120] and NL2 (PDB ID, 3BL8) [136], while the structure of Slitrk3 (27-627 residues) was predicted using Slitrk1 (PDB ID, 4RCW)[137] as a template by the RaptorX server [138], showing two LRR1 and LRR2 domains. (b) Schematic structures of engineered synaptic CAMs used in this study in comparison to wild type NL1 (WT). (c) Predicted structure of NL1-R-Nrx1β complex. The C-terminal tagging module for ectodomain of postsynaptic CAMs minimizes steric hindrance in pre- and postsynaptic CMAs interaction.

To facilitate massive production, purification, quantification, and localization of the ectodomains as well as immobilization of the ectodomains on solid supports, we further engineered the NL1 ectodomain, seeking a general tagging module that can be applied to the other synaptic CAM molecules. On the basis of previous studies showing that both N-terminally YFP-tagged full-length NL1 [139] and glycosylphosphatidylinositol (GPI)-linked NL1 ectodomain [117, 125, 129] are able to instruct excitatory presynaptic differentiation, we first generated N-terminally YFP-tagged and C-terminally GPI-anchored NL1 (Y-NL1-GPI). Unfortunately, the purification yield of the Y-NL1-GPI was extremely low, making us replace the GPI-anchoring motif with AP, a biotin acceptor peptide [140], yielding C-terminally biotinylated Y-NL1. To prevent possible dimerization of YFP, we replaced YFP with TagRFP-T, a photostable monomeric red fluorescence protein (RFP) [141], to

generate R-NL1. We also moved the fluorescence tag from N-terminus to C-terminus of NL1 ectodomain, while keeping the AP-tag at the ultimate C-terminal end of the engineered protein, yielding NL1-R.

The in vivo biotinylation was further simplified by bicistronic expression of ER-specific bacterial biotin holoenzyme synthetase (BirA) (Figure 21).

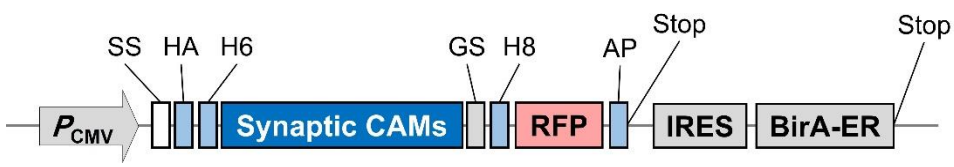

Figure 21[iv]. Genetic engineering of postsynaptic CAMs for facile mass production with in vivo biotinylation. SS, signal sequence; HA, hemagglutinin affinity tag; H6, hexa-His tag; GS, Gly-Ser rich linker; H8, octa-His tag; AP, biotin acceptor peptide; IRES, internal ribosome entry site. The SS, HA and H6 vary depending upon the type of the postsynaptic CAMs

3.2. Generation of stable cell lines

In order to make a stable cell line, the appropriate cell line and antibiotics must be selected. G418 is an antibiotic that is widely used to produce genetically engineered

[iv] Dr. Inseong Hwang contributed to this figure.

proteins in mammalian cells, and HEK-293T cells are resistant to G418. Thus, we selected HEK-293H cells to perform the viability assay using G418. Figure 25 shows a DIC image that demonstrates viability over time in an 800 μg/ml concentration of G418. HEK-293H cells, which are adherent cells, grew well at first, while they were attached to the dish (Figure 22a) but were all dead after one week, when they became detached.

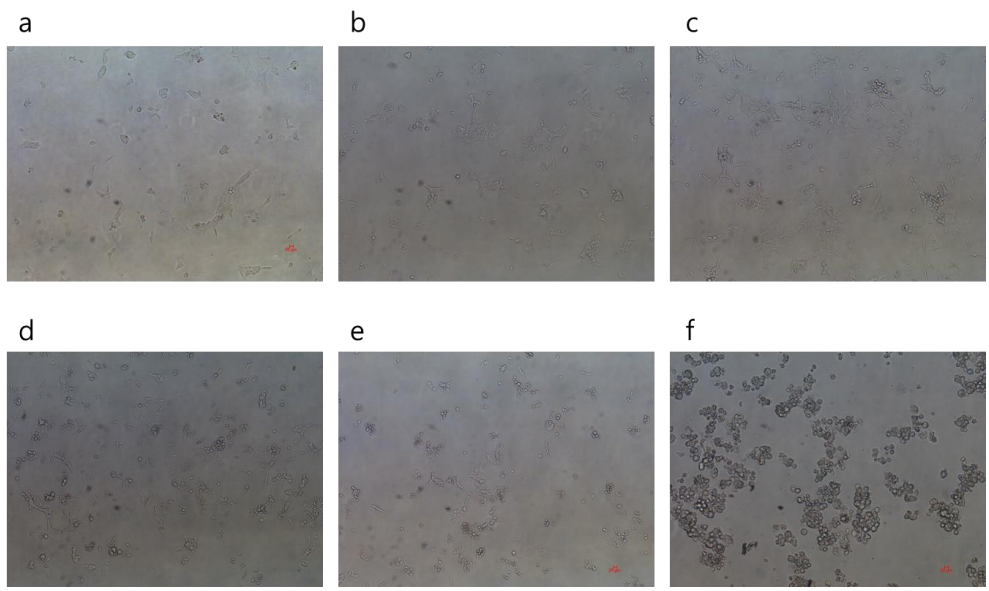

Figure 22. HEK-293H cell viability assay in 800 μg/ml G418 for (a) 0, (b), 1, (c) 2, (d) 3, (e) 5, (f) 7 days.

Next, we optimized the conditions for transient transfection. As shown in Figure 25, green fluorescent protein (GFP) was expressed in HEK-293H cells using either

calcium phosphate, lipofectamine 2000, or polyethyleneimine. The experimental results showed that the best transfection efficiency was obtained using polyethyleneimine (Figure 23c). The highest fluorescence levels were seen after 72 hours, and this became reduced at 100 hours after transfection, due to GFP gene deletion. Thus, we added G418 to the culture media on the third day after transfection to select for synaptic CAMs-expressing cells.

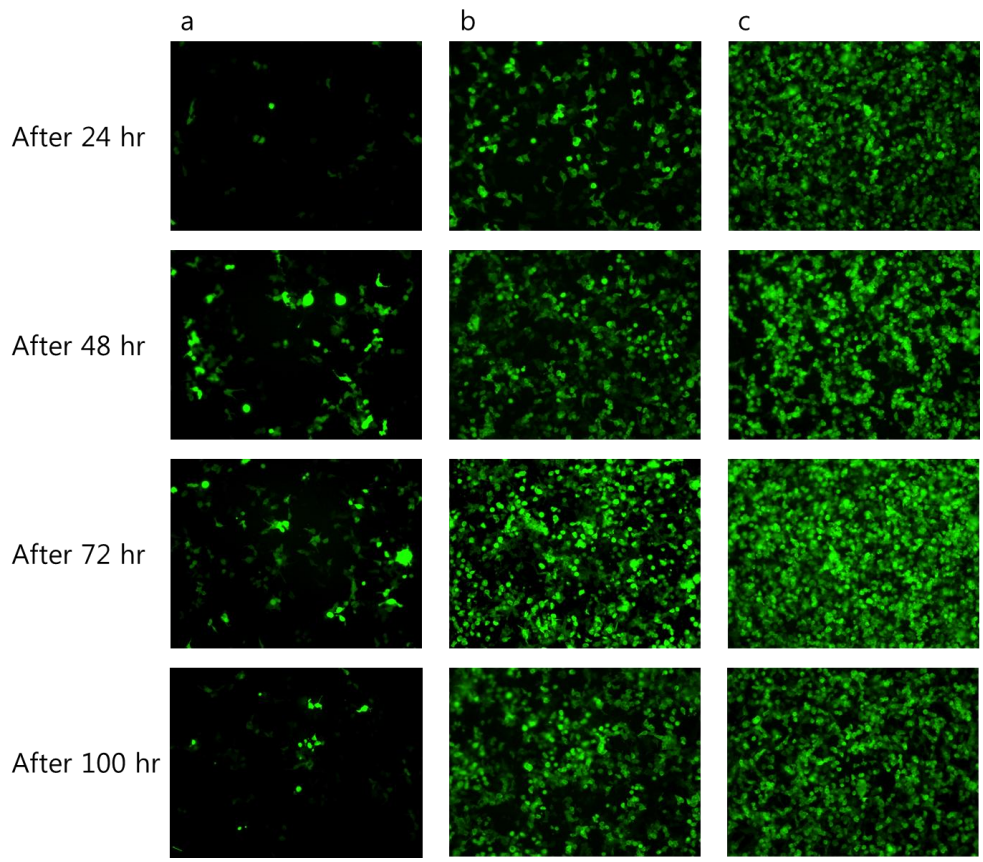

Figure 23. Optimization of transfection methods for a HEK-293H cell line.

Fluorescent images of GFP-transfected HEK-293H cells in three independent transfection experiments. (a) Calcium phosphate, (b) Lipofectamine 2000, (c) Polyethyleneimine.

Figure 24 shows the transfection and selection results using the aforementioned conditions. It also shows the results of selection over time via fluorescence (Figure 24a-c), and a single colony whose size was 0.5–1 mm (Figure 24d). We monitored expression, purification, and immobilization by tagging fluorescent proteins at the synaptic CAMs. It took at least 2 weeks to generate a stable cell line from G418-treated HEK-293H cells. Two to four weeks after transfection, a selected cell had formed into a single colony that could be picked.

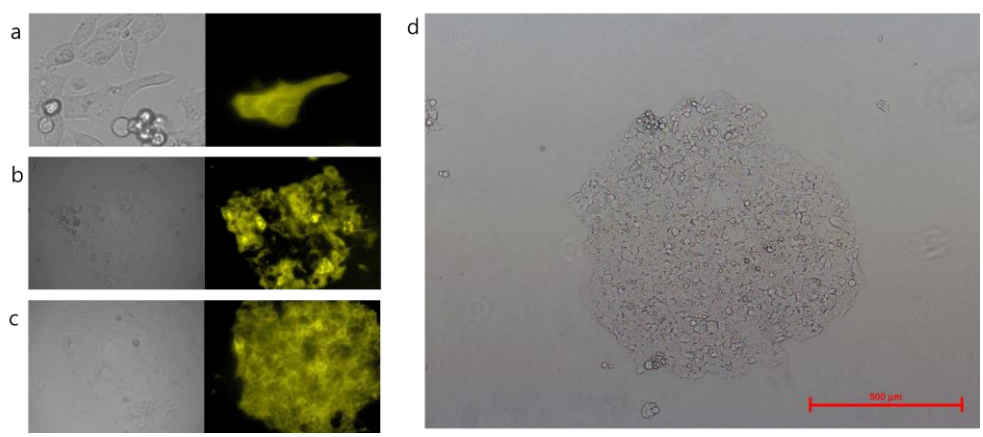

Figure 24. (a) 4, (b) 9 and (c) 12 days after transfection. (d) DIC image of a single colony in which G418 selected NL1-R was expressed two weeks after transfection.

After identifying a colony that was the appropriate size and that displayed bright fluorescence, it was picked using a micropipette on a fluorescence microscope and seeded into a 24-well plate. The established stable cell line was sub-cultured in the presence of 100 μg/mL G418 in a 10 cm-diameter culture dish (Figure 25). Each of the synaptic CAMs were well expressed, as verified by fluorescence. Synaptic CAMs in the cell media, which were secreted during sub-culture, were purified.

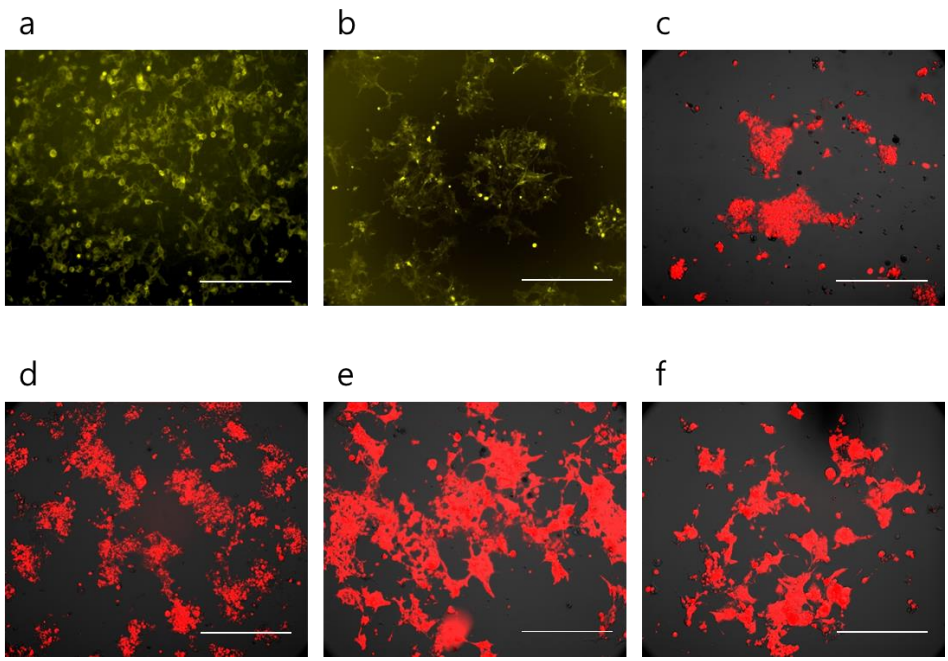

Figure 25. Merged fluorescence and DIC images of stable cell lines in which synaptic CAMs of (a) Y-NL1-G, (b) Y-NL1, (c) R-NL1, (d) NL1-R, (e) NL2-R, and (f) SL3-R were expressed.

3.3. Purification of synaptic CAMs

We employed biotin-streptavidin binding as a strategy to attach the synaptic CAMs to the solid surface. Two methods for binding biotin to synaptic CAMs are *in vivo* biotinylation, which expresses the BirA enzyme inside cells via transfection, and *in vitro* biotinylation, which uses the BirA enzyme in purified synaptic CAMs. The former purifies secreted biotin-conjugated synaptic CAMs by transfecting ER-specific BirA plasmid into the stable cell line, while the latter purifies secreted synaptic CAMs in the stable cell line to perform additional biotinylation. Culture media containing synaptic CAMs were subjected to column purification using 2 mL of Ni-NTA resin according to the manufacturer's protocol. Western blotting (Figure 26) verified that the NL1 derivatives band was successfully purified.

Quantification of the purified synaptic CAMs was verified by silver staining, western blot, and fluorescence intensity. A known amount of BSA was loaded and compared with a known volume of the synaptic CAMs elution fraction to yield the synaptic CAMs concentration (Figure 27). However, despite successful experimental results from *in vivo* and *in vitro* biotinylation of synaptic CAMs, those that were generated by *in vitro* biotinylation did not induce an artificial synapse. Thus, synaptic CAMs were attached to the streptavidin-coated dynabeads using the *in vivo* biotinylation method to induce an artificial synapse. Figure 30 shows the fluorescence image of NL1-R immobilized dynabeads. Since RFP is included, as shown in (Figure 30b), red fluorescence was observed in addition to the shape of the bead. However, RFP fluorescence was disappeared during the

immunocytochemistry (ICC) process for the synaptogenic activity test.

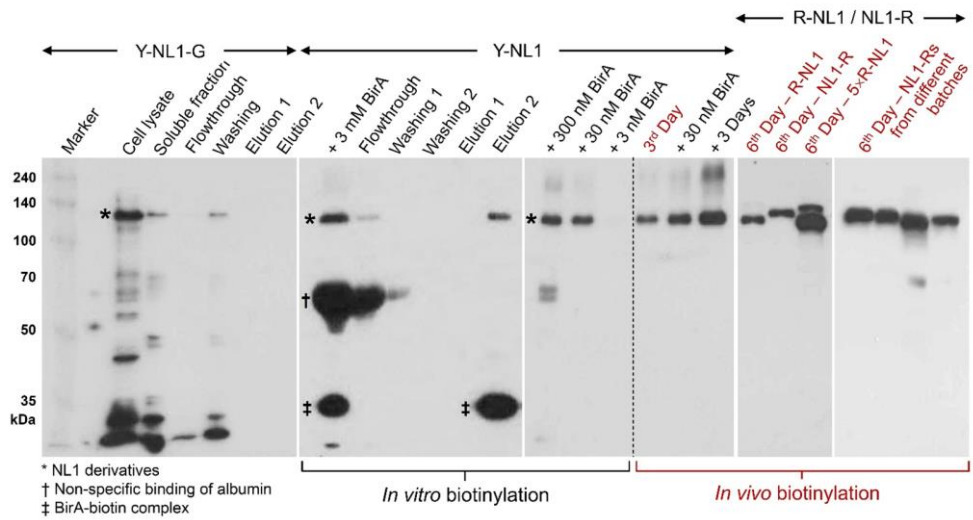

Figure 26. Western blot profiles for the partially purified and labeled NL1s. The YFP-tagged NL1-GPI (Y-NL1-G) rarely appeared in the elution fraction despite its presence in the total cell lysate. When the GPI motif was replaced with AP, the YFP-NL1-AP (Y-NL1) was secreted into the culture medium, and was retained in a Ni-NTA resin. Both *in vitro* and *in vivo* biotinylation revealed biotinylated NL1 regardless of the position of the fluorescence protein. Y-NL1-G was probed by anti-NL1 antibody while the AP-tagged NL1s were detected using streptavidin-HRP.

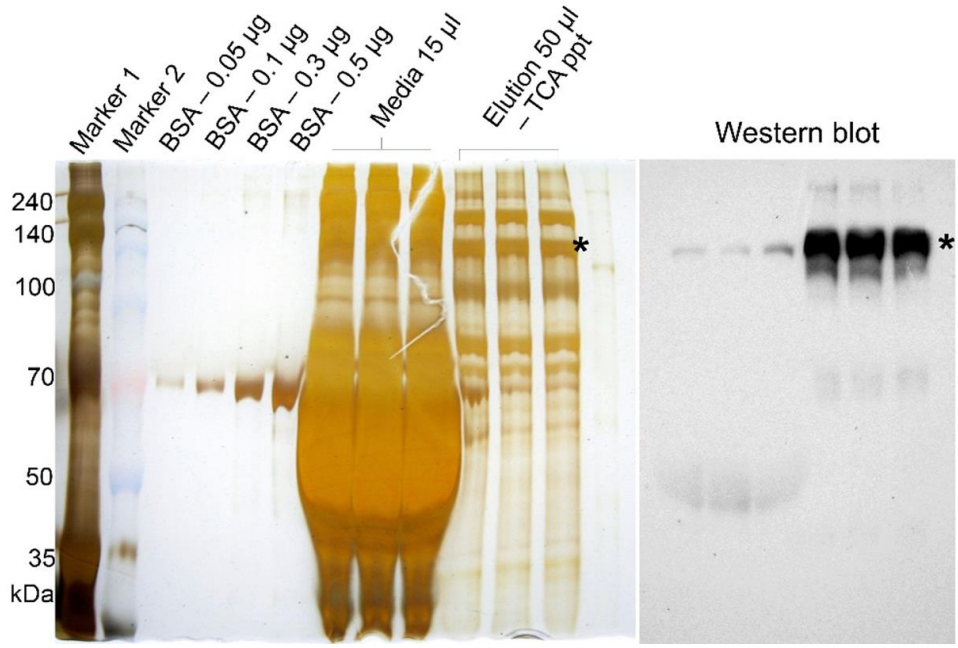

Figure 27. Partially purified NL1-R was quantified using BSA standards. The biotinylated band was verified using western blot (right panel). The relationship between fluorescence intensity and concentration of NL1-R was determined to be 19,000 MFI/µg NL1-R when measured using a microplate reader.

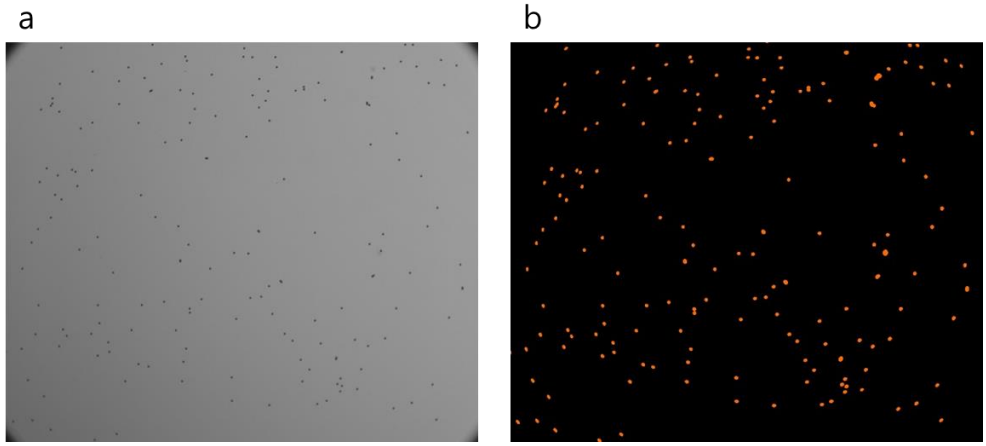

Figure 28. Purified biotin tagged NL1-R was immobilized on streptavidin contained 2.8 μm Dynabeads. (a) DIC image, (b) Fluorescence image. Since RFP is included, as shown in (b), red fluorescence was observed in addition to the shape of the bead.

3.4. Identification of induced artificial synapse

We then compared the synaptogenic activity of the engineered NL1 ectodomains by incubating them with DIV16 cultured neuronal cells for 24 h followed by immunocytochemistry (ICC) to identify immunopositive beads where synapsin I, a representative synaptic marker protein, was prominently clustered as a result of the formation of hemisynaptic boutons (figure 29).

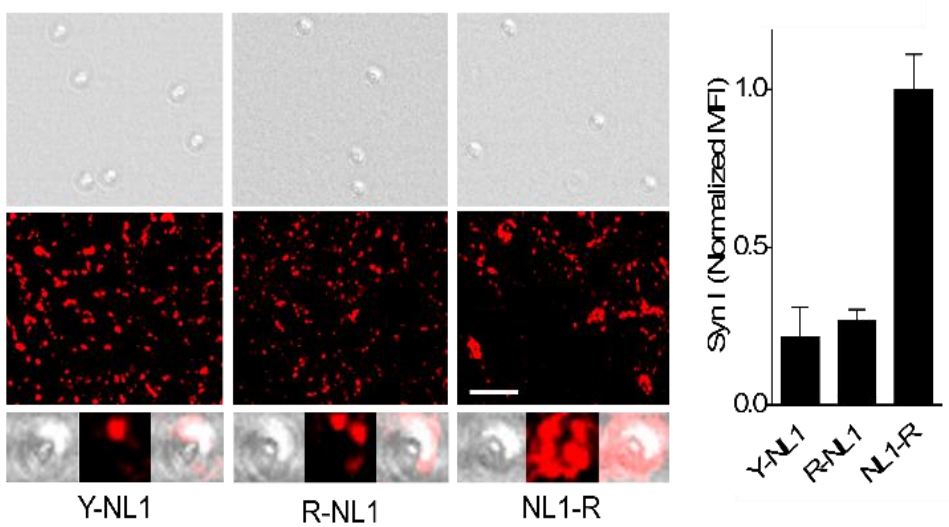

Figure 29[v]. NL1-R induces artificial synapse independently of SLB membrane. NL1-R has the strongest synaptogenic activity streptavidin coated Dynabeads when incubated with DIV14 hippocampal neuron culture for 2 days. Synapsin I (Syn I) aggregation were induced by NL1-R on streptavidin coated Dynabeads. Scale bars = 10 μm.

The dynabeads (Figure 29, left, upper images) to which each of the biotinylated NLs derivatives was fixed formed an artificial synapse by joining with randomly cultured hippocampal neurons. We found that although the N-terminally YFP-tagged NL1 was proven to have synaptogenic activity, biotin-tagged Y-NL1 was barely

[v] Eun Joong Kim contributed to this experiment.

functional compared to NL1-R when immobilized on the dynabeads. On the other hand, we observed that strong fluorescence was emitted by the C-terminally RFP-tagged NL1 on the microspheres and the most robust artificial synapse was induced. This indicated that the structural difference was important because synapses were induced through pairing with Nrxs even when the other components were the same. Furthermore, we separated and purified not only NL1 derivatives that induced an excitatory synapse but also NL2-R and SL3-R that induced an inhibitory synapse using the same experimental procedure, thereby verifying that an artificial synapse could be successfully induced.

4. Conclusion and Perspective

We have demonstrated the feasibility of engineered synaptic CAMs for the induction of artificial synapses. The synaptic CAMs can easily be biotinylated *in vivo*, purified, and quantified from their initial production to the final assay steps. The NL1 ectodomain allows C-terminal tagging for optical tracking and surface immobilization that dispenses with lipid bilayers for its synaptogenic activity. Removal of the lipid bilayer on inorganic substrates can greatly reduce the complexity and workload for establishing artificial synapses. This biased preference to a specific type of synapse induced by synaptic CAMs, if combined with other neuroengineering techniques such as micro- and nano-architectures for neural stimulation and recording, will provide unique possibilities for novel artificial neural interfaces. Moreover, this method will be used as the basis for studying the interaction between the cell and solid surface.

References

[1] K. Landsteiner, Harvard University Press, Cambridge, Massachusetts, 1945

[2] E. Engvall, P. Perlmann, *Immunochemistry* 1971, 8, 871-874

[3] N. Leffers, M. J. Gooden, R. A. Jong, B. N. Hoogeboom, K. A. Hoor, H. Hollema,H. M. Boezen,A. G. Zee, T. Daemen, H. W. Nijman, *Cancer Immunol. Immunother.* 2009, 58, 449-459

[4] S. Birtwell, H. Morgan, *Integr. Biol.* 2009, 1, 345-362

[5] M. Han, X. Gao, J. Z. Su, S. Nie, *Nat. Biotechnol.* 2001, 19, 631-635

[6] H. Fenniri, S. Chun, L. Ding, Y. Zyrianov, K. Hallenga, *J. Am. Chem. Soc.* 2003, 125, 10546-10560

[7] F. Cunin, T. A. Schmedake, J. R. Link, Y. Y. Li, J. Koh, S. N. Bhatia, M. J. Sailor, *Nat. Mater.* 2002, 1, 39-41

[8] Z. L. Zhi, Y. Morita, Q. Hasan, E. Tamiya, *Anal. Chem.* 2003, 75, 4125-4131

[9] D. C. Pregibon, M. Toner, P. S. Doyle, *Science* 2007, 315, 1393-1396

[10] E. J. Moran, S. Sarshar, J. F. Cargill, M. M. Shahbaz, A. Lio, A. M. Mjalli, R. W Armstrong, *J. Am. Chem. Soc.* 1995, 117, 10787-10788

[11] G. Shan, C. Lipton, S. J. Gee, B. D. Hammock, Handbook of Residue Analytical Methods for Agrochemicals, 2003

[12] P. Bostrom, J. Wu, M. P. Jedrychowski, A. Korde, L. Ye, J. C. Lo, K. A. Rasbach, E. A. Bostrom, J. H. Choi, J. Z. Long, S. Kajimura, M. C. Zingaretti, B. F. Vind, H. Tu, S. Cinti, K. Hohlund. S. P. Gygi, B. M. Spiegelman, *Nature.*

2012, 481, 463-469

[13] M. Sinha, Y. C. Jang, J. Oh, D. Khong, E. Y. Wu, R. Manohar, C. Miller, S. G. Regalado, F. S. Loffredo, J. R. Pancoast, M. F. Hirshman, J. Lebowitz, J. L. Shadrach, M. Cerletti, M. Kim, R. Serwold, L. J. Goodyear. B. Rosner, R. T. Lee, A. J. Wagers, *Science* 2014, 344, 649-652

[14] J. K. Lee, K. C. Ahn, O. S. Park, S. Y. Kang, B. D. Hammock, *J. Agric. Food Chem.* 2001, 49, 2159-2165

[15] https://en.wikipedia.org/wiki/Reference_ranges_for_blood_tests

[16] P. Lode, *Clin. Biochem.* 2005, 38, 591-606

[17] G. Amodia, G. Antonelli, F. D. Serio, *Curr. Vasc. Pharmacol.* 2010, 8, 388-393

[18] B. B. Haab, *Curr. Opin. Biotechnol.* 2006, 17, 415-421

[19] L. G. Feinberg, *Nature* 1961, 192, 985-986

[20] W. Zheng, L. He, *Advances in Immunoassay Technology.* 2012, 143-164

[21] M. F. Templin, D. Stoll, M. Schrenk, P. C. Traub, C. F. Vohringer, T. O. Joos, Trends Biotechnol. 2002, 20, 160-166

[22] D. A. Vignali, *J. Immunol. Methods* 2000, 243, 243-255

[23] Y. Li, E. C. Y. Liu, N. Pickett, P. J. Skabara, S. S. Cummins, S. Ryley, A. J. Sutherland, P. OKBrien, *J. Mater. Chem.* 2005, 15, 1238-1243

[24] H. Fenniri, L. H. Ding, A. E. Ribbe, Y. Zyrianov, *J. Am. Chem. Soc.* 2001, 123, 8151-8152

[25] R. Jin, Y. C. Cao, C. S. Thaxton, C. A. Mirkin, *Small* 2006, 2, 375-380

[26] N. P. Gerry, N. E. Witowski, J. Day, R. P. Hammer, G. Barany, F. Barany, *J. Mol. Biol.* 1999, 292, 251-262

[27] M. J. Dejneka, A. Streltsov, S. Pal, A. G. Frutos, K. Yost, P. K. Yuen, U. Muller, J. Lahiri, Proc. *Natl. Acad. Sci. USA* 2003, 100, 389-393

[28] K. C. Nicolaou, X. Y. Xiao, Z. Parandoosh, A. Senyei, M. P. Nova, Angew. Chem. Int. Ed. 1995, 34, 2289-2291

[29] M. J. Benecky, D. R. Post, S. M. Schmitt, M. S. Kochar, *Clin. Chem.* 1997, 43, 1764-1770

[30] F. E. Craig, K. A. Foon, *Blood* 2008, 111, 3941-3967

[31] D. P. Schrum, C. T. Culbertson, S. C. Jacobson, J. M. Ransey, *Anal. Chem.* 1999, 71, 4173-4177

[32] K. B. Kim, H. Chun, H. C. Kim, T. D. Chung, *Electrophoresis* 2009, 30, 1464-1469

[33] S. Joo, K. H.. Kim, H. C. Kim, T. D. Chung, *Biosens. Bioelectron.* 2010, 25, 1509-1515

[34] J. R. Askim, M. Mahmoudi, K. S. Suslick, *Chem. Soc. Rev.* 2013, 42, 8649-8682

[35] http://www.cardiogenics.com/market_advantages/CGNH_Magnetic_Beads_The_Needs.pdf

[36] M. J. Fritzler MJ, M. L. Fritzler, *Expert Opin. Med. Diagn.* 2009, 3, 81-89

[37] www.bangslabs.com

[38] www.thermofisher.com

[39] www.microspheres-nanospheres.com

[40] www.luminexcorp.com

[41] www.affymetrix.com

[42] www.miltenyibiotec.com

[43] www.bioneer.com

[44] Y. Yamamoto, S. Takeda, H. Shiigi, T. Nagaoka, *J. Electrochem. Soc*. 2007, 154, D462-D466

[45] S. Tokonami, Y. Yamamoto, Y. Mizutani, I. Ota, H. Shiigi, T. Nagaoka, *J. Electrochem. Soc.* 2009, 156, D558-D563

[46] H. Zhang, M. E. Meyerhoff, *Anal. Chem.* 2006, 78, 609-616

[47] Y. Cao, X. Hua, X. Zhu, Z. Wang, Z. Huang, Y. Zhao, H. gro, M. Lie, *J. Immunol. Methods* 2006, 317, 163-170

[48] R. Javier, Y. Tomoyuki, M. Fumio, *Biosens. Bioelectron.* 2011, 28, 443-449

[49] www.sekisuichemical.com

[50] J. R. Lee, J. Lee, S. K. Kim, K. P. Kim, H. S. Park, W. Yeo, *Angew. Chem. Int. Ed.* 2008, 47, 9518-9521

[51] J. Lee, J. Lee, T. D. Chung, W. Seo, *Anal. Chim. Acta* 2012, 736, 1-6

[52] J. Lee, J. Lee, H. Oh, H. Mok, W. Yeo, *Bull. Korean Chem. Soc.* 2012, 33, 3076-3078

[53] H. Seo, S. Kim, J. I. Kim, H. Kang, W. Jung, W. Yeo, *Anal. Biochem.* 2013, 434, 199-201

[54] S. Kwon, C. S. Jeon, N. Y. Hong, K. P. Kim, I. Hwang, T. D. Chung, *Chem.*

Commun. 2014, 50, 10066-10069

[55] G. P. Smith, V. A. Petrenko, *Chem. Rev.* 1997, 97, 391-410

[56] M. Mammen, S. Choi, G. Whitesides, *Angew. Chem. Int. Ed.* 1998, 37, 2754-2794

[57] C. Fasting, C. A. Schalley, M. Weber, O. Seitz, S. Hecht, B. Koksch, J. Dernedde, C. Graf, E. Knapp, R. Haag, *Angew. Chem. Int. Ed.* 2012, 51, 10472-10498

[58] C. B. Mao, A. Liu, B. Cao, *Angew. Chem. Int. Ed.* 2009, 48, 6790-6810

[59] G. P. Smith, *Science* 1985, 228, 1315-1317

[60] I. Hwang, *Sensors* 2014, 14, 13592-13612

[61] V. A. Petrenko, G. P Smith, X. Gong, T. Quinn, *Protein Eng*. 1996, 9, 797-801

[62] F. N. Dultsev, R. E. Speight, M. T. Fiorini, J. M. Blackburn, C. Abell, V. P. Ostanin, D. Klenerman, *Anal. Chem.* 2001, 73, 3935-3939

[63] E. Uttenthaler, M. Schraml, J. Mandel, S. Drost, *Biosens. Bioelectron.* 2001, 16, 735-743

[64] E. V. Olsen, I. B. Sorokulova, V. A. Petrenko, I.-H. Chen, J. M. Barbaree, V. J. Vodyanoy, *Biosens. Bioelectron.* 2006, 21, 1434-1442

[65] J. Brigati, D. D. Williams, I. B. Sorokulova, V. Nanduri, I.-H. Chen, C. L. Turnbough, Jr., V. A. Petrenko, *Clin. Chem.* 2004, 50, 1899-1906

[66] V. A. Petrenko, G. P. Smith, *Protein Eng.* 2000, 13, 589-592

[67] M. D. Sheets, P. Amersdorfer, R. Finnern, P. Sargent, E. Lindqvist, R. Schier, G. Hemingsen, C. Wong, J. C. Gerhart, J. D. Marks, *Proc. Natl. Acad. Sci.*

USA 1998, 95, 6157-6162

[68] T. Pulli, M. Hoyhtya, H. Soderlund, K. Takkinen, *Anal. Chem.* 2005, 77, 2637-2642

[69] M. Wikman, E. Rowcliffe, M. Friedman, P. Henning, L. Lindholm, S. Olofsson, S. Stahl, *Biotechnol. Appl. Biochem.* 2006, 45, 93-105

[70] S. Daly, P. Dillon, B. Manning, L. Dunne, A. Killard, R. OKennedy, *Food Agric. Immunol.* 2002, 14, 155-274

[71] Y. Jia, M. Qin, H. Zhang, W. Niu, X. Li, L.Wang, X. Li, Y. Bai, Y. Cao, X. Feng, *Biosens. Bioelectron.* 2007, 22, 3261-3266

[72] M. Sarikaya, C. Tamerler, A. Jen, K. Schulten, F. Baneyx, *Nat. Mater*. 2003, 2, 577-585

[73] K. T. Nam, D. Kim, P. J. Yoo, C. Chiang, N. Meethong, P. T. Hammond, Y. Chiang, A. M. Belcher, *Science* 2006, 312, 885-888

[74] J. H. Lee, P. F. Xu, D. W. Domaille, C. Choi, S. Jin, J. N. Cha, *Adv. Funct. Mater.* 2014, 24, 2079-2084

[75] H. Lee, H. K. Lee, H. Chang, H. Ahn, N. Erdene, H. Lee, Y. Lee, D. H. Jeong, J. Chung, K. T. Nam, *Small* 2014, 10, 3007-3011

[76] L. M. Chen, A. J. Zurita, P. U. Ardelt, R. J. Giordano, W. Arap, R. Pasqualini, *Chem. Biol.* 2004, 11, 1081-1091

[77] R. Edgar, M. McKinstry, J. Hwang, A. B. Oppenheim, R. A. Fekete, G. Giulian, C. Merril, K. Nagashima, S. Adhya, *Proc. Natl. Acad. Sci. U.S.A.* 2006, 103, 4841-4845

[78] K. Li, Y. Chen, S. Q. Li, G. N. Huong, Z. W. Niu, S. J. You, C. M. Mello, X. B. Lu, Q. A. Wang, *Bioconjugate Chem.* 2010, 21, 1369-1377

[79] S. Horikawa, D. Bedi, S. Q. Li, W. Shen, S. C. Huang, I. H. Chen, Y. T. Chai, M. L. Auad, M. J. Bozack, J. M. Barbaree, V. A. Petrenko, B. A. Chin, *Biosens. Bioelectron.* 2011, 26, 2361-2367

[80] J. A. Arter, J. E. Diaz, K. C. Donavan, T. Yuan, R. M. Penner, G. A. Weiss, *Anal. Chem.* 2012, 84, 2776-2783

[81] G. R. Souza, D. R. Christianson, F. I. Staquicini, M. G. Ozawa, E. Y. Snyder, R. L. Sidman, J. H. Miller, W. Arap, R. Pasqualini, *Proc. Natl. Acad. Sci. U.S.A.* 2006, 103, 1215-1220

[82] L. M. C. Yang, P. Y. Tam, B. J. Murray, T. M. McIntire, C. M. Overstreet, G. A. Weiss, R. M. Penner, *Anal. Chem*. 2006, 78, 3265-3270

[83] L. M. C. Yang, J. E. Diaz, T. M. McIntire, G. A. Weiss, R. M. Penner, *Anal. Chem*. 2008, 80, 933-943

[84] N. F. Steinmetz, E. Bock, R. P. Richter, J. P. Spatz, G. P. Lomonossoff, D. J. Evans, *Biomacromolecules* 2008, 9, 456-462

[85] J. S. Park, M. K. Cho, E. J. Lee, K. Y. Ahn, K. E. Lee, J. H. Jung, Y. J. Cho, S. S. Han, Y. K. Kim, J. Lee, *Nat. Nanotechnol*. 2009, 4, 259-264

[86] J. A. Arter, D. K. Taggart, T. M. McIntire, R. M. Penner, G. A. Weiss, Nano Lett. 2010, 10, 4858; g) J. H. Lee, J. N. Cha, *Anal. Chem*. 2011, 83, 3516-3519

[87] K. C. Donavan, J. A. Arter, R. Pilolli, N. Cioffi, G. A. Weiss, R. M. Penner, *Anal. Chem*. 2011, 83, 2420-2424

[88] J. H. Lee, D. W. Domaille, J. N. Cha, *ACS Nano* 2012, 6, 5621-5626

[89] R. Wilson, A. R. Cossins, D. G. Spiller, *Angew. Chem. Int. Ed*. 2006, 45, 6104-6117

[90] J. C. Love, L. A. Estroff, J. K. Kriebel, R. G. Nuzzo, G. M. Whitesides, *Chem. Rev*. 2005, 105, 1103-1169

[91] M. Schaeferling, S. Schiller, H. Paul, M. Kruschina, P. Pavlickova, M. Meerkamp, C. Giammasi, D. Kambhampati, *Electrophoresis* 2002, 23, 3097-3105

[92] C. J. Huang, Y. T. Li, S. Y. Jiang, *Anal. Chem*. 2012, 84, 3440-3445

[93] C. F. Barbas, Phage display : a laboratory manual Cold Spring Harbor Laboratory Press, Cold Spring Harbor, NY 2001

[94] W. Humphrey, A. Dalke, K. Schulten, *J. Mol. Graph. Model*. 1996, 14, 33-38

[95] Y. S. Nam, T. Shin, H. Park, A. P. Magyar, K. Choi, G. Fantner, K. A. Nelson, A. M. Belcher, *J. Am. Chem. Soc*. 2010, 132, 1462-1463

[96] J. R. Newton, Y. B. Miao, S. L. Deutscher, T. P. Quinn, *J. Nucl. Med*. 2007, 48, 429-436

[97] J. Muzard, M. Platt, G. U. Lee, *Small* 2012, 8, 2403-2411

[98] C. Jeppesen, J. Y. Wong, T. L. Kuhl, J. N. Israelachvili, N. Mullah, S. Zalipsky, C. M. Marques, *Science* 2001, 293, 465-468

[99] B. E. Collins, J. C. Paulson, *Curr. Opin. Chem. Biol*. 2004, 8, 617-625

[100] S. H. Wang, E. E. Dormidontova, *Soft Matter* 2011, 7, 4435

[101] D. Reeves, K. Cheveralls, J. Kondev, *Phys. Rev. E* 2011, 84, 021914

[102] M. F. Bear, B. W. Connors, M. A. Paradiso, Neuroscience : exploring the brain, Lippincott Williams & Wilkins, Philadelphia, PA 2007

[103] G. Greicius, L. Westerberg, E. J. Davey, E. Buentke, A. Scheynius, J. Thyberg, E. Severinson, *Int. Immunol*. 2004, 16, 353-364

[104] H. Connell, W. Agace, P. Klemm, M. Schembri, S. Marild, C. Svanborg, *Proc. Natl. Acad. Sci. U.S.A.* 1996, 93, 9827-9832

[105] J. Lederberg, E. L. Tatum, *Nature* 1946, 158, 558

[106] S. R. Kwon, C. S. Jeon, N. Y. Hong, K. P. Kim, I. Hwang, T. D. Chung, *Chem. Commun.* 2014, 50, 10066-10069

[107] M. Howarth, A. Y. Ting, *Nat. Protoc*. 2008, 3, 534-545

[108] A. N. Zacher, C. A. Stock, J. W. Golden, G. P. Smith, *Gene* 1980, 9, 127-140

[109] M. D. Scholle, U. Kriplani, A. Pabon, K. Sishtla, M. J. Glucksman, B. K. Kay, *Chembiochem* 2006, 7, 834-838

[110] P. Holliger, L. Riechmann, R. L. Williams, *J. Mol. Biol*. 1999, 288, 649-657

[111] E. Saxon, C. R. Bertozzi, *Science* 2000, 287, 2007-2010

[112] R. H. Christenson, H. M. E. Azzazy, *Clin. Biochem*. 2009, 42, 150-157

[113] E. G. Gray, *J. Anat*. 1959, 93, 420–433

[114] X. Yang, D. Hou, W. Jiang, C. Zhang, *Protein Cell* 2014, 5, 420–444

[115] E. R. Graf, X. Z. Zhang, S. X. Jin, M. W. Linhoff, A. M. Craig, *Cell* 2004, 119, 1013-1026

[116] C. Nam, L. Chen. *Proc Natl Acad Sci U S A*. 2005, 102, 6137-6142

[117] M. M. Baksh, C. Dean, S. Pautot, S. DeMaria, E. Isacoff, J. T. Groves,

Langmuir 2005, 21, 10693-10698

[118] K. Czöndör, M. Garcia, A. Argento, A. Constals, C. Breillat, B. Tessier, O. Thoumine. *Nat Commun.* 2013, 4, 2252

[119] K. Ichtchenko, Y. Hata, T. Nguyen, B. Ullrich, M. Missler, C. Moomaw, T. C. Sudhof, *Cell* 1995, 81, 435-443

[120] D. Arac, A. A. Boucard, E. Ozkan, P. Strop, E. Newell, T. C. Sudhof, A. T. Brunger, *Neuron* 2007, 56, 992-1003

[121] P. Scheiffele, J. H. Fan, J. Choih, R. Fetter, T. Serafini, *Cell* 2000, 101, 657-669

[122] Chubykin AA1, Liu X, Comoletti D, Tsigelny I, Taylor P, Südhof TC. J Biol Chem. 2005 Jun 10;280(23):22365-74

[123] A. Lucido, Suarez Sanchez F, Thostrup P, Kwiatkowski AV, Leal-Ortiz S, Gopalakrishnan G, Liazoghli D, Belkaid W, Lennox RB, Grutter P, Garner CC, Colman DR. J Neurosci. 2009 Oct 7;29(40):12449-66. doi: 10.1523/JNEUROSCI.1381-09.2009.

[124] M. B. Dalva, A. C. McClelland, M. S. Kayser, *Nat. Rev. Neurosci.* 2007, 8, 206-220

[125] C. Dean, F. G. Scholl, J. Choih, S. DeMaria, J. Berger, E. Isacoff, P. Scheiffele, *Nat. Neurosci*. 2003, 6, 708-716

[126] B. Chih, H. Engelman, P. Scheiffele, *Science* 2005, 307, 1324-1328

[127] B. Chih, L. Gollan, P. Scheiffele, *Neuron* 2006, 51, 171-178

[128] J. Y. Song, K. Ichtchenko, T. C. Sudhof, N. Brose, *Proc. Natl. Acad. Sci. U.S.A.*

1999, 96, 1100-1105

[129] G. Giannone, M. Mondin, D. Grillo-Bosch, B. Tessier, E. Saint-Michel, K. Czöndör, M. Sainlos, D. Choquet, O. Thoumine, *Cell Reports* 2013, 3, 1996-2007

[130] H. Takahashi, K. Katayama, K. Sohya, H. Miyamoto, T. Prasad, Y. Matsumoto, M. Ota, H. Yasuda, T. Tsumoto, J. Aruga, A. M. Craig, *Nat. Neurosci.* 2012, 15, 389-398

[131] Y. S. Yim, Y. Kwon, J. Nam, H. I. Yoon, K. Lee, D. G. Kim, E. Kim, C. H. Kim, J. Ko, *Proc. Natl. Acad. Sci. U.S.A.* 2013, 110, 4057-4062

[132] X. Chen, H. Liu, A. H. R. Shim, P. J. Focia, X. He, *Nat. Struct. Mol. Biol.* 2008, 15, 50-56

[133] D. Comoletti, R. Flynn, L. L. Jennings, A. Chubykin, T. Matsumura, H. Hasegawa, T. C. Sudhof, P. Taylor, *J. Biol. Chem.* 2003, 278, 50497-50505

[134] S. Pautot, H. Lee, E. Y. Isacoff, J. T. Groves, *Nat. Chem. Biol*. 2005, 1, 283-289

[135] K. T. Oneil, W. F. Degrado, *Science* 1990, 250, 646-651

[136] J. Koehnke, K. Jin, E. C. Budreck, S. Posy, P. Scheiffele, B. Honig, L. Shapiro, *P Natl Acad Sci USA* 2008, 105, 1873-1878

[137] J. W. Um, K. H. Kim, B. S. Park, Y. Choi, D. Kim, C. Y. Kim, S. J. Kim, M. Kim, J. S. Ko, S. G. Lee, G. Choii, J. Nam, W. D. Heo, E. Kim, J. O. Lee, J. Ko, H. M. Kim, *Nat Commun* 2014, 5, 5423

[138] M. Kallberg, H. P. Wang, S. Wang, J. Peng, Z. Y. Wang, H. Lu, J. B. Xu, *Nat.*

Protoc. 2012, 7, 1511-1522

[139] E. R. Graf, X. Z. Zhang, S. X. Jin, M. W. Linhoff, A. M. Craig, *Cell* 2004, 119, 1013-1026

[140] M. Howarth, A. Y. Ting, *Nat. Protoc*. 2008, 3, 534-545

[141] N. C. Shaner, M. Z. Lin, M. R. McKeown, P. A. Steinbach, K. L. Hazelwood, M. W. Davidson, R. Y. Tsien, *Nat. Methods* 2008, 5, 545-551

List of Publications

1. **Chang Su Jeon**, Inseong Hwang* and Taek Dong Chung*, "Virus-tethered Magnetic Gold Microshells with Biomimetic Architectures for Enhanced Immunoassay", *Adv. Fucnt. Mater*. 2013, 23, 1484-1489 (Cover paper)
2. Changrok Choi, Inseong Hwang, Young-Lai Cho, Sang Han, Donghyun Cho, Donggeun Jung, Dae Won Moon, Eun Joong Kim, **Chang Su Jeon**, Jeong Hun Kim*, Taek Dong Chung* and Tae Geol Lee*, "Fabrication and characterization of plasma-polymerized poly(ethylene glycol) film with superior biocompatibility", *ACS Appl. Mater. Interfaces* 2013, 5, 697-702
3. Hyoungseon Choi, Kwang Bok Kim, **Chang Su Jeon**, Inseong Hwang, Saram Lee, Hark Kyun Kim*, Hee Chan Kim* and Taek Dong Chung*, "Label-Free DC Impedance-based Microcytometer for Circulating Rare Cancer Cell Counting", *Lab Chip* 2013, 13, 970-977
4. Saram Lee, **Chang Su Jeon**, Inseong Hwang, Taek Dong Chung* and Hee Chan Kim*, "Simultaneous Detection of SERS and Fluorescence Signals Using a Single Excitation Laser Source for Microbead-Based Analysis", *J. Biomed. Nanotechnol.* 2013, 9, 1241-1244
5. Hyoungseon Choi, **Chang Su Jeon**, Inseong Hwang, Juhui Ko, Saram Lee, Jaebum Choo, Jin-Hyo Boo, Hee Chan Kim* and Taek Dong Chung*, "Flow Cytometry–based Submicron-Sized Bacterial Detection System using Movable Virtual Wall", *Lab Chip* 2014, 14, 2327-2333

6. Seung-Ryong Kwon, **Chang Su Jeon**, Nam Yong Hong, Kwang Pyo Kim*, Inseong Hwang* and Taek Dong Chung*, "Gold-plated magnetic polymers for highly specific enrichment and label-free detection of blood biomarkers under physiological conditions", *Chem. Commun.* 2014, 50, 10066-10069
7. Jangho Kim, Subeom Park, Yoen Ju Kim, **Chang Su Jeon**, Ki Teak Lim, Hoon Seonwoo, Sung-Pyo Cho, Taek Dong Chung, Yun-Hoon Choung*, Byung Hee Hong* and Jong Hoon Chung*, "Monolayer graphene-directed growth and neuronal differentiation of mesenchymal stem cells" J. Biomed. Nanotechnol. 11, 1-10 (2015), 2015
8. Eun Joong Kim‡, **Chang Su Jeon**‡, Soo Youn Lee, Inseong Hwang* and Taek Dong Chung*, "Fabrication of Robust Type-specific Hemisynapses Using Artificial Dendrites", *submitted*

요약 (국문초록)

고체상 추출은 시료를 전처리 하는 방법의 하나로 분석 분야에서는 복잡한 미지시료에서 관심 종을 분석하기 위한 분리, 농축 및 정제의 수단으로 사용되며, 최근에는 생체 모사 표면 공학을 통해 결합 친화성을 높이고 민감도와 선택성을 증가시키려는 노력들이 진행되고 있다. 혈액과 세포와 같은 복잡한 생체시료를 분석하기 위해서는 고체상 표면과 관심 종과의 물리/화학적 상호작용이 매우 중요하며, 관심 분석물질이 고체표면에 직접적으로 상호작용하는 유형과 세포와 같은 분석대상을 표면에 도입하여 분비되는 물질을 관찰하는 유형으로 구분할 수 있다. 본 학위 논문은 (i) 향상된 분석물질−고체표면 상호작용을 위한 생체 영감 표면 수식화 와 (ii) 인공시냅스 유도와 생분석을 위한 신경 세포 부착 단백질 정제의 응용사례를 보고했다.

파트1. 분석물질−고체 표면 상호작용: 향상된 면역분석법을 위한 생체 모사 건축물을 가진 바이러스로 꾸며진 자성 금 마이크로쉘

섬사상 파지 바이러스는 세포의 기능을 높이는 많은 가늘고 긴 구조와 유사한 구조적 차원들을 가지고 있다. 이 연구의 목적은 생물체의 시스템을 닮은 바이러스와 마이크로 입자의 결합이며, 그렇게 함으로써 독특한 형태에서 유래된 증가요소가 있다. 우리는 자기조립분자층을 형성하기 위해 마이크로 쉘 위에 금 층을 형성하고 이는 스트렙타아비딘을 사용한 화학조작과 비특이적 흡착을 방지하는데 도움이 된다. 파지 비리온들은 스트렙타아비딘으로 개질 된 금 마이크로쉘에 선택적으로 결합하기 위해 그들의 꼬리에 바이오틴이 결합되어 있다. 우리는 표면 대 부피 비

율 증가로 인해 바이러스 개질 된 금 마이크로쉘 위에 고정되는 항체의 양이 증가되는 것을 확인했다. 실제로 카디악 트로포닌I 와 마이오글로빈 각각이 검출되는 민감도가 증가했다. 이 연구는 바이러스와 비 생체 물질의 결합이 정량분석 가능한 향상된 면역분석을 위한 생체모방 수단이 될 가능성을 설명하고 있다.

파트2. 세포-고체 표면 상호작용: 인공 시냅스 유도를 위한 신경 세포 부착 물질 정제

전통적인 신경 인터페이스는 오로지 신경세포와 비 생물체의 수동적인 물리적 접촉에 의존한다. 하지만 뇌에서의 신경세포는 시·공간상의 특수함이 정교하게 조절된 시냅스를 통해 의사소통 한다. 이 시점에 우리는 새롭게 조작된 형광과 바이오틴이 붙어 정제, 정량, 추적, 무기 기질 위에 고정이 가능하게 하는 시냅스 후 세포 부착 물질을 보고한다. 방향성이 조절된 고정으로부터 유래된 지질 막 위의 시냅스 후 세포 부착 물질의 독립성은 신경세포와 다양한 무기 고체 기질간에 인공 시냅스 형성에 맞게 단백질의 기능성을 확장한다. 또한 세포와 고체 표면과의 상호작용을 연구하기 위한 기초로 활용될 것이다.

주요어: 골드 마이크로쉘, 서스펜션 어레이, 비특이적 흡착, 바이러스, 인공 시냅스, 뉴로라이긴, 신경세포 접착물질

학번: 2009-22920